AD-A118 877 NORWEGIAN DEFENCE RESEARCH ESTABLISHMENT KJELLER F/G 20/5
CONTINUOUSLY-TUNABLE HIGH-REPETITION RATE RF-EXCITED CO2 WAVEGU--ETC(U)
JUL 82 S LOEVOLD
UNCLASSIFIED NDRE/PUBL-82/1002 NL

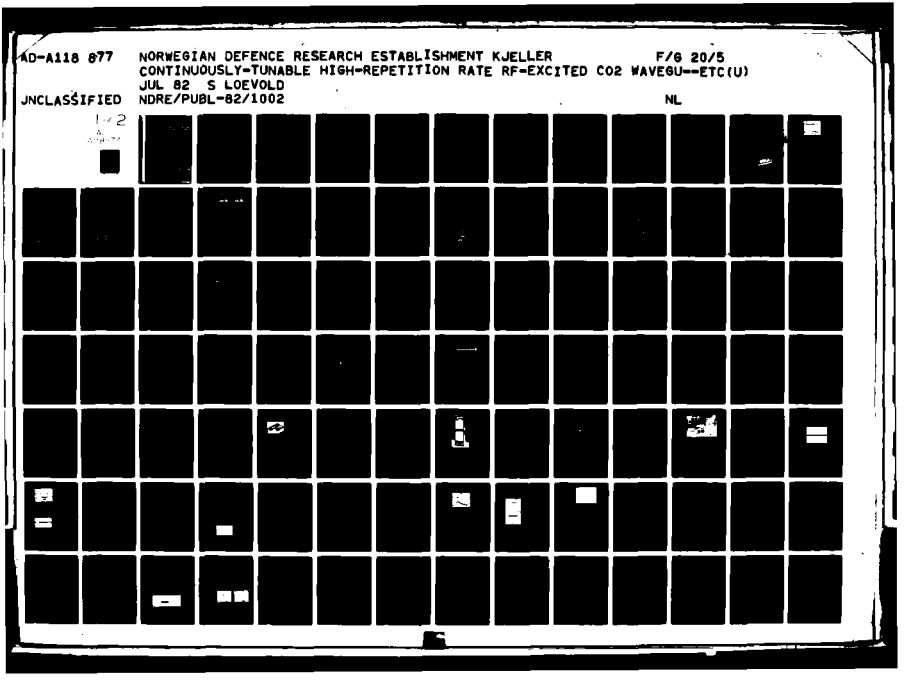

CONTINUOUSLY-TUNABLE HIGH-REPETITION RATE RF-EXCITED CO_2 WAVEGUIDE LASER

BY

STIAN LØVOLD

NDRE/PUBL-82/1002

FORSVARETS FORSKNINGSINSTITUTT
NORWEGIAN DEFENCE RESEARCH ESTABLISHMENT
P O Box 25 - N-2007 Kjeller, Norway

CONTINUOUSLY-TUNABLE HIGH-REPETITION RATE RF-EXCITED CO_2 WAVEGUIDE LASER

BY

STIAN LØVOLD

NDRE/PUBL-82/1082

FORSVARETS FORSKNINGSINSTITUTT
NORWEGIAN DEFENCE RESEARCH ESTABLISHMENT
P O Box 25 - N-2007 Kjeller, Norway

July 1982

NORWEGIAN DEFENCE RESEARCH ESTABLISHMENT (NDRE)
FORSVARETS FORSKNINGSINSTITUTT (FFI)
POST OFFICE BOX 25
N-2007 KJELLER, NORWAY

UNCLASSIFIED
SECURITY CLASSIFICATION OF THIS PAGE
(when data entered)

REPORT DOCUMENTATION PAGE

1) PUBL/REPORT NUMBER	2) SECURITY CLASSIFICATION	3) NUMBER OF PAGES
NDRE/PUBL-82/1002	UNCLASSIFIED	100
1a) JOB REFERENCE	2a) DECLASSIFICATION/DOWNGRADING SCHEDULE	
FFIE/415	–	

4) TITLE

CONTINUOUSLY-TUNABLE HIGH-REPETITION RATE RF-EXCITED CO_2 WAVEGUIDE LASER

5) NAMES OF AUTHOR(S) IN FULL (surname first)

LØVOLD Stian

6) DISTRIBUTION STATEMENT

Approved for public release. Distribution unlimited
(Offentlig tilgjengelig)

7) INDEXING TERMS

IN ENGLISH:	IN NORWEGIAN
a) Laser	a) Laser
b) Carbon Dioxide Laser	b) Karbondioksyd-laser
c) Radio Frequency Discharge	c) Radiofrekvensutladning
d) Waveguide	d) Bølgeleder
e) Tuning	e) Avstemming

THESAURUS REFERENCE:

8) ABSTRACT (continue on reverse side if necessary)

The concept of pumping a CO_2-laser with a radio-frequency discharge at multiatmospheric pressures in order to obtain continuous frequency tuning has been investigated both theoretically and experimentally. Experimentally 40.68 MHz rf-excitation of discharges between parallel plate electrodes with up to 7–8 kW peak rf-power has been investigated. Emphasis has been laid on how to attain a stable glow-discharge with sufficiently long duration before arcing for integration of enough rf-power in the discharge to reach threshold for laser oscillation. A 10 atm rf-excited CO_2 waveguide laser has been developed. With no dispersive elements in the laser resonator and with a 2% output coupler, input rf-power threshold for laser oscillation was 2 kW at 10 atm. Peak output power was 1.5 kW for 7–8 kW input rf-power. The output pulse has the form of a ≈300 ns duration gain-switched pulse followed by a tail at lower power. An efficiency (input rf-energy/laser output-energy) of 2% has been measured for the gain-switched pulse. The laser has been operated with pulse repetition rates in excess of 1 kHz, limited primarily by the available gas-flow capacity. Continuous frequency tuning between the R(12) and R(14) lines in the 10.4 μm band has been demonstrated.

9) DATE	AUTHORIZED BY	POSITION
12 July 1982	Finn Lied	Director

UNCLASSIFIED
SECURITY CLASSIFICATION OF THIS PAGE
(when data entered)

CONTENTS

CONTINUOUSLY-TUNABLE HIGH-REPETITION RATE RF-EXCITED CO_2 WAVEGUIDE LASER

SUMMARY

The concept of pumping a CO_2-laser with a radio-frequency discharge at multiatmospheric pressures in order to obtain continuous frequency tuning has been investigated both theoretically and experimentally. Experimentally 40.68 MHz rf-excitation of discharges between parallel plate electrodes with up to 7–8 kW peak rf-power has been investigated. Emphasis has been laid on how to attain a stable glow-discharge with sufficiently long duration before arcing for integration of enough rf-power in the discharge to reach threshold for laser oscillation. A 10 atm rf-excited CO_2 waveguide laser has been developed. With no dispersive elements in the laser resonator and with a 2% output coupler, input rf-power threshold for laser oscillation was 2 kW at 10 atm. Peak output power was 1.5 kW for 7–8 kW input rf-power. The output pulse has the form of a ≈300 ns duration gain-switched pulse followed by a tail at lower power. An efficiency (input rf-energy/laser output-energy) of 2% has been measured for the gain-switched pulse. The laser has been operated with pulse repetition rates in excess of 1 kHz, limited primarily by the available gas-flow capacity. Continuous frequency tuning between the R(12) and R(14) lines in the 10.4 μm band has been demonstrated.

1 INTRODUCTION

The intention of this work has been to investigate whether it is possible to develop a continuously tunable CO_2 waveguide laser based on a radio-frequency (rf) discharge in a CO_2 laser–gas mixture at high pressure. Work performed at low and medium gas pressures (100 torr – 2 atm) (1–6) has shown that application of rf excitation technique has several advantages, which may also be valid at high pressures. The necessary operating pressure for continuous frequency tuning is approximately 5 atm when a mixture of CO_2 isotopes is used (7) and 10 atm when a single isotope is used (8). A continuously tunable rf-excited CO_2 waveguide laser would be particularly attractive for spectroscopy, remote sensing, short pulse generation and optical pumping of other infrared lasers.

In this report is described a theoretical and experimental investigation into the pumping of a high-pressure molecular gas laser with an electrical rf discharge. Several tunable resonator designs suitable for continuous frequency tuning of such a laser are evaluated. The first operation of an rf excited CO_2 waveguide laser at 10 atm gas pressure is reported. Frequency tunability has been demonstrated by continuous tuning between vibrational–rotational line centres.

Tunable coherent light sources have wide applications in areas like high resolution spectroscopy (9–11) in the study of ultrafast phenomena in atoms and molecules (12) and in photochemistry (13). There is a large research activity on development and application of tunable lasers in remote sensing (14) and in isotope separation (15). Medium- and high-power tunable sources may be used to pump other laser media (11, 15, 16). At the Norwegian Defence Research Establishment (NDRE) remote sensing of pollutants, exhaust gases and toxic gases in the atmosphere have motivated the work described in this report.

Tunable coherent light sources can be realized in different ways. One way is to use a laser with a broad gain profile. The laser frequency may be tuned across the gain profile by using dispersive elements in the laser resonator. Dye lasers, excimer lasers and high-pressure gas lasers are examples of this type. Another possibility is to utilize the shift of energy levels in a laser active medium by external perturbations. In this way the gain profile may be frequency tuned and the laser resonator need not be tunable. The level shift may be caused by an external magnetic field (spin-flip Raman

lasers and Zeeman-tuned gas lasers) or by temperature or pressure changes (semiconductor lasers). A third possibility for generation of tunable coherent radiation is based on optical frequency mixing in media with a sufficiently large non-linear susceptibility. When sufficiently intense laser radiation is incident on such a medium, radiation at multiples of the incident frequency may be generated (frequency doubling, tripling). When two beams are inserted, radiation at both the sum and difference frequency may be generated. In a molecular or atomic gas the incident radiation may be frequency shifted by the Raman effect (Raman laser). In all these examples of frequency mixing one of the incident frequencies must be tunable in order to produce tunable radiation. The advantage is that tunable radiation may be generated in a frequency domain where no other practical tunable sources exist.

The optical parametric oscillator may generate tunable radiation from a fixed frequency which is incident upon a crystal with non-linear susceptibility. The incident wave may be split into two waves with different frequencies and wavevectors. By varying the angle of incidence against the optical axis of the birefringent crystal or controlling the refractive index through the crystal temperature, the frequencies of the two waves may be varied within wide ranges.

Today the whole spectral region from the ultra-violet (~100 Å) to the far infrared (~100 μm) is covered by tunable coherent sources, see Figure 1.1. In the ultra-violet and visible, excimer lasers and dye lasers are the most commonly used. Colour centre lasers, spin-flip Raman lasers, semiconductor lasers and optical parametric oscillators are used in the visible and infrared. Frequency mixing techniques may cover all spectral regions. A good survey over the various sources and techniques can be found in (11).

The tunable lasers and techniques vary considerably in complexity, reliability, lifetime, output power, frequency bandwidth and stability, and price. For example, the spin flip Raman laser requires a high-power pump laser, a 100 kGauss tunable magnet

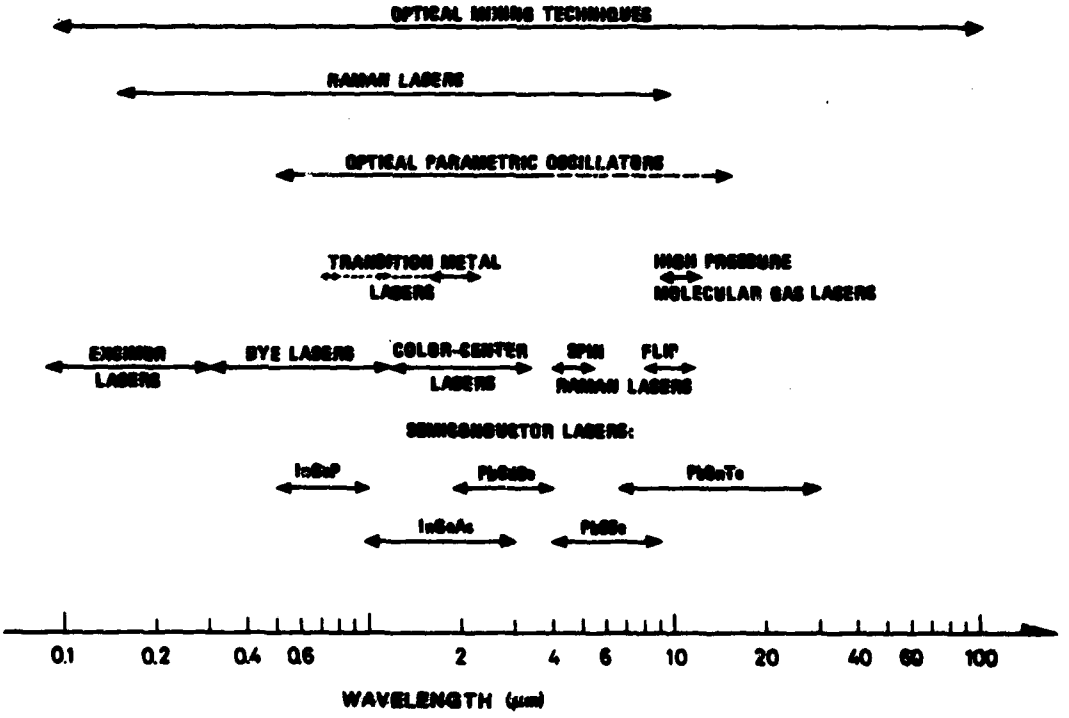

Figure 1.1 Spectral ranges of different tunable coherent sources (after (11, 17, 18))

for frequency tuning, and it must be operated at liquid He temperatures. The semiconductor lasers have output powers in the mW power range, there are problems with regard to frequency control and mode jumping, and in the infrared spectral region they must be operated at liquid He or liquid N_2 temperatures. The dye laser is perhaps the most highly developed tunable laser with respect to reliability, narrow bandwidth and frequency stability. Continuous wave output powers up to 100 W and peak pulse power up to 10^6 W may be achieved. Nonlinear frequency mixing techniques rely on advanced crystal technology. Colour centre lasers and the transition metal lasers (17) are promising sources which are under development. Recently the Alexandrite transition metal laser has become commercially available (18).

In general the various sources are suited for quite different applications. Most of them are only suitable for use in the laboratory. Thus there is extensive research activity on development of practical and reliable tunable coherent sources. It is the author's hope with the present work to make a contribution in this field.

The CO_2 molecule has many fortunate properties which make it suitable for light amplification by stimulated emission of radiation. CO_2 lasers oscillate within many closely spaced rotational–vibrational lines between 9 and 11 μm. This region falls within the good transmission window between 8 and 12 μm in the atmosphere. CO_2 lasers have been operated cw with several kW output power, with several GW peak pulse output powers and with pulse energies of several kJ. CO_2 lasers can be made fairly compact (~10 cm long), they can operate at room temperature, and the frequency stability can be very good (one part in $10^9 - 10^{10}$ (19)). Sealed-off tube lifetimes have exceeded many thousand hours. Operating efficiency can approach 30%. The gain medium (CO_2, N_2 and He gas) is commercially available with very good purity at a reasonable price, and is easy to handle. The CO_2 laser can be Q-switched and has been electrically, optically, gas-dynamically and chemically pumped.

There exists an enormous amount of literature on CO_2 lasers, which is rapidly becoming out of date. DeMaria wrote a good review article in 1973 (20).

At the normal low operating pressures (~20–30 torr) the CO_2 laser-active transitions have a ~50 MHz wide Doppler broadened linewidth. The lines are separated by 20–70 GHz. The pressure broadening of the lines is approximately 4 GHz per atm (full width at half maximum, = FWHM). A frequency tuning range of 1.2 GHz within a single line has been achieved in a continuous wave (cw) CO_2 waveguide laser (21). At approximately ten atmospheres the pressure-broadened lines overlap sufficiently to allow continuous tuning between the line centres. At this pressure only pulsed operation has been possible, mainly due to the pump power and cooling requirements.

Continuously tunable CO_2 lasers have been demonstrated both with optical pumping (23, 24) and direct current (dc) electric discharge pumping with some sort of preionization (7, 8, 25–28). Optical pumping has several general advantages, for example it can selectively excite only one energy state. Since negligible dissociation occurs, it is feasible to use rare and expensive isotopes of atoms and molecules in sealed-off cavities. The main problem is that a high-power pump laser oscillating on a specific frequency is required. Electric discharge pumping has the advantage that it may be realized with more readily available and less expensive components. In high pressure CO_2 lasers the electric pumping is accomplished by electron impact on CO_2 and N_2 in a short duration glow discharge. The main problems are formation of arcs in the glow discharge, which is detrimental to laser performance, and gas dissociation, which makes sealed-off operation difficult. Also sputtering of the electrodes may limit the laser lifetime. DC electric discharge pumping requires very high voltages, typically 40–70 kV. Some of the lasers use an electron beam to preionize and sustain the discharge (25,26). This requires large installations, which usually need frequent maintenance. A common problem with both optical and electric discharge pumping is

damage to the optical components in the tunable laser resonator caused by the high-power optical fields.

High-pressure electric glow discharges may be preionized by uv-radiation from an arc discharge (8, 22, 27–29). A well-known technique is to first ignite an arc and then rapidly apply a voltage with reversed polarity and with the right magnitude for a glow discharge (29, 30). Subsequent reversals of the voltage polarity is exactly what happens in an rf discharge.

In an rf glow discharge arcs should not so easily develop since the oscillating "pulses" may be made very short, and local development of arcs should be quenched by the subsequent reversals of voltage polarity. The rf discharge may be "electrodeless", for example with parallel plate metal electrodes covered by a dielectricum. With an appropriate choice of frequency and electrode separation the electrons may oscillate within the discharge region without colliding with the boundary. In this way the problem with sputtering of the electrodes should be reduced. The dielectric electrodes may form an optical waveguide which both confines the gas discharge and guides the optical field (96–97). This allows for a compact laser construction. With the short electrode separation typical for a waveguide laser, a lower discharge voltage will be required compared to what is typical in high-pressure dc-excited lasers. Also the voltage may be transformed to the appropriate level at the laser head, which eliminates the need for the very high voltage power supply.

Several gas lasers have been made with rf excitation. The first CO_2 laser was pumped by the rf discharge generated by the electromagnetic field from a coil surrounding the laser gas (31). The noise in the output from He–Ne lasers has been found to be less when the laser is pumped by an rf discharge than by a dc discharge (32). RF fields in the MHz and GHz frequency domain have been used both alone and together with a dc field to pump CO_2 lasers at low pressures (1, 2, 5, 6, 31, 33–37), a Xe-He laser (38), He-Ne lasers (32, 39, 40), a CO laser (41) and Br, C, Cl, S and Si lasers (42). Pulsed and cw small compact rf-excited CO_2 waveguide lasers operating in the 100 torr pressure range have been developed (1, 2, 5, 6). CW rf CO_2 waveguide lasers are now commercially available (43, 44). An excimer laser has been pumped with 9.375 GHz microwave power up to 2 atm gas pressure, limited by the gas handling equipment (45)*. High pressure operation of rf-excited CO_2 HF, F and Xe lasers have been reported (4). Lachambre *et al* (3) have operated an rf CO_2 waveguide laser up to 1 atm using a 1 kW amplifier at 21 MHz. Christensen *et al* (4) reported operation of an rf CO_2 waveguide laser up to 2 atm using a 100 kW amplifier at 30 MHz, and Bakarev *et al* (46) reported operation up to 3 atm with a 30 MHz amplifier. These are the highest pressures at which rf-excited lasers have been operated so far.

At the Norwegian Defence Research Establishment, Stig Landrø has made two rf-excited CO_2 waveguide lasers operating at pressures up to 400 torr (47). He used a 100 W rf amplifier at 40.68 MHz. This work formed a basis for the work described in this report. From the start it was chosen to use an industrial band frequency because radiation was considered unavoidable, at least under the experimental situation. 40.68 MHz was chosen because it was the highest industrial band frequency before the GHz domain. First a laser suitable for operation up to 1–2 atm was built. After a successful operation of this laser, a small discharge chamber was built to study discharge parameters and optical gain at up to 10 atm gas pressure. Based on the studies in the high pressure discharge chamber, a laser was built with a housing suitable for more than 10 atm pressure. This laser was operated at up to 11 atm at 1 kHz pulse repetition rate with only 2 kW rf pump power (48). Since then, experiments have been made in order to tune the rf laser continuously between the line centres.

---

* Note added in proof: Results from studies of microwave-excited excimer laser has recently been reported by the same authors at up to 5 atm gas pressure (124).

In this report, a short description will first be given of the characteristics of the 10 atm rf CO_2 laser and the equipment used to drive it. It will be compared to characteristics of dc-discharge excited multiatmospheric-pressure CO_2 lasers. In Chapters 3 and 4 will be treated the two main parts of the laser, that is, the broadband amplifying medium and the tunable resonator. These chapters are based on a literature survey. Several tunable resonator designs suitable for the rf CO_2 waveguide laser are evaluated in Chapter 4. In Chapter 5 the experimental apparatus that has been used will be described, and the experimental results will be given in Chapter 6.

2 DESCRIPTION OF THE 10 ATMOSPHERES HIGH-REPETITION RATE RF-EXCITED CO_2 WAVEGUIDE LASER

In direct-current (dc) excitation of multiatmospheric pressure CO_2 lasers the electrical energy stored in large capacitors is coupled into the discharge in very short duration pulses (8, 22, 25–29, 49–52). In this way very high pump powers are obtainable. Typical pump pulse durations may be $0.1 - 1\ \mu s$ and peak pump powers in the 100 MW range are obtainable. The short pulse duration is necessary to avoid formation of arcs. The pulse repetition rates are usually low, typically from single shot to 50 Hz (52).

The rf discharge for pumping of the rf CO_2 waveguide laser is characterized by a much lower power level and a much longer pump pulse duration. Long pulse durations are necessary because rf power sources cannot easily deliver the very high power obtainable by discharging the high energy capacitors. Long duration pulses are obtainable in rf glow discharges because arcs do not so easily develop as in dc glow discharges. In the experiments described in this report it has been necessary to use He-rich gas mixtures (typically 96% He, 2% CO_2 and 2% N_2). Also the metal electrodes had to be covered by a dielectricum, and the separation between the dielectric plates had to be small, typically 1 mm, to obtain long duration arc-free discharge pulses.

A cross-section of the laser and schematic diagram of the excitation circuitry are shown in Figure 2.1. The optical axis is normal to the paper plane. The copper electrodes are 135 mm long. The ungrounded electrode is 2 mm thick, and is clamped to the room temperature heath sink with a boron nitride block for efficient cooling.

The parallel plate waveguide is formed by polished sapphire ribbons which are 0.75 mm thick, 150 mm long and 12 mm wide, and which are epoxied on the electrodes. The gap between the sapphire ribbons is variable. 1 mm to 1.5 mm gaps were used in most of the experiments. The gas is flowed through the waveguide transversely to the optical axis.

The optical resonator elements are mounted inside the pressure-tight chamber, close to the waveguide. The chamber is made of an aluminium baseplate and Lucite side

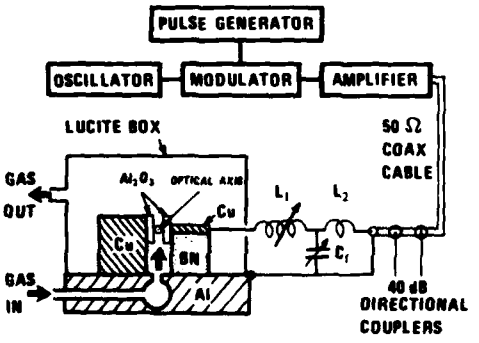

Figure 2.1 *Cross-section of the laser and schematics of the excitation circuitry*

The optical axis is normal to the paper plane. Gas flows through a slit having the same length as the electrodes.

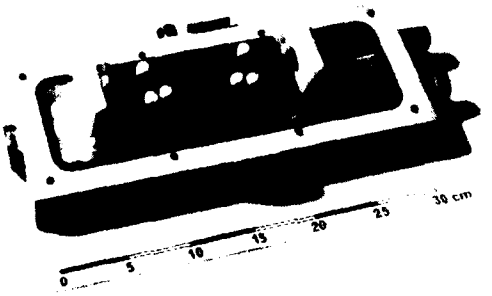

Figure 2.2 *Photograph of the laser with top cover and side-walls removed*

Two mirrors are mounted close to the waveguide

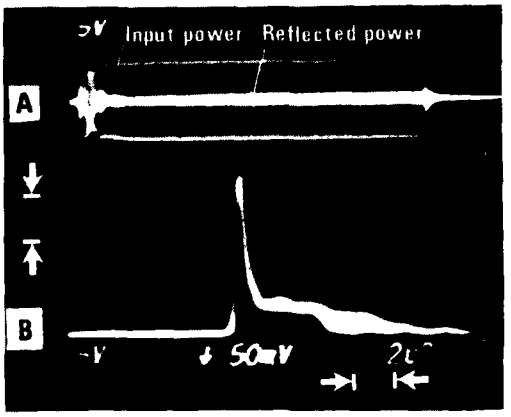

Figure 2.3 Input and reflected rf pulses, and overlay of approximately 10 consecutive laser pulses at 10 atm gas pressure

Input rf power is approximately 2 kW.
A: Input and reflected rf pulses from ~40 dB directional couplers (superposed), (5 V/div).
B: Laser pulses (40 W/div). Horizontal scale is 2 μs/div.

walls and top cover. The optical elements may be adjusted from the outside. The rf amplifier is connected to the laser with an impedance matching network. The overall length of the laser is 32 cm.

A picture of the laser with top cover and side-walls removed is shown in Figure 2.2. Under operation, both the laser head and the impedance matching network are covered by rf shielding boxes. The rf power source consists of a 40.68 MHz oscillator, a pulse modulator, a 50 W preamplifier and a 7–8 kW final power stage.

Typical output pulses at 10 atm gas pressure are shown in Figure 2.3. A pulse consists of an approximately 300–400 ns duration gain-switched spike followed by a tail with lower power. With 7.5 kW pump power, a peak pulse power of 1.5 kW has been obtained. The good pulse stability is illustrated by the fact that Figure 2.3 shows a superposition of approximately 10 consecutive pulses. The laser has been operated with pulse repetition rates from 20 Hz to above 1 kHz. Good pulse to pulse stability and high pulse repetition rate are important for applications of the laser in spectroscopy and remote sensing.

3 RADIO-FREQUENCY DISCHARGE EXCITATION OF A MULTIATMOSPHERIC-PRESSURE CO_2 WAVEGUIDE LASER

In this chapter the concept of pumping a multiatmospheric-pressure molecular gas laser with a radiofrequency (rf) electrical discharge between parallel plate electrodes is analysed. Quantitatively, only the CO_2 laser will be considered. The analysis should be qualitatively relevant for rf excitation of other gases like N_2O, CS_2, OCS, CO, HF, DF and others, and for various isotopes of these gases. Continuous tuning between vibrational-rotational line centres have been demonstrated in $C^{12}O_2^{16}$ (the standard isotope) and $C^{13}O_2^{16}$ at 10 atm, in N_2O at 5 atm and in $C^{12}S_2^{32}$ and $C^{13}S_2^{32}$ at 4 atm (53), see Figure 3.1.

A large amount of literature exists on direct-current (dc) excitation of CO_2 lasers. In the gas pressure regimes used in this work the electron/neutral-particle collision frequency is much larger than the oscillation frequency of the rf field. Therefore, the dc discharge characteristics form a natural base for a discussion of the rf discharge.

In this chapter, emphasis will be laid on how much of the power coupled into a dc discharge will go into excitation of the upper laser level in CO_2. This is a function of the E/N ratio (electric field strength/neutral particle density) and the gas mixture. The excitation efficiency has been calculated by Lowke, Phelps and Irwin (54) from electron impact cross-sections versus electron energy and from calculated electron energy distributions versus E/N.

In general the E/N required to break down the gas to a plasma is much higher than the E/N for which most efficient excitation occurs (54, 55). This is one of the main reasons why separate preionization of the gas is necessary for efficient pumping of dc short-pulse – excited lasers. Preionization of the gas is important to attain a homogenous glow discharge with no arcs in the pump pulse. In general the E/N ratio in glow discharges lies within a regime for which efficient excitation occurs, while the E/N in arc discharges does not. The precise E/N ratio for which a self-sustained glow discharge operates is determined by the electron production and loss rates. Various production and loss mechanisms under conditions relevant for a high pressure CO_2 waveguide laser will be discussed. The mechanism of glow-to-arc transitions in a dc-discharge will also be discussed.

The characteristics of alternating current (ac) glow discharges vary with several parameters like gas pressure, gas mixture, the frequency of the ac field, the way in which the ac field is coupled into the discharge and the discharge confinement geometry. Little information has been found in the literature on characteristics of rf-discharges for the gas mixtures and pressures of interest for this work. Most of the literature covers conditions for gas breakdown at low pressure regimes, typically a few torr. In

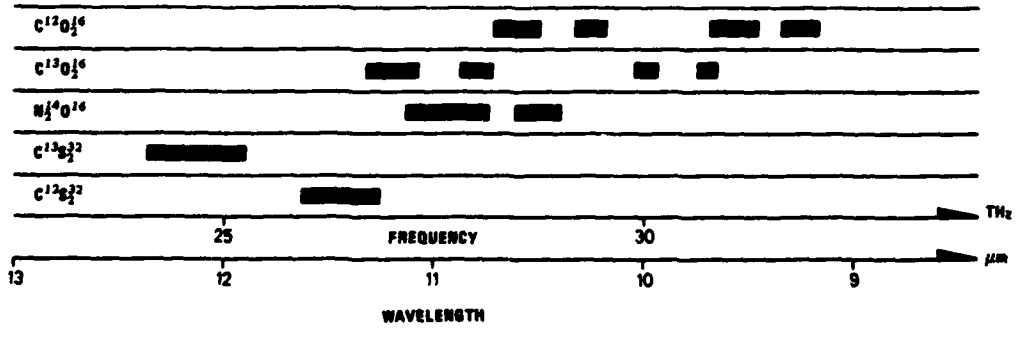

Figure 3.1 Tuning range of multiatmosphere lasers (from (53))

this work we are concerned with the gas breakdown and the stability of an rf glow discharge in a CO_2 laser gas mixture at up to 10 atm, and the excitation efficiency of the upper laser level of CO_2 in such a discharge.

In this chapter will be discussed parameters of importance for the establishment of a stable glow discharge between parallel plate electrodes (a capacitor discharge). The discussion is based on a literary survey and observations made under the experimental part of this work. In the first operation of a CO_2 laser the rf field from a coil surrounding the laser gas mixture was used to pump the laser (31). Because of the high field strengths required to pump the laser at multiatmospheric pressures (~3–10 kV/cm atm) the main emphasis in this work has been laid on capacitor discharges. High power microwave excitation will be only briefly mentioned. A model which describes a stationary rf discharge between parallel plate electrodes will be discussed. It is useful for a derivation of the electrical circuit equivalent of the discharge. This is important for dimensioning an impedance-matching circuit which must be used for efficient coupling of the rf energy into the discharge. It will be pointed out that when the impedance matching circuit is correctly dimensioned the voltage amplitude in the first rf oscillations of the pulse will be large enough to break down the gas to a plasma. After breakdown the voltage amplitude will primarily be determined by the electron production and loss rates. Thus, separate preionization is not necessary in an rf-excited laser. The model describing the stationary rf discharge is also useful for a discussion of the stability of such a discharge.

Finally, the pumping efficiency of the upper laser level of CO_2 in an rf discharge will be discussed. It is important to estimate how much rf power is required for pumping a continuously tunable CO_2 laser. Such an estimate will be made based on the discussion of the dc pumping efficiency versus E/N derived by Lowke *et al* (54) and measurements of small signal gain in pulsed dc-excited CO_2 lasers.

The chapter opens with a description of the CO_2 molecule and its laser active vibrational-rotational transitions.

3.1 Laser active transitions in CO_2

The CO_2 molecule is linear with one axis of symmetry and one plane of symmetry perpendicular to this axis. The four normal modes of vibration of the molecule are shown in Figure 3.2a. Two modes are degenerate. The three nondegenerate normal modes may be denoted by ν_1, ν_2 and ν_3. The energy levels of the vibrational modes

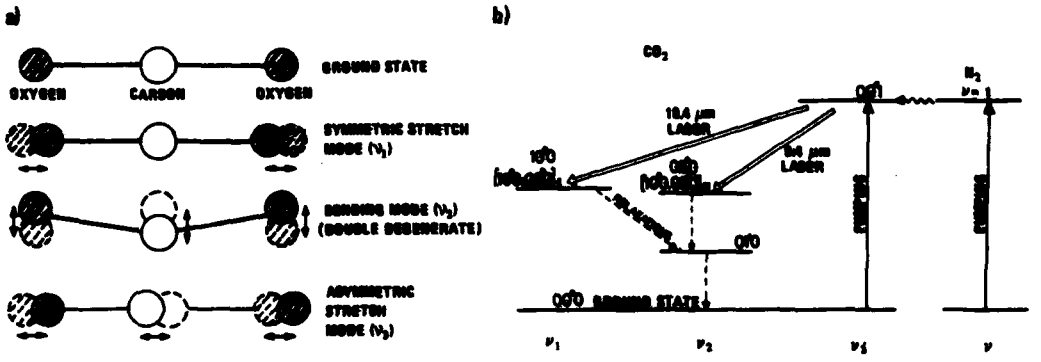

Figure 3.2 The CO_2 molecule

a) The CO_2 molecule in the unexcited state and the three nondegenerate normal modes of vibration.

b) The vibrational energy diagram for the first excited states of the vibrational modes of CO_2. Also shown is the first excited vibrational state of N_2.

are to a good approximation those of a simple harmonic oscillator. An arbitrary vibrational energy level may be denoted by $(n_1\ n_2^l\ n_3)$ where n_i is the number of excited quanta of the i'th mode. The superscript l denotes the rotation around the symmetry axis for the degenerate ν_2 mode.

The energy level diagram of the first excited states of these modes is shown in Figure 3.2b. The first excited state of the asymmetric stretch mode (the $00^0 1$ state) is the upper laser level. The energy difference between the first excited state of the symmetric stretch mode (the $10^0 0$ state) and the second excited state of the bending mode (the $02^0 0$ state) is very small ($\sim$5 cm^{-1}). The lower laser levels are linear superpositions of these two vibrational states. They are often denoted $(10^0 0,02^0 0)_I$ and $(10^0 0,02^0 0)_{II}$. The wavelengths corresponding to the energy difference between the upper and the two lower laser levels are approximately 10.4 μm and 9.4 μm.

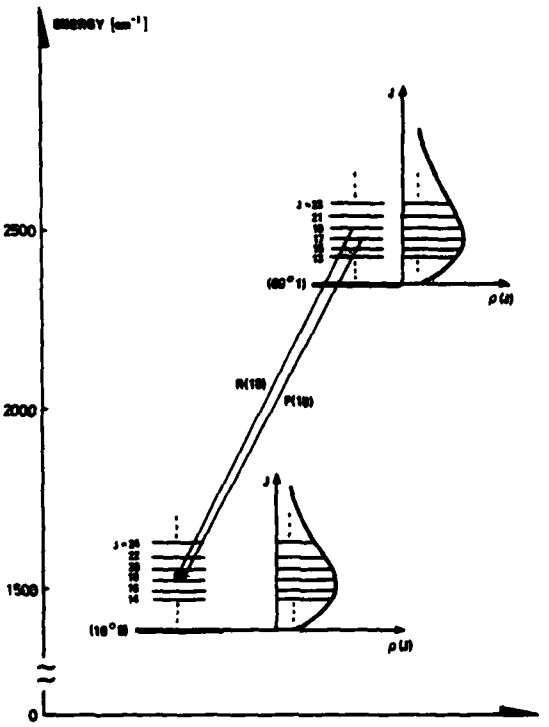

Figure 3.3 Rotational sublevels for two vibrational levels

Also shown are approximate population distributions $\rho(J)$ for the rotational manifold at room temperature, and two laser transitions.

The rotational energy sublevels associated with two of the vibrational states are shown in Figure 3.3. The degeneracy of each level is 2 J (J+1), where J is the rotational quantum number. A typical population of the rotational manifold is included in Figure 3.3, assuming a Boltzmann distribution at room temperature and the above-mentioned degeneracy. Because of the symmetry of the standard CO_2 isotope, only odd J-values are present in the ν_3 mode and only even J-values are present in the ν_1 and ν_2 modes. The property that each second rotational level is missing is the case for linear molecules with a centre of symmetry and zero nuclear spin in atoms outside the symmetry centre (56). The situation is different for some of the other CO_2 isotopes. Selection rules for electric dipole transitions from the upper to lower laser levels allow only transitions where $\Delta J = +1$ (the R-branch) and $\Delta J = -1$ (the P-branch). Each transition may be denoted by its branch (P or R), the rotational quantum number of the lower level, and approximate wavelength, for example P(20) 10.6 μm. In the standard CO_2 isotope the frequency difference between neighbouring transitions varies from about 22 GHz (0.77 cm^{-1}) to about 67 GHz (2.24 cm^{-1}). (The difference in interline spacing is a consequence of a centrifugal distortion term in the rotational energy (56).)

At room temperature the Doppler broadened linewidth of each transition is approximately 50 MHz (full width at half maximum = FWHM). The line broadening from collisions between CO_2 molecules (the self-broadening) is approximately 5.75 GHz per atm (FWHM) (139). In a laser, N_2 and He are usually added to CO_2. (This will be discussed later.) The pressure broadening due to collision with N_2 and He are 0.73 and 0.64 times the self-broadening, respectively, measured for the P(20) 10.6 μm transition (139). The content of He is normally dominant. Thus the pressure broaden-

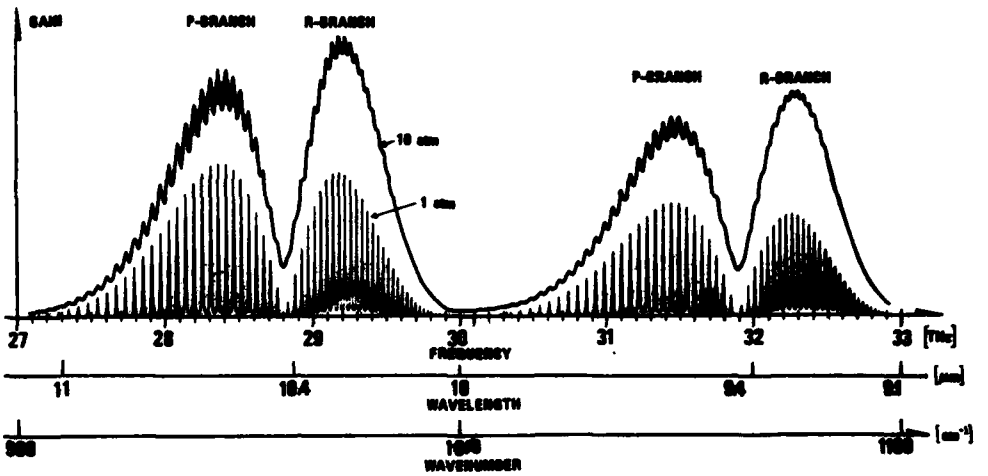

Figure 3.4 Calculated CO_2 laser gain spectrum at 1 atm and 10 atm gas pressure (after (22))
Peak gain is typically 1–3% per centimeter. The highest gain is for the R(16)–R(20) and P(16)–P(20) transitions approximately.

ing of the transitions will be approximately 4 GHz (FWHM) per atm. At approximately 10 atm the line spectrum emerges into continuous bands. Calculated spectra for the $(10^00,02^00)_{I,II} - (00^01)$ transitions are shown in Figure 3.4 at 1 atm and 10 atm gas pressure for a $CO_2 : N_2 : He$ mixing ratio of 1 : 1 : 8 (22). The highest gain is for the P(16)–P(20) and R(16)–R(20) transitions approximately.

The various CO_2 isotopes have spectra shifted slightly away from each other. Figure 3.1 showed the locations of the $(10^00,02^00)_{I,II} - (00^01)$ transition spectra for $C^{12}O_2^{16}$ and $C^{13}O_2^{16}$. At least 18 stable isotopes are known to exist. By using these isotopes, a broad frequency range from 9 μm to 13 μm may be completely covered. However, it should be noted that all but the standard isotopes are scarce and expensive.

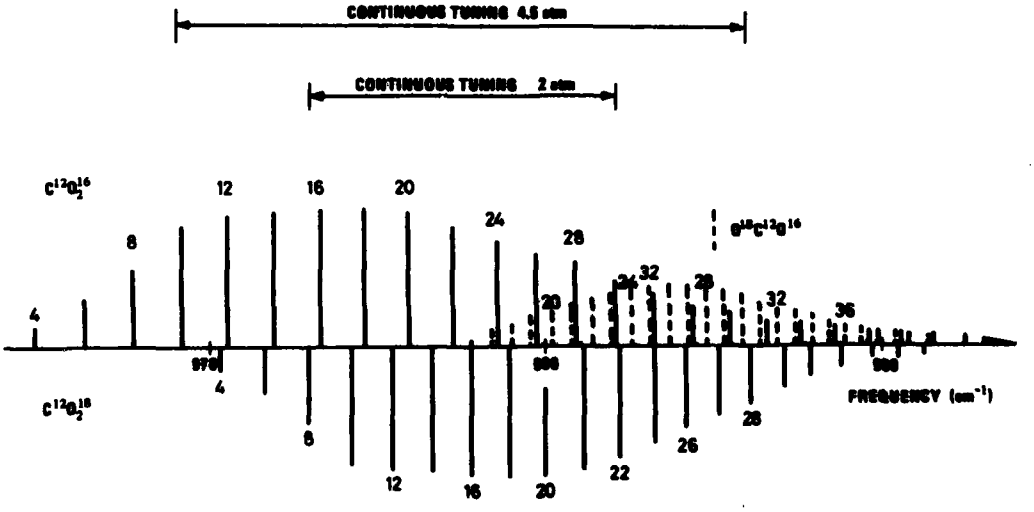

Figure 3.5 Spectral lines for three CO_2 isotopes in the R-branch at 10.2 μm
Approximate relative line strengths, which depend on gas kinetic temperature, are shown (after (7, 57)).

The spectral branches of the $C^{12}O_2^{18}$ and $C^{12}O^{16}O^{18}$ isotopes closely overlap the branches of the standard isotope. The individual lines fall between each other at random. This is shown for the R-branch at 10.2 μm in Figure 3.5 (after (57)). By using a mixture of these isotopes the spectrum will emerge into continuous bands at much lower pressures than when a single isotope is used. Gibson, Boyer and Javan (7) have achieved continuous frequency tuning at 2 – 4.5 atm gas pressure using a mixture of the above-mentioned isotopes.

Finally, it should be noted that the so-called hot-band and sequence-band transitions may aid in filling the gap between the regular lines. An energy level diagram showing these transitions is given in Figure 3.6. At high gas pressures the contribution from these transitions may be important (50). At low pressures they do not contribute significantly to the spectral gain profile unless the gas is heavily pumped. Laser action has been obtained at low pressures on the hot-band and the sequence-band transitions (58, 59).

The line centre frequencies for hot-band and sequence-band transition of the standard CO_2 isotope and for the regular transitions in various CO_2 isotopes is listed in (57–59).

3.2 Population distribution and relaxations in the vibrational/rotational energy manifold

3.2.1 The four-temperature model

Energy exchange between rotational levels and between rotational levels and translation occurs fast. Energy exchange between vibrational levels within each vibrational mode is a nearly resonant process which occurs much faster than the exchange between different modes. Because of these fast energy exchange processes the population within the vibrational modes and within the rotational levels can be considered to have a local Boltzmann equilibrium distribution with a temperature T_i for each mode. In the overall nonequilibrium situation when energy is pumped into one or more modes, these temperatures may be very different. The rotational energy is usually assumed to be in equilibrium with the translational energy at temperature T. The ν_1 and ν_2 modes are strongly coupled through the Fermi resonance between the (10^00) and (02^00) levels. They are usually assumed to have a common temperature T_1. The population within the ν_3 mode is characterized by the temperature T_3. The vibrational temperatures T_1 and T_3 are determined by the number of excited vibrational quanta per molecule. Since the rate of energy exchange within each mode is very fast, almost all the energy quanta stored in the ν_3 mode and in the rotational manifold may be converted into photons in the laser even for very short laser pulses.

3.2.2 Population inversion decay time-constant

Assuming there is a given population inversion between the upper laser level (00^01) and the lower laser levels $(10^00, 02^00)_{I,II}$, the question arises: how long does this population inversion last? The decay of the population in the lower laser levels in general is at least an order of magnitude faster than the decay out of the (00^01) level (65). The population of the (00^01) level is usually assumed to decay out via the (11^10) level, which is rather close in energy to the (00^01) level (65). The decay rates due to collisions between CO_2 and various species have been measured by a number of authors (126–128). There is a relatively large spread in the derived decay time constants. They seem to depend on whether they have been derived from fluorescence-decay or gain decay experiments.

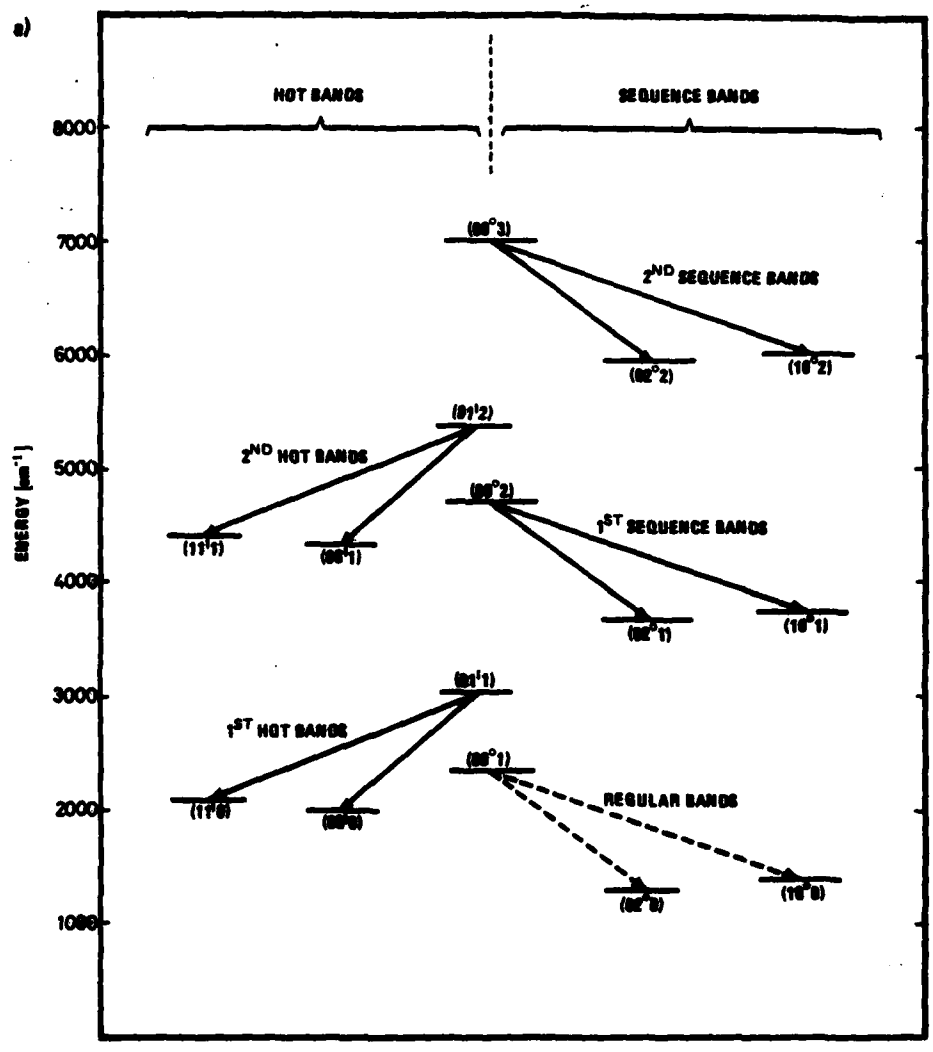

Figure 3.6 *Sequence-bands and hot-bands*

a) Extended CO_2 vibrational energy level diagram showing sequence-band and hot-band transitions

b) The frequency ranges of the first sequence-bands and hot-bands (after (58, 59))

According to (126, 128) the decay out of the $(00^0 1)$ level of CO_2 due to collisions between CO_2-molecules and N_2, He and other CO_2-molecules is given by a decay time-constant τ'

$$\frac{1}{\tau'} = P \cdot 760 \cdot (410\psi_{CO_2} + 115\psi_{N_2} + 64\psi_{He}) \qquad (3.1)$$

P — gas pressure in atm

ψ_x — fractional content of specie x in the gas

In a gas mixture containing 5% CO_2, 5% N_2 and 90% He the decay time-constant τ' would be 15.7 μs at 1 atm.

In a high-pressure CO_2-laser the content of N_2 is usually equal to the content of CO_2. This will be considered later. The vibrational energy levels of N_2 are close to the levels in the ν_3-mode of CO_2. This was shown in Figure 3.2b. Vibrational energy is rapidly shared between these modes. The main decay of the N_2 vibrational energy is via energy transfer to the ν_3 mode of CO_2 and the subsequent decay out of the CO_2 ν_3-mode described by eq (3.1) (65). Thus when there is an equal amount of vibrational energy stored in the CO_2 ν_3 mode and in N_2, the net decay out of the $(00^0 1)$ level of CO_2 will be given by a decay time-constant $\tau = 2\tau'$. When the decay out of the lower laser level is much faster than τ, the decay time-constant of the $(00^0 1)$ level will be the same as the gain-decay time-constant.

3.3 *Electrical dc discharge pumping of* CO_2

Pumping of the upper laser level of CO_2 may be done either gas-dynamically (61), chemically (62, 63), optically (23, 24, 64) or electrically. Gas-dynamical and chemical pumping have not been demonstrated at gas pressures relevant for continuous tuning. Optical pumping of CO_2 has been demonstrated up to 112 atm (23). At the Norwegian Defence Research Establishment a new optical pumping technique has recently been demonstrated up to 19 atm (24, 64).

Electrical discharge pumping of CO_2 lasers is by far the most used pumping technique. It allows simple, compact, reliable, efficient and high-power solutions. It can be used for both cw and pulsed lasers, and from a few torr to at least 20 atm gas pressure (50). An enormous amount of literature exists on the various aspects of electrical discharge pumping. It comprises electrode configurations, glow discharge parameters, glow-to-arc transitions, gas dissociation, gas mixtures, conditions for long life operation, gain saturation, discharge circuitries, etc. In this section only the basic physics of glow discharge pumping of CO_2 lasers will be discussed.

3.3.1 The role of N_2 and He

The electrical discharge pumping relies on the fact that the electron impact excitation of the CO_2 asymmetric stretching mode may be very efficient. Also the electron impact excitation of the N_2 vibration may be even more efficient. The N_2 vibrational mode is metastable and the first excited state is only 18 cm^{-1} (≈ 0.1 kT at room temperature) below the $(00^0 1)$ state of CO_2. This was shown in Figure 3.2. The vibrational energy gained by the N_2 molecule is thus rapidly shared with the upper laser level of CO_2.

Helium is assumed to play several important roles in the CO_2 laser. Helium is efficient in depopulating the $(01^1 0)$ vibrational level of CO_2. The self-deactivation of this level is relatively slow, and this level may serve as a bottle-neck for depopulation of the lower laser levels (20). Helium plays an important role for the energy distribution

of the electrons in the discharge, and He has very good thermal conductivity (20, 55). In general, the higher the gas pressure the higher should be the content of He to achieve a stable glow discharge without arcs ((50) and Chapter 6). According to (126) the relaxation rate of the upper laser level due to He–CO_2 collisions is less than 0.16 times the self-relaxation, see eq (3.1). The broadening of the laser transition due to He–CO_2 collisions is as large as 0.64 times the self-broadening (139). In a long-duration pump pulse, like the rf discharge pump pulse, it is important that the upper laser level lifetime is as long as possible.

It should be noted that several other species like CO, H_2, H_2O, Xe and $(CH_3)_3N$ may also be added to the laser gas mixture to improve performance. The roles of all these are not completely understood. CO aids in the chemical balanse through the reaction $CO + 1/2O_2 \rightarrow CO_2$. This is important especially in sealed-off lasers because CO_2 dissociates into CO and O_2 in the discharge (65). O_2 is detrimental to the laser performance, both in the relaxation of the upper laser level and in the formation of arcs. Vibrationally excited CO can play a similar role to N_2 in pumping of the upper laser level. It is not as efficient as N_2 however, since it is not metastable. Xe and $(CH_3)_3N$ have low ionization potentials. They are sometimes added to aid in the initiation of the discharge (7, 20). The role of these species will not be discussed further. They have not been used in these experiments.

3.3.2 Excitation processes

Cross-sections for electron excitations of CO_2 and N_2 versus electron energy are shown in Figure 3.7 (54, 66). (The first excited vibrational state of N_2 has an energy of approximately 0.2 eV. The cross-section indicates that the vibrational states of N_2 are not excited directly, but rather through the formation of a compound negative ion state (66).) From the cross-sections, the excitation of N_2 and CO_2 can be calculated when the electron energy distribution function is known.

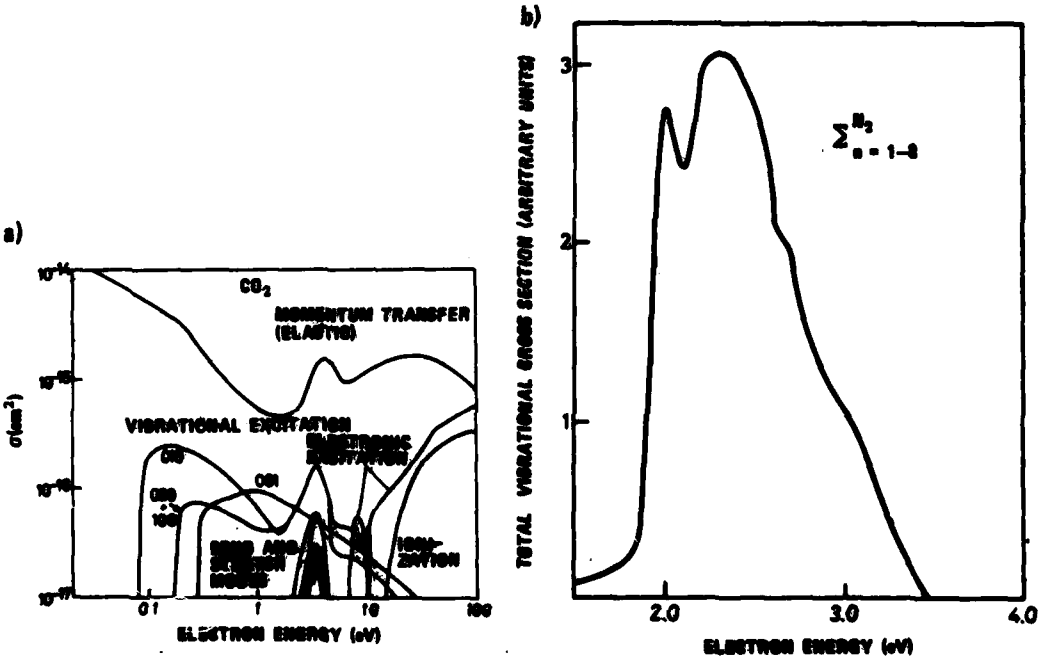

Figure 3.7 Cross-sections for excitations in CO_2 and N_2

a) Cross-sections for various excitations in CO_2 (after (54))

b) Cross-sections for excitation of vibrational levels in N_2 (after (66)). Peak cross-section is approximately $5 \cdot 10^{-16}$ cm^2 (54, 66). Peak cross-section of the n=1 state is approximately $2 \cdot 10^{-16}$ cm^2 (66)

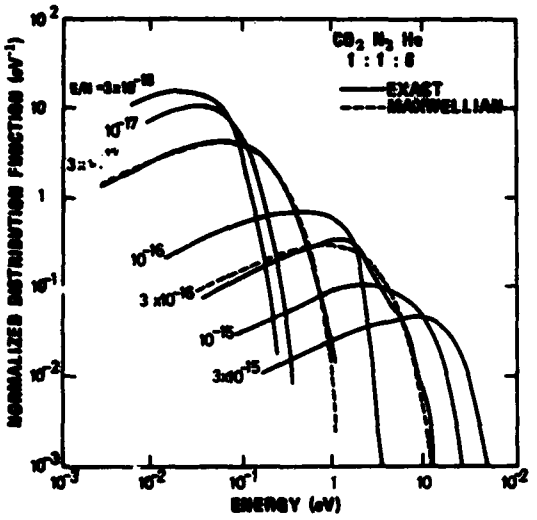

Figure 3.8 Derived electron distribution functions in the gas mixture $CO_2 : N_2 : He = 1:1:8$, for various values of E/N (Vcm^2)

Broken curves indicate a Maxwellian distribution, (from (54)).

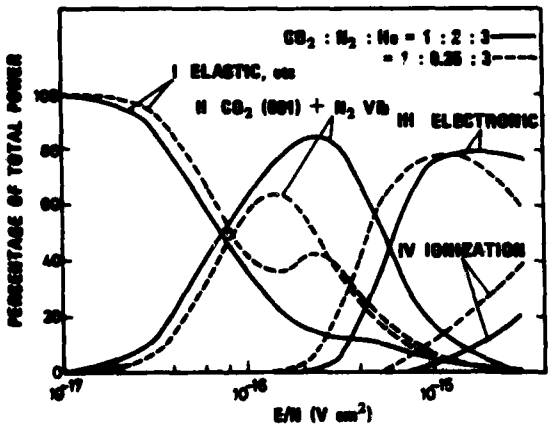

Figure 3.9 Percentage of power lost to (I) elastic collisions, rotational excitation of N_2 and excitation of bend and stretch modes of CO_2, (II) CO_2 $00^0 1$ level and the first eight vibrational levels of N_2, (III) electronic excitation, and (IV) ionization, (from (54))

The motion of the electrons in a discharge is dominated by a high random velocity with a much lower net drift velocity along the electric field. The complete energy or velocity distribution $f(\vec{r},\vec{v},t)$ can usually be expanded into two parts (55)

$$f(\vec{r},\vec{v},t) = f_0(\vec{r},v,t) + f_1(\vec{r},v,t)\cos\theta \qquad (3.2)$$

θ is the angle between the velocity vector $\vec{v}$ and the electric field vector $\vec{E}$. ($\vec{r}$ is the space position coordinate for which the distribution function is calculated.) f_0 is the isotropic part representing the distribution of the high random velocity. f_1 is the perturbation part which is due to the interaction with the electric field and represents the lower net drift velocity along the field. The two distributions interact with each other in the way that f_1 gains energy from the electric field and loses it to f_0 via collisions. f_0 gains its energy from f_1 and loses it in various excitation processes (vibrational excitation, ionization). Mathematically, even the equations of motion for f_0 and f_1 may be very complicated (55).

Because the inelastic collisions play an important role, the electron distribution function f_0 may become markedly non-Maxwellian. Lowke, Phelps and Irwin (54) have calculated distribution functions f_0 for various E/N and various $CO_2 : N_2 : He$ mixing ratios from the Boltzmann equation. They used altogether 31 different inelastic collision cross-sections which had been adjusted to give consistency between measured and calculated transport coefficients. Figure 3.8 shows electron distribution functions for a $CO_2 : N_2 : He$ mixing ratio of 1 : 1 : 8 for various E/N. By using these functions and the cross-sections in Figure 3.7, the percentage of power transferred to the various excitations may be calculated as a function of E/N. This is shown in Figure 3.9 for 1 : 2 : 3 and 1 : 0.25 : 3 $CO_2 : N_2 : He$ mixing ratios (from (54)).

The most important curves in Figure 3.9 are curves II, which show the excitation efficiency of the upper laser level and the N_2 vibrational levels. They show that theoretically more than 80% of the power of the electrons may go into excitation of these levels when the E/N ratio is $\approx 2 \cdot 10^{-16}$ Vcm^2 or E/P $\approx$ 5 kV/cm atm (P is the gas pressure at room temperature.) They also show the effect of reducing the N_2 content. It should be noted that the vibrational energy stored in N_2 does not contribute to the small signal gain. Thus, since theoretically the maximum of curve II is only reduced from $\approx$ 80% to $\approx$ 60% when the content of N_2 is reduced from 33% (the 1:2:3 mixture) to 6% (the 1 : 0.25 : 3 mixture), the small signal gain will be much higher in the 1 : 0.25 : 3 mixture. Experiments performed at multiatmospheric pressures show that an equal content of CO_2 and He is best for maximum small signal gain (49).

It was noted earlier in this section that a high content of He is necessary for a stable self-sustained discharge, especially at several atmospheres. The most pronounced effect of increasing the He content on curve II in Figure 3.9 is to decrease the E/N for maximum percentage power transfer. For a $CO_2 : N_2 :$ He mixing ratio of 1:1:8 curve II has a theoretical maximum of 74% at E/N = $1.2 \cdot 10^{-16}$ Vcm^2 or at E/P = 3 kV/cm atm (54).

3.4 The E/N ratio in a self-sustained glow discharge

The E/N ratio for which a discharge with no separate electron sources operates is determined by the electron production and loss terms. Depending on the pressure, the current density and gas medium, the dominant loss mechanism can be diffusion out of the plasma region, recombination with positive ions, or attachment to neutral molecules forming negative ions. At steady state, this can be written as (55)

$$\frac{dn}{dt} = D\nabla^2 n + n\nu_i - n\nu_a - \beta n^2 = 0 \qquad (3.3)$$

n – electron number density
D – diffusion coefficient
ν_i – one-step ionization coefficient
ν_a – attachment coefficient
β – electron–ion recombination coefficient

In the recombination term it is assumed that electron and positive-ion densities are equal. This may be a poor approximation if significant attachment occurs without subsequent rapid detachment.

For current densities normal for several high-pressure CO_2 lasers (50–52, 67, 68) the recombination term is negligibly small compared to the others. The electron densities are usually so high that ambipolar diffusion dominates free diffusion (55). (Ambipolar diffusion is much slower than free electron diffusion because when the charge densities are large, a space charge field is created between the electrons and ions which retard the electron diffusion (55).) Thus the ambipolar diffusion coefficient must be used in eq (3.3). The diffusion loss decreases with increasing gas pressure and increasing discharge diameter. In most dc excited high-pressure lasers the discharge diameter is so large that the diffusion loss may be neglected. The criterion for attachment loss to dominate diffusion loss has been calculated by Lowke, Phelps and Irwin (54) as

$$0.25\,(aE)^{-1/2} \ll R \qquad (3.4)$$

a — ν_a/v expressed in cm^{-1}

v — electron drift velocity (see Figure 3.12)

E — electric field amplitude in V/cm

R — radius of the discharge in cm

When attachment loss is dominating, the discharge will operate at an E/N for which the ionization and attachment coefficients are equal. E/N will be independent of the current density, the gas pressure and the discharge diameter. Lowke *et al* (54) and Denes and Lowke (68) have calculated the ionization, recombination and attachment coefficients versus E/N for various CO_2 laser gas mixtures, see Figure 3.10. Denes and Lowke (68) measured the E/N in discharges with these mixtures under conditions where the diffusion and recombination loss terms can be neglected. This is shown in Figure 3.11, which shows excellent agreement between theory and experiment.

It may be seen from a comparison between values of E/N for which efficient excitation of the upper laser level occurs that a self-sustained attachment loss dominated discharge operates at an E/N ratio which is good for excitation of a CO_2 laser. This is very fortunate for cw lasers and also for a long-pulse-duration laser since then no separate electron source is necessary. It may be seen that the E/N ratio in the self-sustained discharge is slightly above the value for most efficient pumping. For a $CO_2 : N_2 : He$ mixing ratio of 1:1:8 the ionization and attachment processes balance at

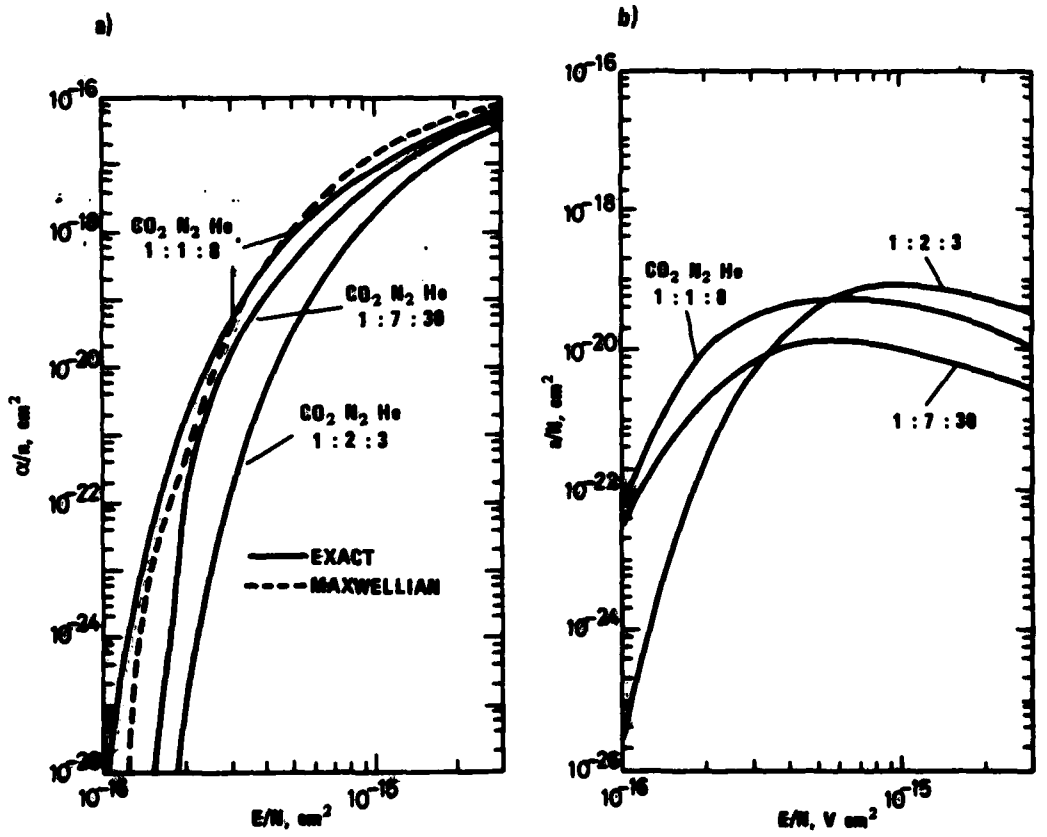

Figure 3.10 Calculated values of the ionization and attachment coefficients (after (54))

a) The ionization coefficient α/N for various gas mixtures. N is the neutral particle density. The relation between α and ν_i (equation (3.1)) is $\alpha = \nu_i/v$. v is the electron drift velocity (see Figure 3.12). Broken curve indicates values obtained assuming a Maxwellian distribution of the 1:1:8 mixture.

b) The attachment coefficient a/N for various gas mixtures.

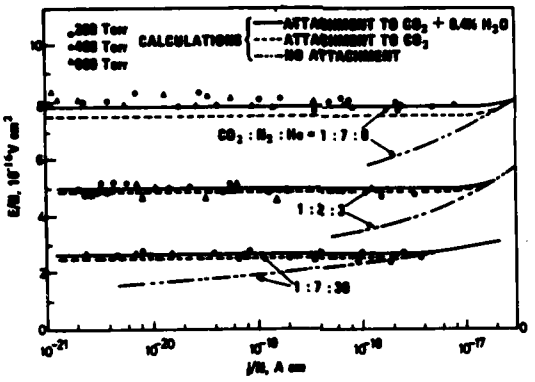

Figure 3.11 Measured and calculated V–I characteristics for three CO_2: N_2: He gas mixtures

Experimental values at three values of pressure are indicated by data points. Curves represent results of numerical calculations with varying conditions of attachment, (from (68)).

$E/N \approx 2.7 \cdot 10^{-16}$ Vcm^2, while maximum excitation of upper laser level occurs for $E/N = 1.2 \cdot 10^{-16}$ Vcm^2 (54). At this latter E/N the theoretical excitation efficiency is still about 50% (54). Increasing the He content results in a decrease in the E/N operating point, see Figure 3.11. However, it was pointed out in the preceding section that increasing the He content also results in a decrease in the E/N for which maximum pumping efficiency occurs. These effects approximately cancel each other (54).

In the rf excited CO_2 waveguide laser described in this report the content of CO_2 and N_2 has been much lower than in the mixtures shown in Figure 3.10. A $CO_2 : N_2 :$ He mixing ratio of 2 : 2: 96 has been used most of the time. Also the discharge dimensions in the waveguide are much smaller than in most dc-excited discharges. It is therefore not obvious that the discharge will be attachment-loss dominated. For a 1:1:8 mixing ratio the criterion (eq (3.4)) says that the waveguide discharge will be attachment-loss dominated when the attachment coefficients calculated by (54) are used. However, it is seen from Figure 3.10 that the attachment coefficient varies several orders of magnitude for only small variations of E/N. According to (54, 68) several processes may reduce the effective attachment coefficient. If the electron in the negative ion resulting from attachment is rapidly detached in collisions with other species, the attachment coefficient may be effectively zero (54). The dominating attachment process is usually assumed to be formation of negative CO_2 ions (68). Thus a pure He discharge may be diffusion or recombination-loss dominated.

The E/N ratio for which a diffusion-loss dominated discharge operates is determined by the N·R product (55). (N is the neutral particle density and R is the discharge radius.) Thus while in an attachment-dominated discharge the E/N ratio will be independent of pressure, discharge current density and the discharge diameter, the E/N ratio in a diffusion-dominated discharge will decrease with increasing gas pressure for fixed discharge diameter. E/N will increase with decreasing discharge diameter for a fixed gas pressure. This allows manipulation of the E/N ratio towards an E/N ratio for maximum excitation of the upper laser level.

In a recombination-loss dominated discharge the electron loss increases rapidly with the current density. In such a discharge the E/N ratio will increase with the current density. This was shown in Figure 3.11. Thus, such a discharge also permits manipulation with the E/N ratio.

In this report this subject has not been analyzed quantitatively any further. Calculation of the various ionization and loss coefficients and the E/N ratio for maximum pumping efficiency for the gas mixtures that have been used in these experiments is a large project in itself. Also, as has been pointed out, the electron decay processes may not easily be well specified quantitatively.

In the choice of He content, discharge dimensions and current density, several other considerations than those described above must also be taken. These will be discussed in the following sections.

3.5 Glow to arc transitions

Arc discharges differ from glow discharges in that arcs are characterized by much higher electron densities and much lower E/N ratios. They are often restricted to narrow strings, which have a very high electric conductivity and can carry large currents. It should be apparent from the preceding discussion that arcs are not effective in pumping of CO_2 laser gas mixtures.

Glow discharges tend to "collapse" into arc discharges when either the current density or the gas pressure or both are increased. Glow-to-arc transitions are a limiting factor in both high-power and high-pressure lasers. Causes of arcing have been studied both theoretically (69) and experimentally (70).

Nighan and Wiegand (69) have studied theoretically the causes of arcing in self-sustained cw CO_2 laser discharges. Attachment and recombination controlled discharges were considered. Their analysis should be equally well applicable to a self-sustained long duration pulsed high pressure glow discharge since the glow-to-arc transitions may take place on a time-scale much shorter than typical pulse lengths. Here only the essential processes leading to formation of arcs will be discussed (primarily after (69)).

In the absence of pressure fluctuations, a local increase in gas temperature leads to a decrease in gas density. This leads to an increase in E/N and consequently to an increase in both electron temperature and ionization rate (Figure 3.10). The increase in ionization rate leads to a large increase in electron density. A large local increase in electron density causes additional gas heating through elastic collisions and strongly affects vibrational excitation of the molecules. Increased relaxation of vibrational energy also leads to an increase in gas temperature. Thus there are two primary positive feedback mechanisms to the original local increase in temperature, namely enhanced gas heating through vibrational relaxation and through elastic collisions. Such a positive feedback may lead to a rapid local increase in temperature and current, and the subsequent formation of a bright narrow string arc discharge. The high current usually results in a drop in the voltage across the discharge. This terminates the glow discharge, and all the electrical power goes into the arc.

The formation of an arc may be inhibited if the gas has high enough thermal conductivity to carry away the local concentration of heat. Helium has very good thermal conductivity, and this is one of the important effects of He in a CO_2 laser gas.

Boundary effects and other external parameters also play an important role in the formation of stable arc-free glow discharges. Small irregularities at the electrodes cause local variations in the electric field which may lead to local heating and the subsequent formation of an arc. In a gas discharge between parallel plates it is therefore important that the electrode surfaces are smooth and even and that they to a very good accuracy are parallel.

3.6 The rf discharge

The study of alternating current (ac) discharges is naturally divided into two parts: the study of the gas breakdown mechanism and the study of a stationary discharge. General treatment of ac discharges are found in several textbooks on plasmas and gas discharges (71–75). Gänger (76) reported in 1943 measurements of rf breakdown at

100–150 kHz in air, N_2 and Difluordiclormethan at up to 40 atm. Some information is found on characteristics of rf discharges in air (77, 78), in argon (79), and in He and hydrogen (80, 81) at up to 1 atm. Schmieder considers theoretically gas breakdown in combined laser and microwave fields (82). None of the reports on rf-excited gas lasers above 100 torr have been found to cover in detail the characteristics of the discharge. Useful information about a model of a stationary rf-discharge between cylindrical or parallel plate electrodes is found in (83–85). In (85) is considered the application of rf discharge in a sputtering plant, where the operating pressure is in the millitorr range. A similar division of the discharge in dark and luminous zones to that observed in (83–85) is observed in the experiments described in this report (Chapter 6).

Important quantities in an rf discharge are the electron/neutral particle collision frequency ν_m and the oscillation frequency ν of the discharge excitation field. In He, $\nu_m = 1.75 \cdot 10^{12} \cdot P\ (s^{-1})$ where P is the gas pressure in atm (55, 86), while in this work an excitation field frequency $\nu = 4 \cdot 10^7\ s^{-1}$ has been used. Thus the electrons collide several times during an rf period.

In this section (3.6) will first be discussed general conditions for establishing a radio-frequency glow discharge between parallel plate electrodes. Then the time variation of the electron number density and the electron energy distribution in such a discharge will be discussed. The electron number density is a central parameter for the stability and the electrical impedance of the discharge. Based on the previously described CO_2 excitation process in a dc discharge, a discussion of the electron energy distribution in the rf discharge will give an insight into the CO_2 excitation process in the rf discharge. The characteristics of the stationary discharge are discussed based on the three-zone model (83–85). The model forms a basis for calculation of the electric circuit equivalent of the discharge and for a discussion of the stability of the discharge. The problem of coupling the rf power into the discharge will be discussed in general terms. It will be considered more quantitatively in Chapter 5. Finally, the plasma frequency and the expressions for the relative dielectric constant of the discharge will be discussed.

3.6.1 rf discharge between parallel plate electrodes

The general requirement for establishing a stable rf glow discharge between parallel plates is that the electron displacement peak-to-peak is smaller than the electrode separation (71–75). In such a discharge most of the electrons are able to oscillate freely without colliding with the electrodes. Collisions with the electrodes in general represent an electron loss term. If the electron displacement were larger than the electrode separation, the discharge would behave more like a dc discharge.

In an oscillating electric field $E = E_0 \sin \omega t$ the electron displacement ℓ peak-to-peak would be given by

$$\ell = \frac{2 \mu E_0}{\omega} \tag{3.5}$$

if the electron mobility μ were independent of the electric field strength E. When the electron-neutral particle collision frequency ν_m is much larger than the oscillation frequency ω of the electric field, the mobility μ will be given by (55)

$$\mu = \frac{e}{m \nu_m} \tag{3.6}$$

(e and m are the electron charge and mass, respectively). (Eq (3.6) in general requires that ν_m is independent of the electron velocity v. In He this is true to a good approximation (55, 86).) The collision frequency ν_m is proportional to the neutral

particle density N (or to the gas pressure P). This implies that for a fixed frequency the electron displacement

$$\ell \sim \frac{E}{N} \tag{3.7}$$

In general the E/N ratio required to break down the gas to a plasma is larger than the E/N required to sustain the discharge both for dc and rf discharges (55, 71–75). For rf discharges this is usually because before gas breakdown the main electron loss is by free diffusion which is much larger than ambipolar diffusion loss (55, 71–75). When the electrodes in contact with the gas are of metal, the electrons reaching the electrodes are usually lost from the gas. Thus, for striking of a discharge between metal electrodes it is important that the distance between metal electrodes is larger than the electron displacement at the E/N required for breakdown. When the metal electrodes are covered with a dielectricum the electrons reaching the dielectricum are not necessarily lost. Experimentally in this work it is observed that both striking and sustaining a stable glow discharge is much easier when electrodes covered with a dielectricum are used. Thus, in this case the basic requirement for establishment of a glow discharge is probably that the electron displacement is shorter than the electrode separation for the E/N required to sustain the discharge.

In a recombination-loss dominated discharge the E/N ratio after breakdown is independent of the gas pressure. This implies that also the electron displacement amplitude will be independent of the pressure. In a diffusion-loss dominated discharge E/N will decrease with increasing gas pressure for fixed discharge dimension. In the experiments described in this work, the E_0/N ratio after gas breakdown has usually been below $3 \cdot 10^{-16}$ Vcm^2 (Chapter 6). Using the value for He (55, 86)

$$\nu_m = 1.75 \cdot 10^{12} \cdot P \ (s^{-1} \ atm^{-1}) \tag{3.8}$$

this E_0/N gives ℓ = 0.6 mm at 40 MHz.

The simple relations of eq (3.5) and (3.6) do not hold over the large range of E/N encountered in a high pressure rf discharge in a CO_2, N_2 and He gas mixture. In He at low E/N the drift velocity is larger than given by eqs (3.6) and (3.8). Lowke, Phelps and Irwin (54) have calculated the electron drift velocity versus E/N for several $CO_2 : N_2 : He$ mixing ratios. The drift velocities are shown in Figure 3.12. It is seen that the actual electron displacement amplitude must be calculated numerically. At $E_0/N = 3 \cdot 10^{-16}$ Vcm^2 the drift velocity v from Figure 3.12 is $66.7 \cdot 10^5$ cm/s, while v = $75 \cdot 10^5$ cm/s results from eqs (3.6) and (3.8) at the same E_0/N. These two values of the drift velocity are very close. One should therefore be able to draw the conclusion that the electron displacement will be smaller than the electrode separation for electrode separations larger than about half a millimeter at 40 MHz for $E_0/N = 3 \cdot 10^{-16}$ Vcm^2 or E_0/P = 7.5 kV/cm atm.

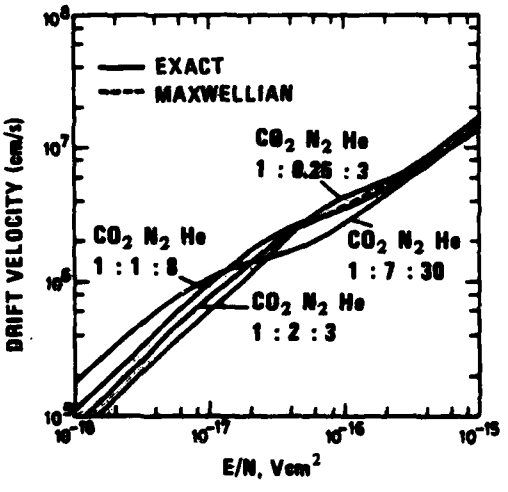

Figure 3.12 Calculated drift velocities of electrons for various gas mixtures of CO_2, N_2 and He (from (54))

Apart from the above-mentioned minimum electrode separation and the possibility to manipulate the E/N ratio mentioned in the previous chapter for a diffusion loss dominated discharge, several other factors determine the optimum electrode separation. The discharge shall be used to amplify an optical field, which must be able to propagate between the electrodes. As will be pointed out in the next chapter, if the electrode separation is too small (typically less than 1 mm) the light propagation losses may be significant and the design of the reflectors in the optical resonator may be more difficult.

The experiments in this work have shown that the electrode separation should not be too large. At a 2 mm electrode separation the discharge tended to be confined to a small volume at the middle of the electrodes, see Chapter 6.

The optical gain is determined by the pump power density. In order to get the maximum obtainable small signal gain with a given pump power, the discharge cross-section should be as small as possible.

Finally, the larger the electrode separation, the larger must be the voltage across the electrodes in order to maintain the right E/N. High voltages, of the order of tens of kilovolts, may cause practical problems like breakdown in the external circuitry.

3.6.2 Time variation of the electron number density and the energy distribution function

Considering there is a given electron number density in the discharge when the oscillating electric field strength is at its maximum value, the question arises: what happens to the electron density n when the electric field strength crosses the zero value? It was shown in Figure 3.10 that when the electric field goes towards zero the ionization and attachment coefficients rapidly decrease several orders of magnitude. The ionization coefficient decreases most rapidly. The time rate of change of n will either be given by attachment, diffusion or recombination loss. It is assumed that the largest possible loss rate which may be taken into consideration is the attachment loss at 10 atm at the E/N ratio for which the attachment and ionization coefficients are equal. Without the ionization term the electron density n will decay according to (54, 55) (eq (3.3) (3.4))

$$\frac{dn}{dt} = -n \left(\frac{a}{N}\right) Nv \qquad (3.9)$$

a/N – the attachment coefficient shown in Figure 3.10

N – neutral particle number density

v – electron drift velocity

The drift velocity versus E/N was shown in Figure 3.12 (from (54)). For the CO_2 : N_2 : He gas mixing ratio of 1:1:8 the ionization and attachment coefficients are equal for E/N ~ $2.7 \cdot 10^{-16}$ Vcm^2 (54). At this E/N, a/N ≈ $2.5 \cdot 10^{-20}$ cm^2 and v ≈ $6 \cdot 10^6$ cm/s. At 10 atm gas pressure at room temperature this gives

$$\frac{dn}{dt} = -\frac{n}{27} (ns^{-1}) \qquad (3.10)$$

This is an exponential decay with 27 ns decay time constant. In the discharge the net electron loss rate will always be smaller than given by this time constant. At 40 MHz the electric field strength goes from its rms value to zero within 3 ns. It is thus evident (see the discussion in section 3.4) that the electron density will not vary appreciably within the rf period. It will settle to a value where the electron production rate averaged over an rf period balances the average loss.

The electron energy relaxation rate due to elastic collisions is given by the electron/neutral-particle collision frequency times twice the ratio of the electron mass to the neutral-particle mass (55). When inelastic collisions play an important role the relaxation rate can be considerably faster (65), since the electron energy loss per inelastic collision is much larger than per elastic collision. Even the electron energy relaxation rate due to elastic collisions is faster than the frequency of the oscillating electric field at multiatmospheric pressures. Thus the electron energy distribution will vary according to the instantaneous E/N during the rf period. The averaged excitation efficiency versus E_0/N has not been calculated in this work since curves showing the upper laser level excitation versus E/N for the gas mixture used in these experiments have not been available. Since efficient excitation occurs over a rather broad E/N range, see Figure 3.9, it may be expected that if the rms value of the E/N ratio is close to the value for which most efficient excitation occurs, the pumping efficiency of the rf discharge is reasonably good. This will be discussed further in section 3.7.

The question may also be asked: How fast do the electron and ion number densities decay after the discharge excitation power is turned off. The attachment and recombination coefficients vary with the electric field strength, gas pressure and gas mixture (54, 55, 119, 120). According to Figure 3.10 the attachment coefficient may be neglected when the discharge excitation field is turned off. According to (54, 119) the recombination coefficient also varies with the electron number density. No values relevant for the conditions of interest for this work have been found. The electron loss by diffusion is expressed by the diffusion coefficient. Its value depends on whether the diffusion is free or ambipolar, and on the electron and ion temperatures. The free diffusion coefficient D_e is given by (55)

$$D_e = \frac{k T_e}{m \nu_m} \tag{3.11}$$

if the electron energy distribution is Maxwellian.

k – Boltzmann constant

T_e – electron temperature

m – electron mass

ν_m – electron/neutral particle collision frequency

Since the electron and ion temperatures adjust on a time scale determined by the collision frequency between these species and neutral particles, it seems reasonable to assume that the electron and ion temperatures will be equal to the gas kinetic temperature after the excitation field has been turned off. According to (55) the diffusion will be ambipolar for electron and ion densities down to several orders of magnitude lower than the densities during the discharge. The ambipolar diffusion coefficient also depends on what is the dominating ion. In (54) the ambipolar diffusion coefficient is taken to be 1/50 of the free diffusion coefficient when the electron and ion temperatures are equal. Assuming these temperatures to be equal to the gas kinetic temperature, the electron decay time constant due to free diffusion will be about 100 μs at 1 atm, proportional to the gas pressure, and the ambipolar diffusion decay time constant will be 50 times longer. Thus, if the electron loss due to attachment and recombination can be neglected compared to diffusion after the discharge excitation has been turned off, one should be able to draw the conclusion that some ionization will remain in the gas volume from one discharge pulse to the next for the pulse repetition rates used in the experiments described in this report. Experimentally it has been observed in this work that the pulses are influenced by the preceding pulses. However, this subject has not been further analyzed quantitatively from a theoretical point of view in this report.

3.6.3 The three-zone model

A discharge between parallel plate electrodes normally appears with a bright luminous zone in the middle and dark space regions near the electrodes. This is illustrated in Figure 3.13. This is the case both when pure metal electrodes and electrodes covered with a dielectricum are used. The divisions in dark and bright zones are considered in (83–85) for gas pressures several orders of magnitude lower than in the experiments described in this work. In this work the same phenomenon is observed. Thus the mechanism leading to this formation of zones seems to be independent of pressure. The phenomenon can be explained by the following.

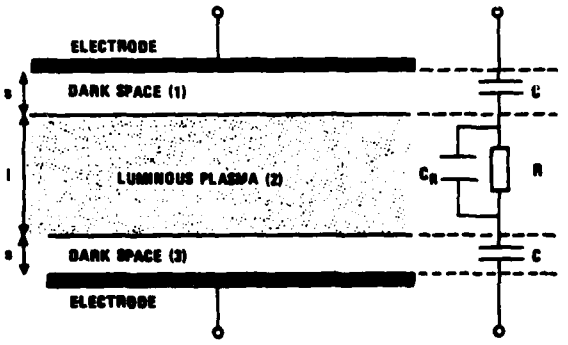

Figure 3.13 The three-zone-model
Cross-section of the discharge and electrical equivalent circuit.

The voltage-current characteristic of a plasma is very nonlinear, due to the different masses of the electrons and the ions. If the electron and positive ion densities are equal near the electrode surface, the electron current towards the electrode when the electrode is positive will be much larger than the positive ion current towards the same electrode when it is negative. This is due to the much smaller mass of the electrons, and is part of the Langmuir-probe characteristics (71–73). At steady state no net current averaged over one rf period will flow to the electrodes. Thus the surface of the electrodes will assume a negative charge with respect to the plasma to repel the electrons. The magnitude of the electrode surface charge will adjust so that the ion current during the negative swing of the oscillating voltage just equals the electron current during the positive swing. In the plasma near the electrode there will be a net positive space charge due to the negative surface charge. This positive space charge will look dark, because very few electrons make collisions there.

Electrically the discharge will look like what is illustrated schematically in Figure 3.13. Close to the electrodes are the dark space regions and in the middle is the plasma with high electron number density. The current density j flowing between the electrodes in general consists of a conduction current and a displacement current. The conduction current in the dark space regions can be disregarded in comparison with the displacement current. Thus electrically these regions will act as a capacitor. In the plasma region there is a high electron density n. The current density j_2 in this region will be

$$j_2 = \left[\frac{e^2}{m}\frac{n}{i\omega+\nu_m} + i\omega\epsilon\right] E_0 \exp(i\omega t) \qquad (3.12)$$

Here

- i – $\sqrt{-1}$
- e – electron charge
- m – electron mass
- n – electron number density
- ω – angular frequency of the applied electric field E
- ν_m – electron/neutral-particle collision frequency
- ϵ – permittivity of the plasma region, see section 3.6.6

Since $\nu_m >> \omega$ the plasma will behave like a pure resistor in parallel with a capacitor. The electrical impedance Z of the whole discharge will be

$$Z = 2\frac{1}{i\omega\epsilon_1}\frac{s}{A} + \left(\frac{e^2 n}{m\nu_m} + i\omega\epsilon_2\right)^{-1}\frac{\ell}{A} \qquad (3.13)$$

$\epsilon_{1,2}$ – permittivity of dark-space and plasma region respectively

s – thickness of the dark-space region

ℓ – thickness of the plasma

A – electrode area

3.6.4 Impedance matching

For rf power to be coupled into a load, the impedance of the load must be equal to the characteristic impedance of the power source. If it is not, part of the power incident on the load will be reflected. Therefore, in general, an impedance matching circuit is needed between the load and the power source to transform the impedance of the load to the characteristic impedance of the source. Equivalently, the impedance matching circuit transforms the voltage and current from the source to values suitable for the load impedance. The situation is illustrated qualitatively in Figure 3.14b.

When the load is a gas, the load resistance will be infinitely large before the gas is broken down to a plasma. After breakdown the resistance will vary with the electron number density (eq (3.13)) which is an increasing function of the input power. It will also depend on the gas pressure and gas mixture.

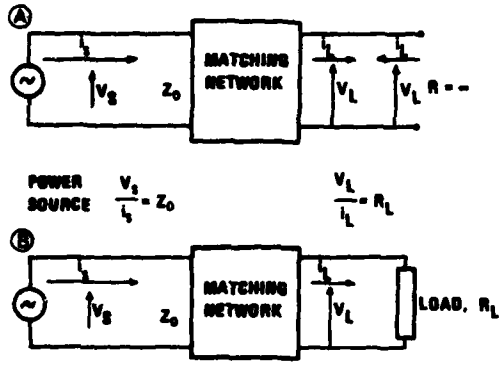

Figure 3.14 Schematic of the impedance matching problem

a) Before gas breakdown, b) After gas breakdown

Figure 3.14 illustrates qualitatively what happens when the impedance matching circuit is adjusted to match the impedance of a discharge to the source impedance. The circuit must be adjusted for the specific gas pressure, gas mixture and for the power level incident on the electrodes. Before the gas is broken down to a plasma there will be an infinitely large impedance at the point where the load should be. This is illustrated in Figure 3.14a. Thus at this point the incident power will be totally reflected. As illustrated in Figure 3.14a the reflected voltage will have the same phase as the incident voltage at the place where the load should be. Thus the total voltage may be up to twice as large across the discharge gap before gas breakdown as it will be after gas breakdown. Experiments (Chapter 6) have shown that the voltage required to break down the gas to a plasma in general is less than twice the plasma sustaining voltage. Thus, when the impedance matching network is adjusted to couple a certain amount of input rf power into the discharge, the necessary overvoltage required for gas breakdown is automatically provided. Consequently, a separate preionization source is not necessary.

Since the discharge impedance varies with input power, gas mixture and gas pressure, the impedance matching circuit should be tunable. The realization of such a circuit is discussed in Chapter 5.

3.6.5 Discharge stability

The electron number density in the plasma will increase with increasing input power. Thus the resistivity of the plasma, which is inversely proportional to the electron number density, will decrease with increasing input power, see equation (3.13). In general, such a negative differential impedance character leads to discharge instabilities. This is because lower resistance gives larger current and larger power dissipation, which in turn give an even lower resistance, if the voltage is kept approximately constant. Since the load resistivity varies with the input power, the voltage and current must in general be stabilized by external circuitry. The positive feedback to a local increase in electron number density also leads to formation of arcs as discussed in section 3.5. In rf discharges it is observed that discharge instabilities do not so easily develop as in dc discharges. This may be explained by the following.

For all the incident power to be coupled into a load, the impedance of the load must be equal to the internal impedance of the power source. This was discussed in the preceding section. Under impedance mismatch conditions, part of the rf power incident on the load will be reflected back to the power source. Thus, a change in the load impedance away from a perfect match condition will result in less power coupled into the load. Also power reflected back into the rf power source usually will reduce the power delivered by the source. To inhibit possible damage to the source caused by the reflected power, a circulator may be used between the source and the load to couple the power reflected from the discharge into a dummy load. In this case the source will operate with a constant output power independent of the load. In all cases, when a certain discharge impedance is matched to the internal impedance of the source, the power coupled into the discharge will be reduced when the discharge impedance changes. The reduction depends on the impedance-matching circuit and on the source and the way in which it is connected to the discharge.

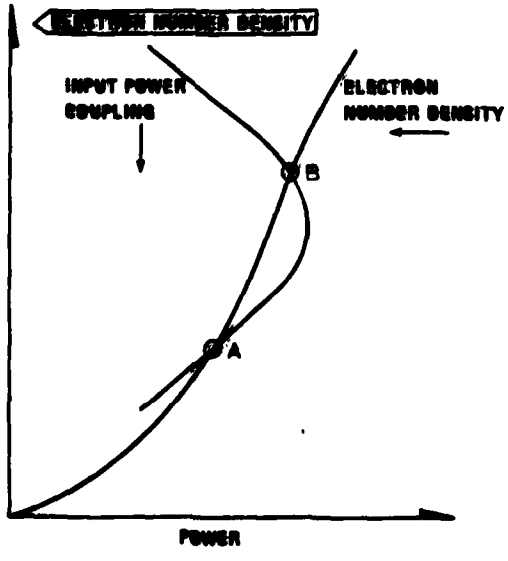

Figure 3.15 Operating point of rf discharge
The electron number density is an increasing function of the input power. The input power coupling varies with variation in the electron number density qualitatively as shown. Stable point of operation is point B.

The situation is illustrated qualitatively in Figure 3.15. The electron number density is an increasing function of the power coupled into the discharge, and the power input coupling varies with variation in the electron number density, as discussed above. A stability analysis shows that the stable point of operation is point B: If the electron number density accidentally increases from point B, the power coupled into the discharge will be reduced. This will in turn reduce the electron number density. In the same way, a small decrease in the electron number density will result in increased power input coupling, which will produce more electrons. The same analysis applied at apoint A will show that a small perturbation in the

electron number density will drive the electron density away from the value at that point.

It should be noted that when the electron number density becomes sufficiently large, the impedance of the plasma region can become much smaller than the impedance of the dark space regions, see Figure 3.13. Thus, for such high electron number densities the overall discharge impedance will be reactive and approximately constant, independent of variation in the input power. It will be so even when pure metal electrodes are used because of the dark space regions. This is probably why rf discharges have been said to have a "positive impedance character" (1). According to the above discussion this so-called "positive impedance character" is not necessary for obtaining a stable point of operation of the rf discharge. Experimentally it is observed that a stable point of operation is obtained also for low input power levels where the resistivity of the plasma region is much larger than the impedance of the capacities in series with the plasma. Under these circumstances the overall discharge impedance can be approximately inversely proportional to the input power.

The variation in power coupled into the discharge is often not a very sharp function of the electron number density. Experiments have shown that if the glow discharge collapses into an arc, very little power is needed to sustain the arc discharge. It was pointed out in the introduction that the subsequent reversals of the voltage polarity in the rf discharge aid in reducing the tendency to arc formation. In addition, this tendency is reduced by the capacitive ballasting of the discharge. Because of the induced capacities at the dark space regions the plasma will be capacitively ballasted even when pure metal electrodes are used. Because of this capacitive ballasting an increase in current density in the plasma region will result in an increased voltage across the capacitor, and when the capacitive ballasting is large enough, the power dissipated in the plasma will be reduced. This will reduce the tendency to arc formation. Mathematically this may be expressed by the average power P dissipated in the plasma, which is given by

$$P = \frac{1}{2} \frac{R V_0}{R^2 + (2X)^2} \tag{3.14}$$

R – resistivity of the plasma

V_0 – voltage amplitude across the electrodes, see Figure 3.13

X – capacitive impedance, $X = 1/\omega c$, where ω is the angular frequency of the oscillating voltage and c is the capacity between the electrode and the plasma

In equation (3.14) it is assumed that $R \ll X_R$, where X_R is the impedance of the capacity in parallel with R. The requirement for stability for constant voltage is

$$\frac{dP}{dR} > 0 \tag{3.15}$$

which is satisfied for $2X > R$. It should be noted that arc-discharges appear like narrow strings with high current dentities. Thus, the simple discharge model and stability analysis described above is not strictly correct because edge-effects have been neglected. Such effects will probably be dominant when arc discharges are concerned. Qualitatively the analysis is assumed to be relevant in the description of the stabilizing effect of capacitors in series with the plasma region. Experimentally it has been observed in this work that the larger the capacitive ballasting of the electrodes, the less is the tendency for arcs to develop in the discharge.

Experiments have shown that when pure metal electrodes are used and when the input power or the gas pressure or both are increased, even the rf glow discharge will eventually collapse into an arc. The dark space region "capacitor" has then been

broken down by the high field strength, and the arcs constitute narrow strings extending the full gap between the electrodes. Because of this it has been necessary in the experiments described in this report to use dielectric ribbons on the metal electrodes. These ribbons stabilize the discharge in the same way as the dark space region capacities. Several dielectric materials have sufficiently high breakdown-field strength to avoid dielectric breakdown under the conditions relevant for this work. The capacitive ballasting of the discharge can be varied by choosing dielectric materials with various thicknesses and various dielectric constants.

It should be noted that the maximum discharge current density, and consequently the maximum power density that can be coupled into the discharge, is limited by the dielectric strength of the dielectric material which is used on the electrodes. This has been considered by Ishchenko *et al* (121) and by Christensen (122) and Christensen *et al* (4). In (122)* dielectric properties of several dielectrics of interest are tabulated. The limitation in the maximum power dissipation due to the dielectric is first of all of importance when excitation with a single pulse through a dielectric is concerned. In the experiments described in this report this limitation has not been a problem.

3.6.6 The skin depth

Skin-depth effects can limit the maximum power that can be coupled into the discharge volume. In a conductor the current will propagate in a surface layer with a depth δ defining the distance from the surface at which the current density has diminished to 1/e of its value at the surface. The skin depth δ is given by (123)

$$\delta = \left(\frac{2}{\sigma\mu\omega}\right)^{1/2} \tag{3.16}$$

σ – conductivity of the conductor

μ – permeability of the conductor

ω – angular frequency of the current

When the conductor is a plasma, the conductivity σ will be given by (55) (eq (3.12))

$$\sigma = \frac{ne^2}{m(\nu_m + j\omega)} \tag{3.17}$$

In the glow discharges the electron densities are usually below 10^{14} cm^{-3} (55). Assuming $\mu = \mu_0$ = permeability of vacuum, $n_e = 10^{14}$ cm^{-3}, $\nu_m = 1.75 \cdot 10^{12}$ sec^{-1} atm^{-1} (55, 86) the skin depth will be $\delta \approx 20$ cm at 40 MHz and 10 atm gas pressure. Thus, the skin-depth limitation has not been a problem at frequencies as low as have been used in this work. It may be of concern when 1 MW magnetrons at 10 GHz are used to excite the discharge (45, 124).

3.6.7 Plasma frequency

The plasma frequency is an important quantity in a gas discharge.

---

*See also Table 5.1

The plasma frequency ω_p is defined as (55)

$$\omega_p^2 = \frac{ne^2}{m\epsilon_0} \tag{3.18}$$

ϵ_0 is the permittivity of vacuum.

In a discharge where collisions between electrons and neutral particles can be neglected, the plasma frequency is the frequency above which an electromagnetic wave can propagate freely through the plasma. The relative dielectric constant ϵ_r will be

$$\epsilon_r = 1 - \frac{\omega_p^2}{\omega^2} \tag{3.19}$$

where ω is the angular frequency of the electromagnetic wave. The index of refraction n of the medium is

$$n = \sqrt{\epsilon_r} \tag{3.20}$$

When collisions between electrons and neutral particles must be taken into consideration, the relative dielectric constant is modified to (55)

$$\epsilon_r = 1 - \frac{\omega_p^2}{\omega^2} \frac{1}{1 - j\frac{\nu_m}{\omega}} \equiv 1 - j\frac{\sigma}{\omega\epsilon_0} \tag{3.21}$$

When ω is the angular frequency of the discharge excitation field, $\omega << \nu_m$ is usually the case, and ϵ_r is to a good approximation given by

$$\epsilon_r = 1 - \frac{\omega_p^2}{\nu_m^2} - j\frac{\omega_p^2}{\omega\nu_m} \tag{3.22}$$

The last term in eq (3.22) is much larger than the second term at 40 MHz. At 10 atm gas pressure the last term becomes unity for $n = 1.4 \cdot 10^{12}$ cm^{-3}.

When ω is the angular frequency of the CO_2 radiation field, ω may become comparable to the electron/neutral-particle collision frequency ν_m at high gas pressures. At 10 atm gas pressure $\nu_m/\omega \approx 0.1$. Thus, at very high pressures and for very high electron number densities, the plasma may attenuate the laser radiation field. In this work this has not been considered to be a problem.

In the experiments described in this report, the following relations in general hold

$$\omega_{rf} < \omega_p < \nu_m < \omega_{CO_2} \tag{3.23}$$

where

ω_{rf} – radiofrequency discharge excitation frequency
ω_p – plasma frequency
ν_m – electron/neutral-particle collision frequency
ω_{CO_2} – frequency of laser radiation field

3.7 rf power requirements

The population inversion in a laser active medium is determined by the energy that goes into excitation of the upper laser level. The time for which pump power can be usefully integrated to give a population inversion is determined by the upper laser level lifetime. This lifetime is inversely proportional to the gas pressure. In a CO_2

laser at 10 atm it is approximately 3 μs, see section 3.2.2 and Chapter 6. When the laser transition is pressure broadened, the peak small signal gain at line centre for a fixed population inversion is also inversely proportional to the gas pressure. Thus the required pump power for a fixed small signal gain at line centre is proportional to the gas pressure squared.

For a fixed pump rate λ of the upper laser level and a fixed upper laser level decay-rate $\gamma = \tau^{-1}$, the population inversion ΔN will vary as

$$\Delta N = \lambda\tau(1 - e^{-t/\tau}) \tag{3.24}$$

The pumping is assumed to be turned on at time t=0 and the population of the lower laser level is assumed to be negligible.

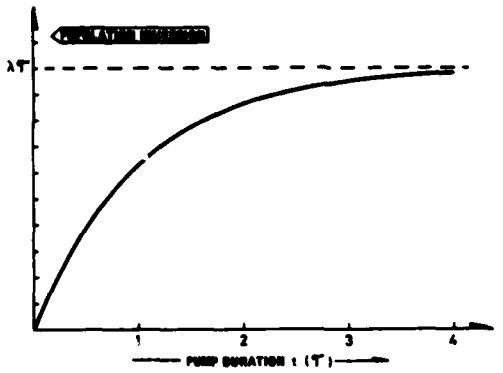

Figure 3.16 Population inversion ΔN versus time for an upper laser level pump rate λ and decay time constant τ, according to equation (3.24)

Pumping is assumed to be turned on at t=0. The population of the lower laser level is assumed to be negligible. The time is expressed in units of τ.

This curve is shown in Figure 3.16. It may be seen that the pump duration t should be approximately t = 2–3 τ to get the maximum obtainable population λ/γ or $\lambda\tau$ of the upper laser level.

In CO_2 at pressures above approximately 5 atm the gain curves from neighbouring transitions begin to overlap significantly enough to contribute to the gain at a line centre frequency. Thus the small signal gain at a line centre will not decrease so fast with increasing gas pressure above this pressure for a fixed pump power. The contribution from sequence-bands and hot-bands (see section 3.1) may also contribute to the gain at above 5 atm gas pressure. Thus the required pump power for a fixed gain will not increase with the pressure as fast as the pressure squared dependence.

Figure 3.17 Theoretical and experimental peak small signal gain for the R(16) 10.4 μm transition versus gas pressure (from (50))

The CO_2:N_2:He gas mixing ratio is 1:1:18, and the pump energy density is 32 J/l atm. The bottom dashed curve represents a model prediction for the gain including regular plus hot band lines. The solid curve includes the additional contribution from sequence bands. The top dashed curve is the final gain prediction corrected for non-Lorentzian line overlap effects. The final theoretical gain prediction was normalized to the 4 atm experimental gain. Experimental points are shown by dots.

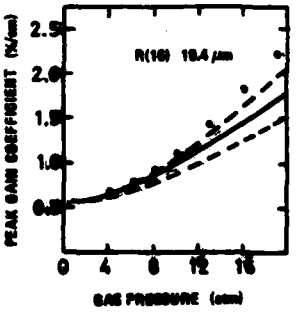

The peak small signal gain versus gas pressure has been calculated and measured at line centre frequencies by Taylor *et al* (50) for fixed pump energies per liter-atm. One of their curves is shown in Figure 3.17. The effect of line overlap and hot-bands and sequence-band transitions is clearly seen for pressures above 3–4 atm.

In Figure 3.17 the calculated gain was fitted to the experimentally measured gain at 4 atm in a UV-preionized pulsed dc-discharge. As was pointed out in section 3.4, a self-sustained glow discharge operates at a higher E/N ratio than is theoretically found to be optimum for most efficient pumping of the upper laser level. This is the case for the discharge in the work of Taylor *et al*, where the E/N in the 1:1:8 and 1:1:18 mixtures of $CO_2 : N_2 : He$ were 3.1 and $2.5 \cdot 10^{-16}$ Vcm^2 respectively. Theoretically the E/N for most efficient pumping is $1.2 \cdot 10^{-16}$ Vcm^2 for the 1:1:8 mixture (54). Wood *et al* (118) have measured the gain in a transversely excited waveguide laser where they could control the E/N ratio with a special preionization scheme. Their results are comparable to measurements of gain in an electron-beam controlled discharge. This is shown in Figure 3.18. It is seen that the gain per pump energy density is larger than in the discharge of Taylor *et al*.

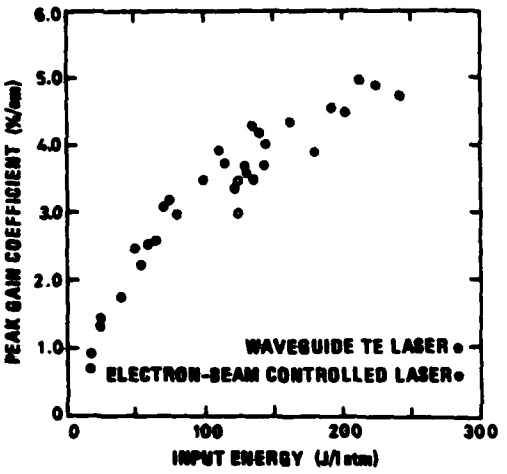

Figure 3.18 Peak gain coefficient (%/cm) vs input energy (J/l atm) for a CO_2 waveguide TE amplifier at 150 torr (solid points) and for CO_2 electron-beam-controlled discharge amplifier at 760 torr (open points) (after (118)).

It is not obvious what the gain will be in an rf discharge. As was pointed out in section 3.6.2 the excitation of the upper laser level will vary with the variation in E/N within the rf period. E/N will probably pass through the value for most efficient upper laser level excitation within the rf period, but it will also pass through values where most energy is lost to other processes. In the dc discharges a significant portion of the power put into the discharge will go into the cathode fall region (97, 118). This will not be the case in the rf discharge, where there is no cathode fall region. Some of the input rf power will obviously be lost in the dark space regions, but this is considered to be a negligibly small loss. Most of the input power will be dissipated in the plasma region, which is not filling the full gap between the electrodes because of the dark space regions. Finally, it is not obvious what sort of gas pressure dependence of the gain one can calculate with. The line overlap effect depends primarily on the gas pressure alone, while the contribution from sequence-bands and hot-bands depends on the excitation of the higher vibrational levels in the ν_3-mode, see sections 3.1 – 3.2. The population of these levels depends on the vibrational temperature T_3 of the ν_3-mode, which is determined by the input energy density per molecule. In this work the input energy density has typically been around 7–9 J/l atm at 10 atm, which is a very low value compared to the input energy densities used by Taylor *et al* (50) and Wood *et al* (118). On the other hand, the content of CO_2 and N_2 has also been lower, typically 2% each. In Figure 3.17 the input energy density was 32 J/l atm and the content of CO_2 and N_2 was 5% each.

In this work an estimate of the gain per pump energy density has been made using the gain per pump energy density measured by Wood *et al* (50) in the waveguide laser (Figure 3.18) and using the pressure dependence calculated by Taylor *et al* taking into

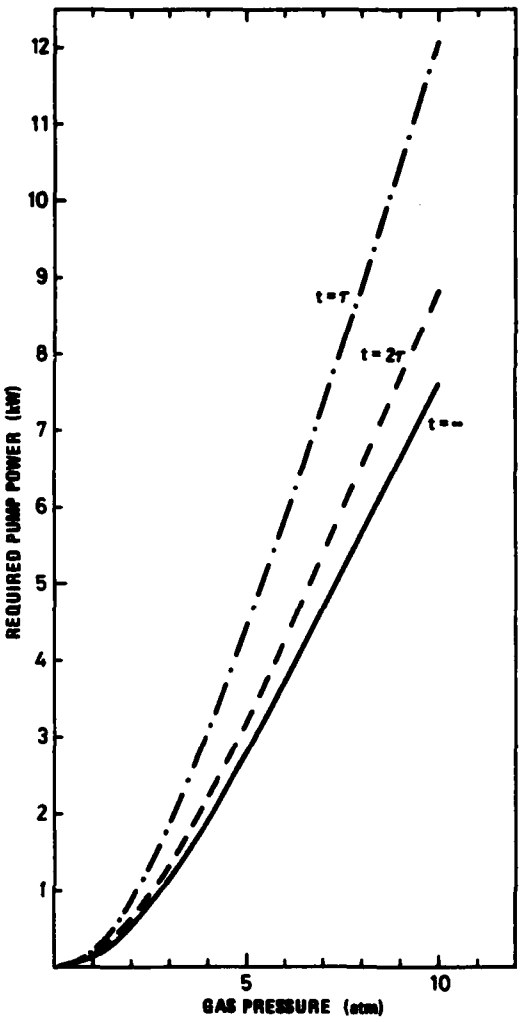

Figure 3.19 Estimated pump power required to achieve 0.5%/cm peak small signal gain in a 1.2 mm x 2 mm x 135 mm discharge volume, versus pressure

The curves are derived from the data in Figures 3.17 and 3.18. Curves for three different values of normalized pulse durations are shown. t is the pulse duration and τ is the gain decay time-constant. $\tau = 30/P$ μs is used, where P is the gas pressure in atm.

account the contribution from sequence-bands and hot-bands. This pressure dependence is the solid curve in Figure 3.17. According to this estimate the pump energy density required to give 0.5%/cm peak small signal gain is approximately 12.5 J/l atm at 1 atm and 7 J/l atm at 10 atm. In Figure 3.19 is shown the calculated rf power required to give a peak small signal gain of 0.5%/cm in a discharge volume of 1.2 mm x 2 mm x 135 mm. This will give a resonator round trip peak small signal gain slightly above 10%, which may be considered to be the minimum required for continuous frequency tuning. The required rf power depends on how long duration the rf discharge pulse can have before considerable amounts of arcs begin to develop. Experimentally it is found that pulse durations longer than twice the gain decay time constants are achievable. In Figure 3.19 the rf power requirements are shown for various normalized pulse durations. The gain decay time constant is taken to be 30 μs·atm.

In Chapters 6.2 and 6.3 the estimate of the small signal gain described above will be compared to measurements of the small signal gain and of the rf power required to reach threshold for laser oscillation.

The required pressure for sufficient gain between the line centres for continuous laser frequency tuning with a single CO_2 isotope is approximately 10 atm (8). When a mixture of CO_2 isotopes is used, continuous tuning has been demonstrated at below

5 atm (7). When such a mixture is used, the pump energy may to a first order approximation be assumed to be spread over the whole frequency range at 5 atm in the same proportion as it is at 10 atm with the single isotope. Thus the small signal gain per Joule/liter should be approximately the same. However, at 5 atm the gain decay time-constant is twice as long as at 10 atm. Consequently, the maximum optainable Joule/liter for a fixed pump power should be twice as large at 5 atm compared to that at 10 atm. Thus the peak small signal gain would be approximately twice as large at 5 atm with a suitable isotope mixture compared to at 10 atm with a single isotope, for the same pump power. This shows that the use of an isotope mixture may be specially attractive for continuous frequency tuning of an rf-excited CO_2 laser.

4 THE TUNABLE RESONATOR

The design of the optical resonator must satisfy the constraints determined by the discharge geometry which must be used to give a stable discharge and as high optical gain as possible. This geometry is shown in Figure 4.1. It is found experimentally in this work that a separation between the dielectric ribbons of less than 1.5 mm is best for a stable discharge. The discharge cross-section should be as small as possible in order to obtain as high gain as possible with a fixed pump energy.

With a separation less than ~ 2 mm between the dielectric ribbons, the ribbons will act as a parallel plate waveguide. The optical modes of circular and rectangular hollow waveguides are well known from the literature (87–90). In the rectangular waveguide the modes are considered to be described as superpositions of modes calculated for each transverse direction independently. In the parallel plate waveguide there are no walls defining a waveguide mode diameter in the open direction. It is reasonable to assume that the resonator can be described as a free space resonator in this direction. The mode profile in this direction will then be determined by the reflectors. The optical mode in the resonator is thus considered to be described as a superposition of a one-dimensional waveguide mode in the x-plane and a free space mode in the y-plane, see Figure 4.1. In the x-plane the resonator reflectors must be designed to couple the radiation emitted from the waveguide back into the waveguide mode. In the y-plane the reflectors must be designed to support a stable free-space mode with a mode diameter less or approximately equal to the discharge width. This is necessary for the free space mode to be homogeneously amplified and to oscillate with low loss.

When a light-amplifying medium with a certain transverse profile of the complex index of refraction is placed in the resonator, it will obviously have some influence on the resonator modes. In solid state lasers, like Nd:YAG, the laser rod is considered

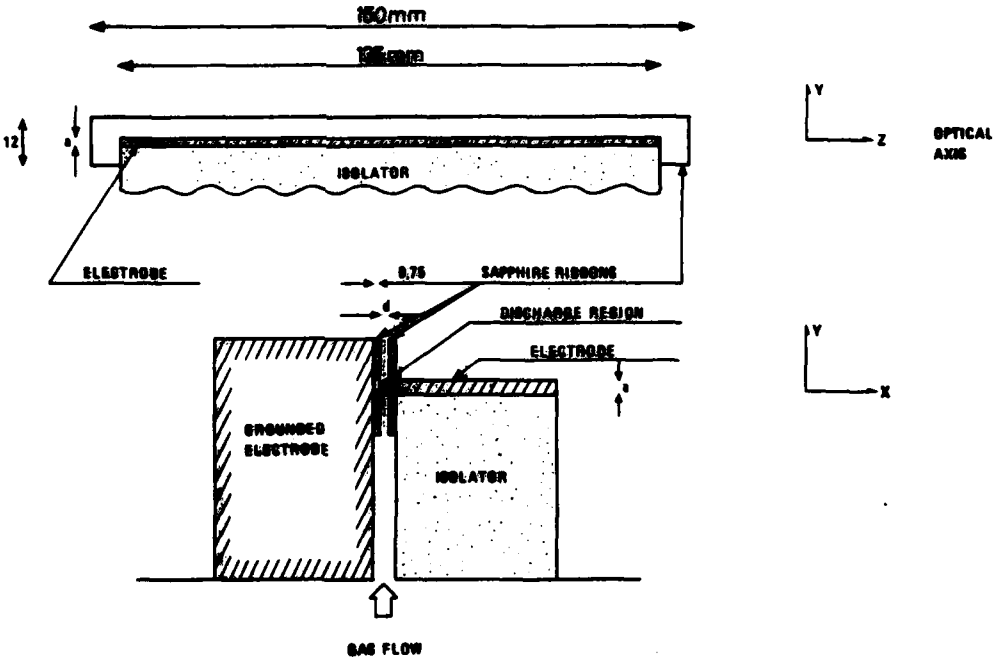

Figure 4.1 The discharge geometry
Dimensions are in millimeters. The cross-section of the discharge region is typically a = 2 mm, d = 1 – 1.5 mm

to act as a distributed lens with a focal length depending on the pumping (91). This is probably also relevant for gas lasers, because both the electron density and the temperature profile in the discharge will cause transverse variations in the index of refraction. Shock waves generated by the pulsed gas discharge may have a detrimental effect on the laser performance (92, 49). In this work these effects have not been considered quantitatively. The input energy density has been so low that shock waves have not been considered to be a big problem. In the experiments, observations have been made which may be attributed to discharge lensing effects.

The necessary frequency resolution and stability of the tunable resonator is determined by several requirements. In the CO_2 laser, even at 10 atm gas pressure, the gain is considerably stronger at line centres than in between. This was shown in Figure 3.4. The basic requirement is thus that the frequency resolution must be large enough to inhibit the laser from oscillating only close to the line centres. In a short pulse laser the laser may oscillate on several longitudinal resonator modes even when the gain is homogeneously broadened. Several applications of tunable lasers require oscillation on only one longitudinal mode. This is often hard to obtain.

Absorption and scattering from the elements in the resonator and mode mismatch and poor coupling into the waveguide may cause large frequency-independent resonator losses. These losses limit the frequency tuning range of the laser and the relative variation in the net gain between line centres may become rather large. High frequency resolution and low frequency independent losses are often in contradiction to each other.

In this work the peak small signal gain has been relatively low (~5% single pass at 10 atm) due to the limited available rf-power. It has thus been important to use a resonator with low frequency-independent losses. This is in general more difficult to obtain with the parallel plate waveguide than with a pure waveguide or free space resonator, since the boundary conditions are different in the two transverse directions in the parallel plate waveguide resonator. The best solutions are in general found with nonspherical optical components, like mirrors and lenses with different radii of curvature in the x- and y-direction. However, spherical optics are much more easily available and may be found with various radii of curvature and reflectivities among the standard inventory in our laboratory. Good solutions with spherical optics are therefore considered to be of great interest.

The design of the tunable resonator should also take into consideration the specific application of the laser. For example, in spectroscopy it may be desirable to be able to easily tune the laser over a broad frequency range. In heterodyne detection and isotope separation the laser will normally be operated at one or more fixed frequencies.

Within the frame of the work described in this report it has not been time to go into a detailed quantitative analysis of the required frequency resolution and stability of the laser resonator and of all possible configurations for low frequency independent losses. In this chapter will be analyzed a few solutions employing dispersive elements that are well-known from other tunable lasers. Designs for single longitudinal mode operation will not be discussed quantitatively. It is probably easier to obtain good frequency resolution with the parallel plate waveguide resonator than with a square or circular bore waveguide. This will be pointed out later. Since the rf-pump pulse has a relatively long duration compared to other pulsed tunable lasers (dye lasers, direct current TE CO_2 lasers) it is probably easier to achieve single longitudinal mode operation with the rf laser. First in this chapter, the basic characteristics of free space resonators and waveguide resonators will be briefly reviewed. The three different reflector positions suitable for low loss coupling to a waveguide will be pointed out. Then various resonator designs will be evaluated. Distributed feedback resonators (93)

and ring resonators will not be discussed, even though ring resonators are extensively used in dye lasers (11) and have also been used in CO_2 lasers (94).

4.1 Waveguide- and free space resonators

4.1.1 The free space resonator

The field configurations for standing waves between two mirrors were first determined by Fox and Lee in 1961 (95). Here will be reviewed only the basic characteristics of the fundamental Gaussian, or TEM_{00} mode between two spherical mirrors. Such a mode is shown in Figure 4.2. The standing wave field configuration is deter-

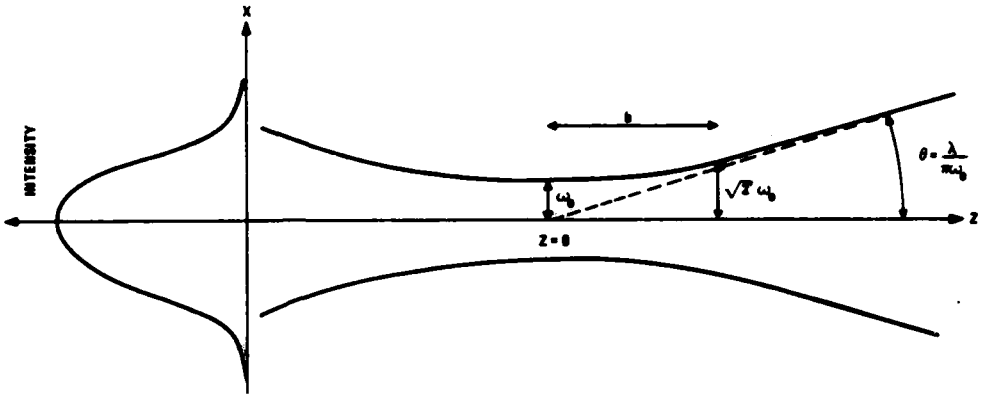

Figure 4.2 Schematic of Gaussian beam

mined by the claim that the radius of curvature R of the wavefront at each mirror must be equal to the mirror radius of curvature. The beam radius ω is the distance from the optical axis where the field amplitude is 1/e of the amplitude on the axis. The beamwaist $2\omega_0$ is the smallest beam diameter. The confocal parameter b is the length measured from the beamwaist where the beam is said to be collimated, that is within which the beam diameter 2ω is less than $\sqrt{2}$ times the beamwaist $2\omega_0$. The parameters $R(z)$, $\omega_0(z)$ and b are linked together by the equations

$$R(z) = z\left(1 + \left(\frac{b}{z}\right)^2\right) \tag{4.1}$$

$$\omega(z) = \omega_0\left(1 + \left(\frac{z}{b}\right)^2\right)^{1/2} \tag{4.2}$$

$$b = \frac{\pi\omega_0^2}{\lambda} \tag{4.3}$$

z is the distance along the optical axis from ω_0.

The beam diameter 2ω should be approximately equal to or less than the width of the light amplifying medium in order for the mode to be homogeneously amplified. The gain length in the rf laser described in this work is 13.5 cm. The mode between two mirrors separated by 15 cm, one mirror with 1 m radius of curvature and the other a plane mirror, will have a beamwaist $2\omega_0$ = 2.14 mm at the plane mirror. At the curved mirror the beam diameter 2ω will be 2.32 mm. As will be shown in the next section, these mirrors may also be suitable for low loss coupling to the waveguide mode. A discharge width of 2 mm is used most of the time in the experiments described in this report.

4.1.2 Hollow waveguide resonators

The modes of hollow optical waveguides are often called "leaky" modes, because some of the radiation will inevitably "leak out" in the guiding material. This is not the case in dielectric waveguides like optical fibers, where the core material has a higher dielectric constant than the surrounding medium. Thereby the light is totally reflected when impinging at a grazing angle on the guide wall. Marcatily and Schmeltzer (87) were the first to point out that the losses in hollow "leaky" waveguides may be very small when the guide diameter is much larger than the optical wavelength. Such waveguides may thus be used in gas lasers both to confine the discharge and to guide the optical mode (96, 97).

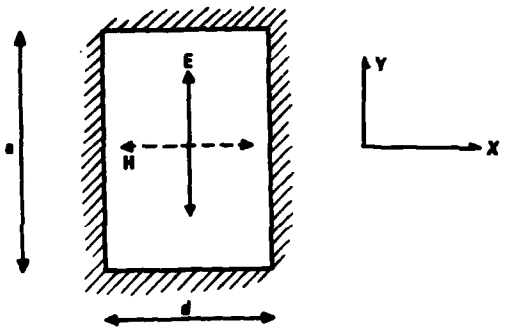

Figure 4.3 Rectangular waveguide cross-section, showing the polarization of the electric and magnetic field vectors for which the attenuation α (equation (4.4)) is derived

The modes of hollow circular waveguides (87) and hollow square and rectangular waveguides (88–90) are now well covered in the literature. In the laser resonator the reflectors are usually mounted outside the waveguide. The problem associated with low loss coupling of the radiated waveguide mode back into itself has been treated by a number of authors (98–102).

The modes of rectangular optical waveguides closely approximate the linearly polarized TEM modes of conventional microwave waveguides. The modes are described as superpositions of modes derived for each transverse direction independently (88–90). The mode amplitude is vanishing small at the boundary. The attenuation constant α of an $E^yH^x_{nm}$ mode in a waveguide as defined in Figure 4.3 is given by

$$\alpha = \frac{n^2\lambda^2}{16d^3}\,\mathrm{Re}\,\frac{1}{(\nu^2-1)^{1/2}} + \frac{m^2\lambda^2}{16a^3}\,\mathrm{Re}\,\frac{\nu^2}{(\nu^2-1)^{1/2}} \qquad (4.4)$$

$\nu = \sqrt{\frac{\epsilon}{\epsilon_0}}$ – the complex refractive index of the wall material

a and d – dimensions of the waveguide cross-section, see Figure 4.3

λ – wavelength

n,m – mode order numbers

It can be seen that the attenuation is lowest for the mode with electric field vector polarization parallel to the longest side wall of the guide.

For alumina the following value of the refractive index has been used at 10 μm (103, 104)

$$\nu = 1.15 - i\,1.42\cdot 10^{-2} \qquad (4.5)$$

This gives $\alpha = 1\cdot10^{-4}$ cm^{-1} in a parallel plate waveguide for d = 1 mm and a >> d. The round trip waveguide loss in a 15 cm long laser will be 0.3%, which is negligibly small compared to the coupling losses, see the following sections.

Additional waveguide losses may be caused by surface irregularities and waveguide bends. In circular bore waveguides the losses caused by even very small bends may become very large (87). In parallel plate waveguides bending losses are not so large (105). Flexible parallel plate waveguides may be suitable for long distance optical transmission lines at 10 μm (105).

The wavefront of the waveguide modes is plane to the first order approximation. From the exit of the waveguide these modes radiate into free space. The field distribution outside the waveguide may be determined by a scalar diffraction calculation using the Huyghens–Fresnel principle (98–102) with the waveguide mode as the radiation source. The wavefront of this radiated mode is not necessarily circular or spherical. However, there are in general three positions where spherical or circular symmetric reflectors may be used to couple the radiation from the lowest order waveguide mode back into the original waveguide mode with low coupling loss.

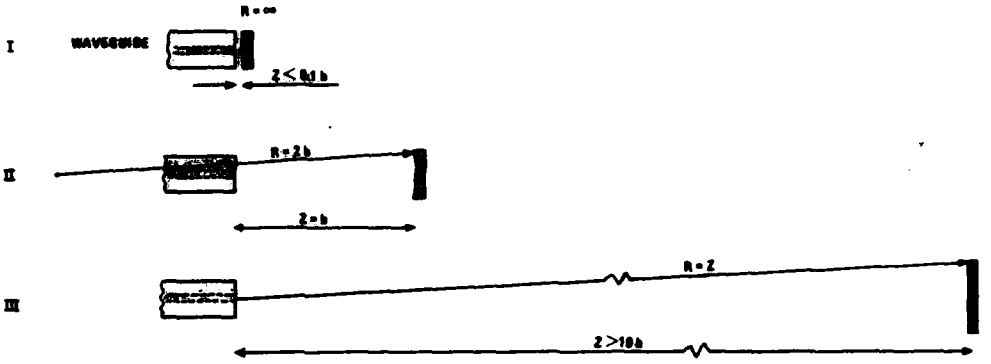

Figure 4.4 Schematic of the three configurations for low-loss coupling of the lowest order circular or rectangular waveguide mode back into the waveguide (after (98–102))
b is the confocal parameter of the Gaussian mode that most closely resembles the fundamental waveguide mode.

The three cases are shown in Figure 4.4. Case I is a plane mirror placed at the waveguide end. Abrams (99) and Degnan and Hall (100) have calculated for a circular waveguide that a displacement of the plane mirror a distance z from the waveguide introduces a coupling loss for the EH_{11} mode given by

$$\text{loss} = 57(z/b)^{3/2}\ (\%) \quad \text{for} \quad (z/b) < 0.4 \tag{4.6}$$

$b = \pi\omega_0^2/\lambda$ is the confocal parameter of the free space Gaussian mode (section 4.1.1) that most closely resembles the waveguide mode. Abrams (99) has calculated that $\omega_0 = 0.64$ a for a circular bore waveguide with bore radius a. Hendersson (102) determined $\omega_0 = 0.70$ a for a square hollow waveguide of half-width a.

Case II corresponds to a mirror with radius of curvature 2b located at a distance b from the waveguide end. The point z=b corresponds to the point where the radius of curvature of the corresponding Gaussian mode is smallest. This is shown in Figure 4.5. Case II is a low loss configuration only for the lowest order mode.

Case III corresponds to a mirror with radius of curvature R equal to the distance z to the waveguide, when $z >> b$.

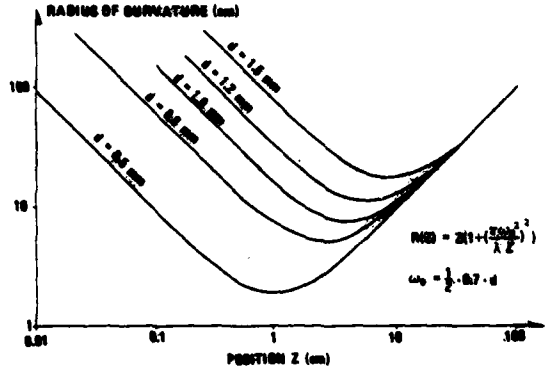

Figure 4.5 Radius of curvature versus distance Z from beam-waist for a Gaussian beam with beam-waist $2\omega_0 = 0.7d$

d is the inner diameter of the waveguide.

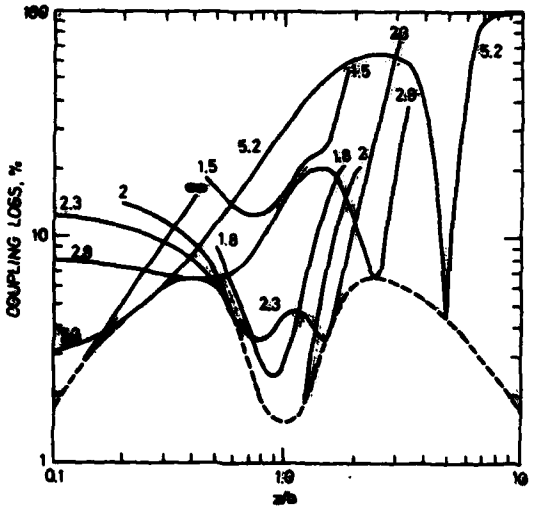

Figure 4.6 Coupling-losses for the EH_{11} *mode in a circular-bore waveguide, versus normalized distance Z/b between the waveguide and the mirror*

Each curve is labelled with a normalized mirror curvature. The dashed line is the coupling loss for a mirror with radius of curvature equal to the radius of curvature of the Gaussian mode which most closely resembles the EH_{11} mode (after Abrams (99)).

The coupling losses for spherical mirrors with radius of curvature matching the Gaussian beam which most closely resembles the waveguide mode has been calculated by Abrams (99) for a circular bore waveguide. The result is shown in Figure 4.6.

It may be seen from Figure 4.5 that a mirror with 1 m radius of curvature matches the approximate Gaussian wavefront from a 1.2 mm diameter square bore waveguide (b = 5.5 cm) at a distance $z \approx 3$ mm. This situation ($z/b \approx 0.05$) gives a coupling loss of less than 1%, see Figure 4.6. From the preceding discussion it seems reasonable to expect that the coupling loss for the same mirror at approximately the same distance from a parallel plate waveguide with 1.2 mm plate separation will be approximately half of that given by equation (4.6). (This is because in the treatment of the rectangular waveguide modes, the mode propagation losses are calculated for each transverse direction separately and added to give the total loss, equation (4.4). It thus seems reasonable to apply the same procedure when calculating the coupling loss.) It was shown in the preceding section that a 1 m radius of curvature mirror and a flat mirror separated by 15 cm may be suitable for low losses in the free space direction. A resonator with two such reflectors close to the waveguide will thus probably have low overall losses. A resonator with parameters close to those described above has been used extensively in this work. However, such a resonator is of course not suitable for continuous frequency tuning.

4.2 Evaluation of various tunable resonators

The frequency tuning problem is illustrated qualitatively in Figure 4.7. The resonance-frequencies ν_q of the laser cavity is given by

$$\nu_q = q \frac{c}{2nL} \qquad (4.7)$$

c – speed of light in vacuum

n – index of refraction of the medium between the resonator reflectors

L – distance between the reflectors

q – number of wavelengths in a round trip in the cavity

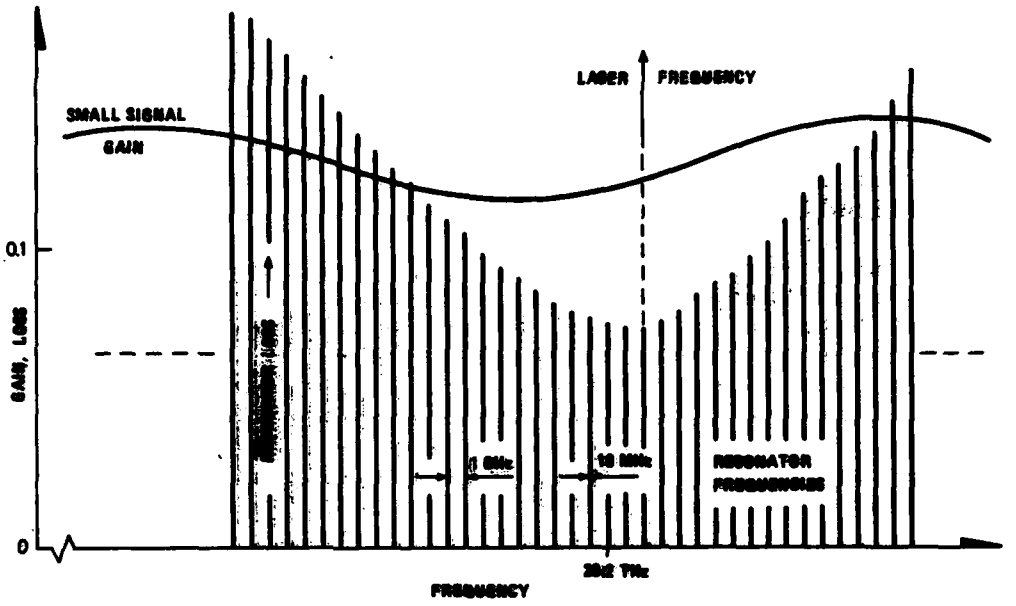

Figure 4.7 *Frequency tuning of a CO_2-laser, schematically*
Typical small signal gain-curve between two line-centre frequencies are shown. The separation between the resonance frequencies of the laser resonator corresponds to a 15 cm long cavity. The resonator must contain dispersive elements which make the resonator losses vary approximately as shown.

For L = 15 cm the frequency separation between neighbouring resonance-frequencies is 1 GHz. Because the resonator operates on very high orders of resonance, the Q-value of the resonator is very high, typically of the order 10^6. The width of each cavity resonance-frequency is typically 10 MHz. The separation between various CO_2 line centre frequencies is typically 40–60 GHz. In Figure 4.7 is illustrated qualitatively the shape of the small signal gain curve between two line centre frequencies.

The laser will oscillate on one or more of the cavity resonance-frequencies that exhibit the highest net small signal gain. For the laser to oscillate on a cavity resonance-frequency between two line-centre frequencies the resonator must contain one or more dispersive elements which make the resonator losses vary typically as shown in Figure 4.7.

It should be noted that in a pulsed laser the index of refraction n of the laser active medium can vary within the laser pulse. This is because the temperature of the medium will increase during the discharge, and because when the laser starts to oscillate the gain will saturate. Thus the cavity resonance-frequency can vary during the pulse according to eq (4.7) and this can cause a laser-frequency chirp. This frequency chirp will usually determine a lower limit of the spectral bandwidth of the

laser pulse. In the work described in this report the input energy has been relatively small so the increase in gas temperature has been relatively low, compared to other pulsed dc-excited lasers. Also the build-up time for the gain has been relatively long so that the variation in the index of refraction of the medium due to saturation of the gain should also be relatively small. Thus the frequency chirp during the laser pulse is estimated to be relatively small compared to in short-pulse excited, high energy lasers. This object has not been analyzed quantitatively any further from a theoretical point of view.

The dispersive elements most commonly used in tunable laser resonators are reflection gratings, prisms and etalons. In combination with these elements may be used beam expanders to enhance the resolution of the grating, and extra partial or totally reflecting mirrors. The mirrors may be used to form interferometers to select a single resonator mode, or may be used in combination with a dispersive element to enhance the maximum reflection. In this section various tunable resonators incorporating one or more of the above-mentioned elements and the parallel waveguide geometry shown in Figure 4.1 will be evaluated.

Only solutions where the optical components are mounted close to the waveguide, inside the pressure chamber, will be discussed. From a practical point of view it may be desirable that the discharge chamber is a separate unit with either antireflection-coated or Brewster-angle oriented windows. Such a solution may also be best for the laser performance because variations in the index of refraction of the gas caused by shock waves generated by the discharge may be detrimental to the resonator mode quality. The part of the resonator which is occupied by the high pressure gas should thus be as small as possible. Also, the shock waves can make the optical components vibrate. In these experiments these problems are considered to be of minor importance because the energy dissipated in the discharge is relatively low compared to other dc-excited pulsed CO_2 lasers. The solution with optics mounted inside the pressure chamber has been chosen because there will inevitably be some losses both in AR-coated and Brewster-angle windows. Also, with such windows, the resonator with optics mounted close to the waveguide will be more difficult to realize. Optics mounted close to the waveguide, which correspond to case I for low coupling loss, give the simplest and most compact resonator construction.

A good survey over various tunable resonators can be found in (11).

4.2.1 The grating resonator

A reflection grating may be used as a dispersive end reflector in a laser resonator. Such a grating will be blazed for a certain wavelength for first order Littrow configuration, that is, the grooves of the grating will be shaped so that almost all of the impinging radiation is diffracted in the first order at a diffraction angle close to the angle of incidence (106, 107). Higher diffraction orders in general will have a diffraction angle larger than 90°, which means that they do not exist.

Such gratings are commercially available and the best gratings can diffract up to 95% of the incident radiation in the first order. Highest efficiency is usually obtained for polarization normal to the grooves (106, 107). Very little (~1%) may be lost through absorption and scattering and the rest is diffracted in 0′ order.

In Figure 4.8 a reflection grating is placed as close as possible to the waveguide, to give as low waveguide coupling loss as possible. According to eq (4.6) and the discussion in section 4.1.2, if the distance between the grating and a 1.2 mm wide waveguide is 5 mm, the coupling loss should be approximately 0.8%. The distance may be reduced if the ends of the dielectric ribbons are cut parallel to the grating surface, but 0.8% is a negligibly small loss term.

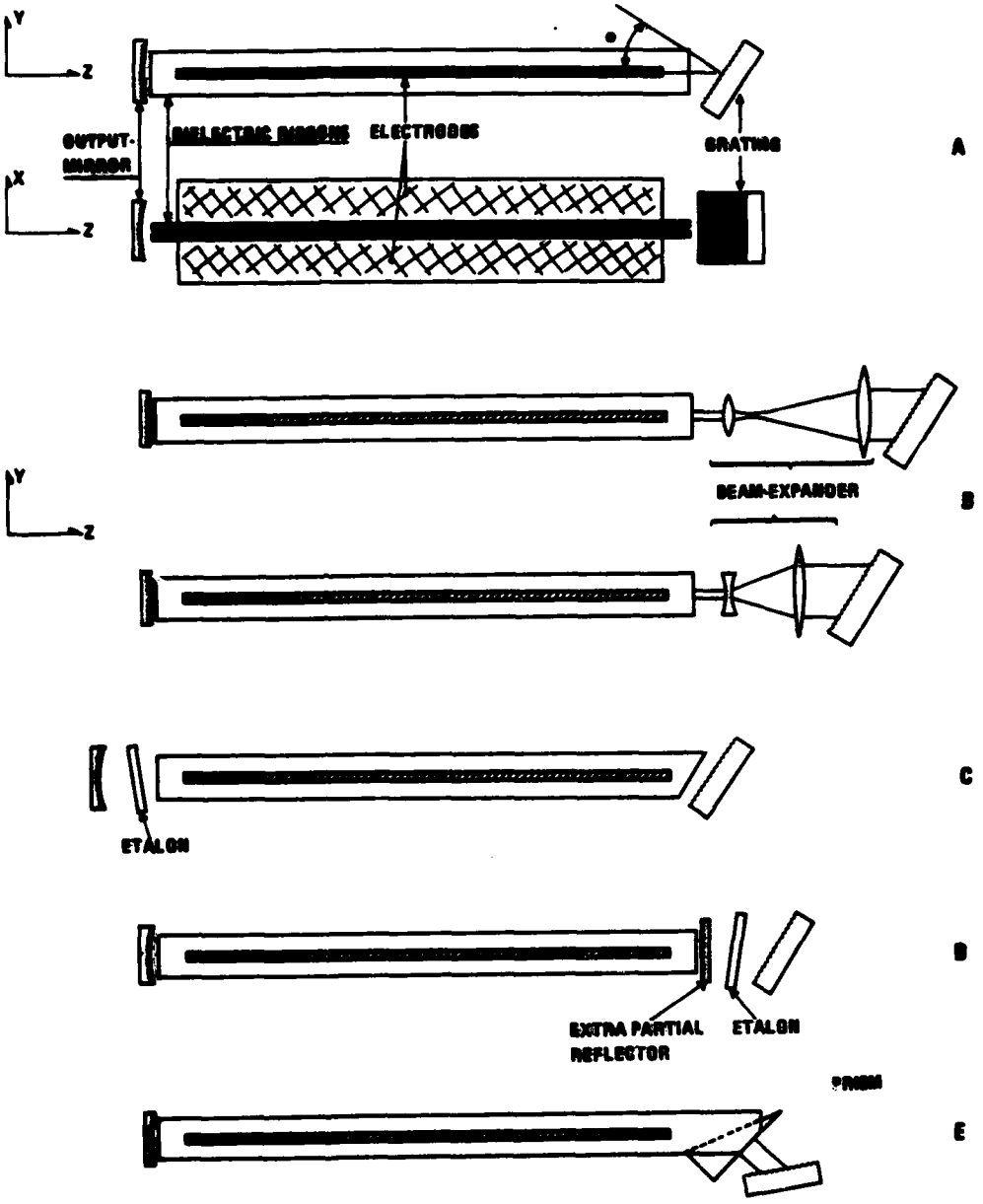

Figure 4.8 Various tunable waveguide-resonators

The grooves must be oriented normal to the waveguide surface so that the angular dispersion is in the free space direction. If the angular dispersion were in the other direction, the frequency resolution of the resonator would be much lower. This is because radiation reflected from the grating a small angle from the optical axis may easily couple into higher order waveguide modes. The angular separation between diffracted beams for two neighbouring CO_2 – line-centre frequencies is typically 0.1°. Since the gain curve versus frequency is not linear, the laser could easily oscillate on combinations of higher order modes which might have only slightly larger waveguide losses, instead of at the frequency which the grating is tuned for and which may have

a lower gain. Also, more grooves will be illuminated when the grooves are normal to the waveguide, since the beam diameter typically is larger in the free space direction than in the waveguide direction.

The efficiency of the grating is best for an electric field vector normal to the grooves. It is very fortunate that when the grating is oriented with the angular dispersion in the free space direction, this electric field polarization which has maximum reflection from the grating is the same as the one which has lowest waveguide loss, see section 4.1.2.

The main problem with this simple tunable resonator, shown in Figure 4.8a, is that the frequency resolution may be too low for frequency tuning between line centres. Since laser reflection gratings must be operated in the first diffraction order, the resolution $R = \nu/\Delta\nu$ is directly proportional to the number of illuminated grooves N. ν is the optical frequency and $\Delta\nu$ is the difference between two frequencies which are just resolved after the Rayleigh criterion. The grating used in these experiments has 135 grooves per millimeter and a blaze angle of ~45°, see Figure 4.7. Thus with a 2 mm wide beam the difference $\Delta\nu$ between two frequencies which are just resolved after the Rayleigh criterion is as large as 80 GHz. Since the difference between two line centre frequencies is typically 40–60 GHz, this resolution is probably too low for frequency tuning between line centres. Also a problem with this simple solution for the rf-excited CO_2 lasers described in these experiments is the frequency independent loss. The peak reflection from the grating will probably not be much larger than 93–94% including the coupling losses. The resolution of the grating may be increased by increasing the beam diameter in the open direction. To do this the discharge width must be increased to match the beam diameter. This will result in reduced gain since the pump energy is fixed.

One problem with a grating can be that the maximum radiation that can be shone on the surface before the surface is damaged in general is lower than what may be the situation in a laser resonator. The damage threshold is usually lower than for the best dielectric or metallic mirrors. This may limit the use of gratings in high power lasers. In general the damage threshold is high enough for line-tunable low pressure cw CO_2 lasers, but too low for 10 atm dc-pulsed TE CO_2 lasers. No problems with grating-damage have been encountered in the 10 atm rf-excited CO_2 laser described in this report.

4.2.2 The beam-expander/grating resonator

A beam expander may be used in front of the grating to increase the number of illuminated grooves, that is, increase the frequency resolution of the grating. Two beam-expander/grating combinations mounted close to the waveguide are shown in Figure 4.8b.

With a 2 mm diameter beam in the waveguide, a magnification M≈8 of the beam-expander is adequate to illuminate a 25 mm squared grating. The frequency resolution R would be $R = \nu/\Delta\nu = N \approx 3000$, which would give $\Delta\nu \approx 10$ GHz. This should be sufficient for frequency tuning between the line centres. Since in general lenses may be diffraction limited when the f-number is larger than 5, such a beam-expander may be constructed with a 1 cm diameter, 1 cm focal length lense and an 8 cm focal length lens.

When the collimator and the grating is correctly positioned and aligned the coupling losses may be assumed to become relatively small. It should be noted that alignment of the beam-expander is very critical. The lenses must be oriented coaxially and parallel to each other with very good accuracy to avoid astigmatism. The separation between the two lenses must be controlled with an accuracy of a few tenths of a millimeter. The movement of the grating normal to the tuning angle direction must

be very small when a spherical-symmetric expander is used. This is because any angular deviation of the diffracted beam away from the optical axis is increased with the magnification M of the beam-expander. This last problem can be overcome by using sylindrical lenses, so the beam is expanded only in the direction perpendicular to the grooves.

Another problem with the beam-expander in these experiments is that there will inevitably be some optical loss in it. Antireflection coatings cannot be made 100 per cent transmissive, especially not over the whole spectral region between 9 and 11 μm. It is also more difficult to make good coatings on surfaces with short radius of curvature. We have measured 2% loss after single pass propagation through a beam-expander made with lenses purchased from one of the best manufacturers of infrared optical components (108). The maximum reflection from the grating/beam-expander combination will thus not be more than about 90%. We will return to a possible solution of this problem after a discussion of the etalon.

4.2.3 Resonators with etalons

An etalon can be used as a dispersive element both in combination with a grating and alone. Harris, O'Neill and Whitney used two etalons as tuning elements in continuously tunable CO_2-lasers (26). One etalon was a very narrow-gap air-spaced etalon for a coarse frequency selection. The other was a solid etalon with a wider gap for fine tuning.

When an etalon is used as a dispersive element in a laser resonator it is slightly tilted with respect to the optical axis. Frequencies for which the transmission through the etalon is low are reflected out of the resonator, that is, the resonator losses are high for these frequencies. A small tilt angle introduces only small "walk-off" losses for the frequencies at the transmission maximum (109). Frequency tuning may be accomplished by varying the tilt angle. Tuning of an air-spaced etalon may also be accomplished by mounting one of the mirrors on a piezoelectric translator or by varying the pressure in the etalon gap.

In a continuously tunable CO_2 laser it is desirable to be able to choose unambiguously a frequency within the gain bands between 9 and 11 μm, that is, between 33 and 27 THz. In order to do so with an etalon, the free spectral range c/2L must be larger than 6 THz, which implies that the etalon gap L in an air-spaced etalon must be smaller than 25 μm. c is the speed of light in the medium between the etalon reflectors. For such an etalon to have a frequency resolution of 50 GHz, which is easily obtainable with a grating, the finesse must be approximately 100. A finesse of 100 implies that the reflection R on each surface must be 97%. With such high reflectivities the peak transmission through the etalon, or the throughput, will be very poor due to absorption, scattering and other inevitable imperfections in the etalon. The throughput, T_{max} is given by

$$T_{max} = [\,1 - \frac{A}{1-R}\,]^2 \qquad (4.8)$$

where A is the power loss at each surface. In Figure 4.9 are shown the throughputs versus reflectivity R on each surface for A = 0.01 and A = 0.02. Also shown are typical values of throughputs obtainable in practice, according to a manufacturer of etalons (110). These values also correspond well with measurements taken during this work.

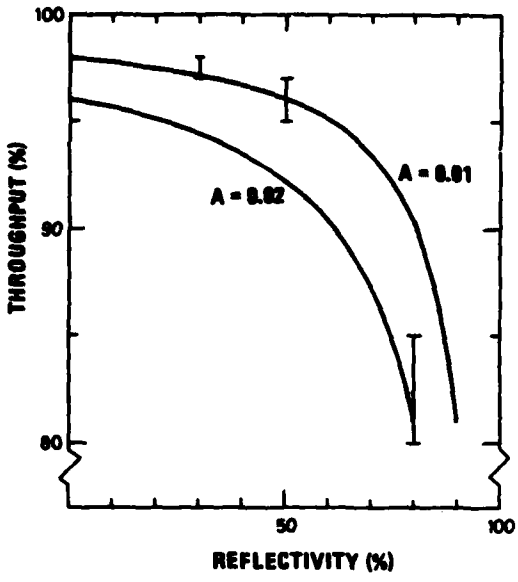

Figure 4.9 *Maximum transmission through an etalon versus power reflectivity R on each surface*

Curves for two values of absorption A on each surface are shown, see equation (4.8). Bars indicate typical maximum transmission obtainable in practice (110).

It may thus be concluded that unless one has very high gain and problems with optical damage of the grating, a grating is superior to an etalon as a main frequency tuning element. However, an etalon with a smaller spectral range and a lower finesse may be useful to increase the frequency resolution of a grating. The free spectral range of the etalon should then be equal to or larger than the resolution bandwidth of the grating. This is shown in Figures 4.8c and 4.10. Figure 4.8c shows schematically the etalon/grating combination in the rf-excited waveguide laser. Figure 4.10 show the frequency tuning characteristics of the etalon/grating combination. The transmission characteristics of the etalon correspond roughly to that of a 0.75 mm thick solid ZnSe etalon with 50% reflectivity on each surface. The transmission frequency ν_E of the etalon versus tilt angle α is given by

$$\nu_E(\alpha) = \nu(0)\,(1-(\frac{\sin\alpha}{n})^2)^{-1/2} \qquad (4.9)$$

n – index of refraction of the etalon

α – tilt angle of the etalon with respect to optical axis

To make the "walk-off" losses as small as possible the tilt angle α should be as close to 0° as possible. However it is important that the frequencies which are not transmitted through the etalon are reflected completely out of the resonator.

An etalon with free spectral range equal to the resolution bandwidth of the grating gives roughly the same improvement in frequency resolution as a beam-expander with magnification M equal to the finesse F of the etalon. A 10–80 GHz free spectral range corresponds to an air gap of 15 mm and 2 mm respectively, or a 6.25 – 0.8 mm thick solid ZnSe etalon. A finesse of 6 is obtained with approximately 50% reflection on each surface of the etalon. With this reflectivity the losses will be approximately 4%, see Figure 4.9.

An advantage with the etalon as a fine-tuning element is that the resonance-frequency of the etalon can be tuned between two CO_2 line-centre frequencies by varying the tilt angle typically 3–5°, see Figure 4.10. Thus tuning between line-centre frequencies can be easily done with good accuracy. As was mentioned in the preceeding section, tuning the laser frequency between two CO_2 line-centres with a grating corresponds to tuning the grating angle only approximately 0.1°. Thus in this case very stable mounts for the grating and high precision tuning mechanics are required. Another advantage with the etalon is that the resonator construction can be made more compact than with a beam-expander, and the alignment of the various optical

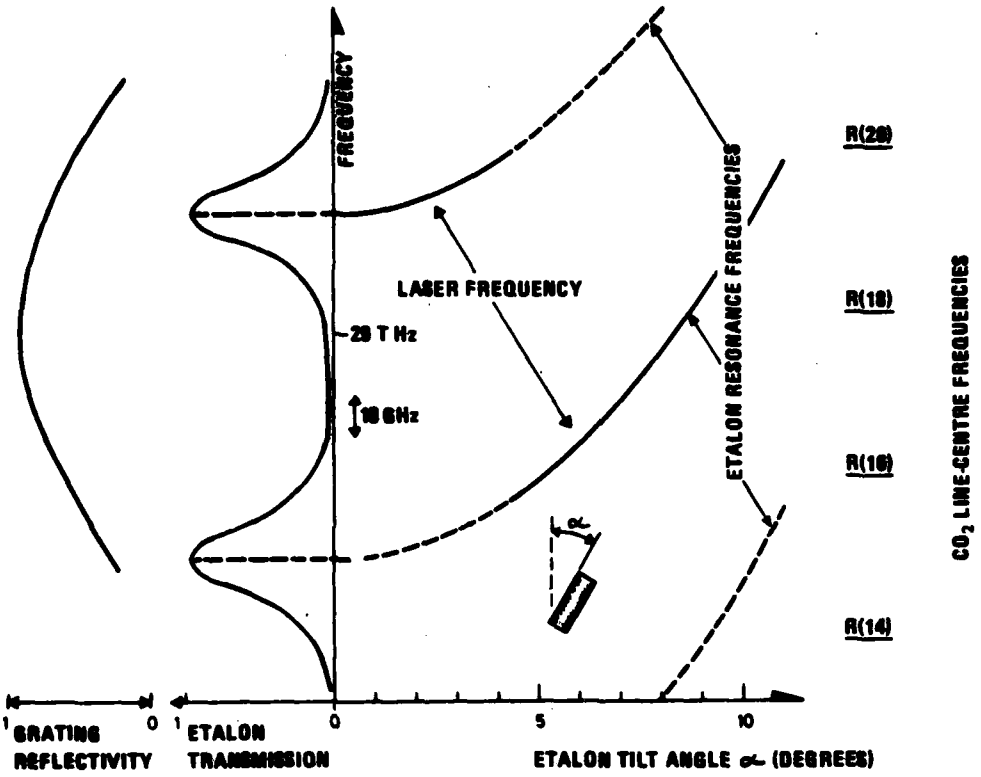

Figure 4.10 Schematics of laser-frequency tuning with grating and etalon
The transmission curve of the etalon is close to that of a 0.75 mm thick etalon with 51% reflectivity of each surface. The grating is used as a coarse frequency-tuning element. The laser frequency is fine-tuned by tuning the etalon tilt angle.

components is not so critical as when a beam-expander is used. On the other hand, the losses in the etalon increase with the finesse, while the losses in the beam-expander are independent of M. When the etalon is placed between the waveguide and one of the reflectors, the distance between the reflector and the waveguide opening will be at least 10–20 mm. This will give waveguide coupling losses. Finally, broad frequency scans are more complicated with the etalon since both the grating and the etalon must be adjusted.

4.2.4 Resonator with a third reflector

The problem with the frequency-independent loss both in the beam-expander/grating and the etalon/grating combinations can be overcome by using an extra partial reflector close to the waveguide. In Figure 4.8d is shown a resonator with an extra reflector in front of an etalon/grating combination.

The improvement in reflectivity obtained by using an extra mirror in front of a reflection grating has been used in several lasers (111, 112). It has also been used to reduce the optical damage to the grating and to achieve single longitudinal mode operation of a continuously tunable TE CO_2 laser (113).

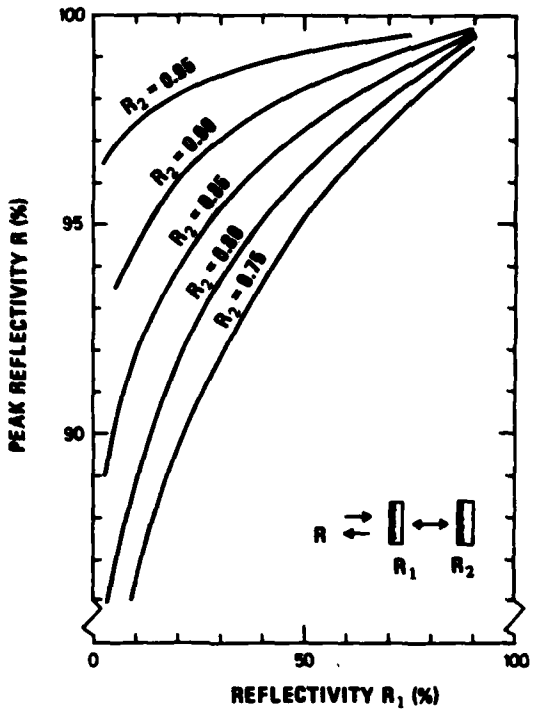

Figure 4.11 Maximum power reflectivity from a two-mirror reflector versus reflectivity R_1 of the first mirror for various reflectivities R_2 of the second mirror

The improvement in reflectivity when the extra mirror is used can be analyzed by first considering the reflection from two parallel reflectors, that is, from an etalon. Maximum reflection occurs when the etalon is at "antiresonance". Maximum reflection is shown versus reflectivity R_1 of the first reflector for various reflectivities R_2 of the second reflector in Figure 4.11.

When the second reflector is a grating, the reflectivity of the second surface can be assumed to have a frequency-dependent reflection coefficient corresponding to the frequency resolution of the grating. When an etalon is inserted between the grating and the extra mirror, the reflectivity R_2 of the second surface can be expressed as

$$R_2 = R_G(\nu)\, T_E^{\,2}(\nu) \qquad (4.10)$$

where

$R_G(\nu)$ – Reflectivity of the grating
$T_E(\nu)$ – Transmission through etalon

(the beam incident on the etalon/grating combination passes through the etalon twice before it comes back, therefore the T^2 term in equation (4.10).)

For sake of simplicity it will be assumed in the proceeding analyses that one resonance-frequency of the etalon is close to the reflection maximum of the grating, and that the other resonance-frequencies can be ignored, see Figure 4.10.

In Figure 4.12 the reflectivity of the extra-mirror/grating/etalon combination is shown versus frequency. Quantitatively, values have been used in Figure 4.12 which correspond to components that have been used in some of the experiments. The distance L between the grating and the extra mirror is 2 cm, the reflectivity of the extra mirror is 70%, R_G has a maximum reflectivity of 87.5% and a reflection bandwidth (FWHM) of 100 GHz. The 0.75 mm thick ZnSe etalon has 51% reflectivity coating.

It is seen in Figure 4.12 that the extra mirror has three pronounced effects: It increases the maximum reflection and it increases the reflection bandwidth of the etalon/grating combination. The first effect is what is necessary to bring the laser above threshold for oscillation. The second effect is a disadvantage with respect to the frequency tuning of the laser. The third effect is that the extra mirror introduces "holes" in the reflection curve. These "holes" correspond to the frequencies where the "etalon" formed by the extra mirror and the grating is at resonance. The separation between these resonance-

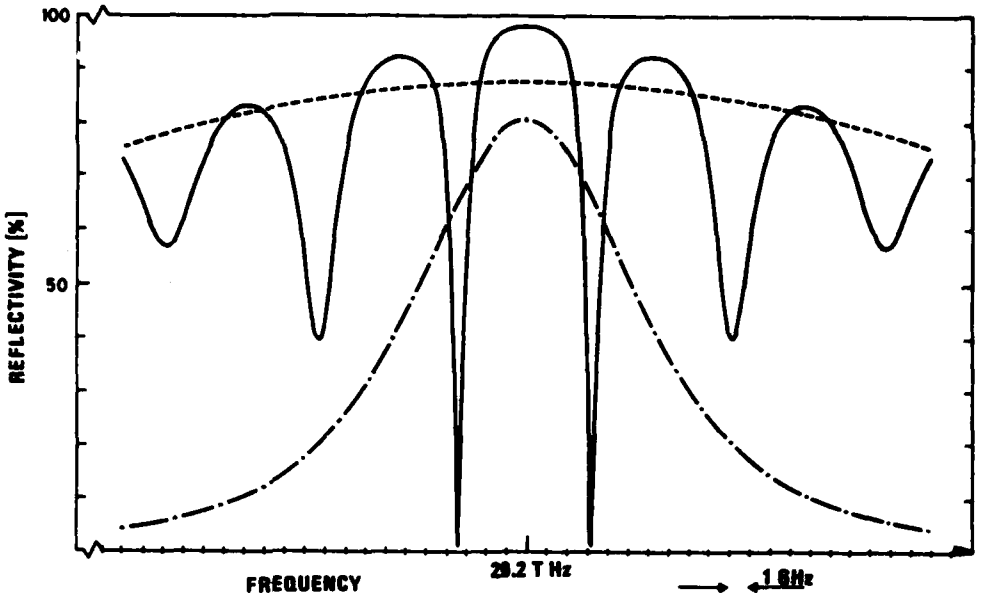

Figure 4.12 Power reflection from a grating/etalon/extra-mirror combination
The dashed line is the grating reflectivity. The dash-dot line is the grating/etalon reflectivity. The solid line is the grating/etalon/extra-mirror reflectivity. The etalon is a 0.75 m thick, 51%/51% coated ZnSe etalon with 0.01% surface loss. The extra mirror has 70% reflectivity. The distance between the grating and the extra mirror is 2 cm, and it is assumed to be adjusted so that maximum reflectivity of the grating/extra-mirror combination occurs for a frequency equal to a resonance frequency of the etalon. The units on the frequency axis correspond to the distance between resonance-frequencies of a 15 cm long resonator.

frequencies is c/2L where L is the distance between the extra mirror and the grating. The width and the depth of the "holes" depend on the reflectivities of the extra mirror and the grating. In general the higher the reflectivity of the extra mirror, the narrower and deeper are the "holes". One should be able to control the "position" of these holes so that they do not fall on the resonance frequency of the etalon. This is best done with the grating mounted on a piezo-electric translator.

In general, the higher the reflectivity of the extra-mirror the higher is the peak reflectivity of the extra-mirror/etalon/grating combination, but also the poorer is the frequency resolution. Thus good frequency resolution and low losses are in contradiction to each other. Several parameters must be chosen to optimize a specific laser with a given peak small signal gain: The grating is the least critical part to choose, it should have as good resolution, good efficiency and high damage threshold as possible. The thickness of the etalon must be chosen so that its resonance frequencies are not so close that the laser frequency jumps back and forth between the resonance frequencies during the tuning. The reflectivities of the etalon surfaces must be chosen so that the losses are not too high (Figure 4.9) and so that the frequency resolution is good enough in combination with the extra-mirror reflectivity. The total frequency resolution and peak reflectivity depend on all the above mentioned parameters. A detailed quantitative analyses of this problem has not been done in this report. Experimentally a few combinations of etalons and extra mirrors have been tried out, see chapter 6.

When the extra mirror is used, a problem with mode matching arises since the total laser resonator then consists of two coupled resonators. It may be necessary to control the position of one or more of the reflectors to make the resonance frequency of the total resonator and the etalon coincide with the maximum reflection for the extra-mirror/grating combination. A more serious problem is the transverse mode matching. The output mirror and the extra mirror form a resonator with a certain transverse mode profile. So does the extra mirror and the grating, or the extra-mirror and the grating/beamexpander or grating/etalon combination. If the two transverse modes do not match, large mode coupling losses will be the result. It was pointed out in section 4.2.2 that when a beam-expander is used in front of the grating, the positioning and alignment of the beam-expander and the grating are very critical. The fact that part of the resonator is a waveguide does not make the situation easier. The alignment of the various components are not at all so critical when the etalon is used and when the extra-mirror, the etalon and the grating are mounted as close to the waveguide as possible.

It should finally be noted that to reduce the coupling losses for the extra-mirror/etalon/grating combination, both the extra-mirror and the etalon, and possibly also the grating, can be mounted inside the waveguide. The components then have to be about 1 mm thick. Also the beam-expander can be mounted inside the waveguide. The lenses should be cylindrical. The beam-expander then expands the beam only in the open direction of the waveguide. These solutions have not been tried experimentally in this work.

4.2.5 Resonator with a prism and a grating

It should be noted that another way to enhance the frequency resolution of the grating is to use a prism in front of it. When a ZnSe prism is used at Brewster's angle of incidence, the magnification will be $M = n = 2.4$. With a 2 mm beam in the waveguide the resolution $\Delta\nu$ of the grating will be $\approx$30 GHz. The prism can be mounted inside the waveguide as shown in Figure 4.8e. The side of the prism which face the grating can be AR-coated, or it can be used as an extra reflector as described in the preceding section. The advantage with a prism compared to a spherical beam-expander is that the prism expands the optical beam in only one direction. Prisms have been used in tunable CO_2 lasers (125). They have not been tried in the experiments described in this report.

5 EXPERIMENTAL APPARATUS AND MEASUREMENT TECHNIQUES

In this chapter will be described the apparatus and experimental techniques that have been used to investigate rf-discharge characteristics at multiatmospheric pressures, and to measure the laser-output characteristi· The laser will be described in more detail than in Chapter 2.

First will be briefly discussed the choice of alternating-current (ac) frequency. Previous work (1, 2) concludes that frequencies both in the MHz and GHz domain are suitable for pumping of gas lasers. The possible discharge geometries and the problem of coupling the ac power into the discharge vary considerably within this wide frequency range. Also it should be taken into consideration that high-power ac sources are not readily available at an, frequency, and that it may be desirable to work within an industrial frequency band.

In the work described in this report it was initially chosen to work within the industrial frequency band at 40.68 MHz. A preliminary 1 atm laser was first built. The construction of this laser will not be described here. Then a multiatmospheric-pressure discharge chamber was constructed for investigation and measurements of the discharge characteristics, the impedance matching problem and the optical gain in the discharge at up to at least 10 atm. Based on the experiments with the discharge chamber, a multiatmospheric-pressure laser was built with a discharge geometry similar to that in the discharge chamber.

A great deal of work has been done in order to get enough rf-power at 40.68 MHz. This has been more difficult than was initially anticipated. It has been chosen to drive an increasing number of modified solid-state 500 W "RF-Power Labs" radio-amateur amplifiers in parallel. These have been found to be reasonably reliable and robust. The amplifier system will be described in section 5.5. It is probably not the best solution for a practical tunable laser system.

5.1 Choice of ac-discharge excitation frequency

In the radio-frequency domain and when rf-discharges between parallel-plate electrodes are concerned, the choice of excitation frequency is connected to the choice of electrode separation through the demand that the electron displacement shall be less than the electrode separation. As was shown in Chapter 3, the displacement amplitude will be less than approximately 1 mm for frequencies above 20 MHz. In addition to this demand, the ac-frequency should probably be as high as possible in order for the time between reversals of the voltage polarity to be too short for development of arcs, see Chapter 3.

When the wavelength associated with the ac-frequency is much longer than the dimension of the discharge region, the electric field will be uniform along the whole electrode length. If the wavelength is of the same magnitude or shorter than the discharge dimensions, a uniform electric field can be achieved by separate feeding of individual electrode segments with individual phase delay and individual reactive ballasting.

A vacuum wavelength longer than 10 times the electrode length L corresponds to a frequency below 200 MHz for L = 15 cm.

Good coupling of the energy into the discharge requires that the impedance of the discharge as seen from the rf-power source is equal to the internal impedance of the source. In general, good coupling can be achieved at any frequency. At frequencies up to about 100 MHz the impedance matching can be accomplished with lumped-circuit components like solenoides and capacitors. At these frequencies the inductive loads caused by current-loops between the lumped-circuit components is relatively low.

Above about 100 MHz these inductive loads become comparable to and larger than the reactive loading of the discrete components. At these frequencies transmission-line matching is probably more appropriate.

If frequencies in the GHz domain are used, microwave waveguides or microwave resonators must be used to couple the power into the discharge. A carrier frequency of 9.375 GHz has been used to pump a pulsed high-pressure XeCl excimer laser by coupling the microwave power from the primary waveguide into a secondary waveguide embracing the laser gas (45). The laser optical axis was parallel to the propagation of the microwave field. A tapered waveguide has also been used in pumping of a low-pressure CO_2-laser with 2.45 GHz microwave pulses (34). The gas was located in the tapered section and the optical axis was perpendicular to the propagation of the microwave field.

In the choice of ac-frequency the availability of rf-power sources should also be taken into consideration, since the development of a power source may be a rather large project. In section 3.7 it was concluded that at least 10 kW is required for pumping of a continuously-tunable CO_2-laser. Such high power ac sources are not readily available.

Up to about 30 MHz there exist several rf amplifiers which have been designed for use as short-wave transmitters (114, 115). Between 30 MHz and about 100 MHz there are few available high-power sources. FM broadcasting station amplifiers typically give 10 kW cw output in the 80–120 MHz band. Such an amplifier can probably be modified to an even higher peak-power pulsed rf-source (117). In the GHz frequency domain magnetrons with very high output power (~1 MW) and very good efficiency are available.

Perfect shielding of the laser and the power source can be difficult. To avoid interference with communication frequencies, it may be desirable to work within an industrial frequency band. Between 13 MHz and 10 GHz these are: 13.51 MHz ± 0.05%, 27.12 MHz ± 0.6%, 40.68 MHz ± 0.05%, 2.425–2.450 GHz, 5.725–5.875 GHz and 10–10.5 GHz.

In this work an ac-frequency of 40.68 MHz has been chosen for several reasons. Radiation from the discharge was considered to be unavoidable, at least under the experimental conditions. It was therefore chosen to use an industrial-band frequency. 40.68 MHz was chosen because it is the highest industrial frequency band below the GHz-domain. At 40 MHz the impedance matching may be accomplished by easily available lumped-circuit components, and the voltage across the discharge can be measured relatively accurately with a commercial high-voltage probe.

5.2 The high-pressure discharge chamber

The high-pressure discharge chamber is designed for at least 20 atm gas pressure. A cross-sectional view is shown in Figure 5.1. The base-plate and side-walls are made out of one block of aluminium. Holes are drilled through the block for water cooling. The top cover is made of 25 mm thick Lucite for visual observation of the discharge. The inner dimensions are 8 cm×6 cm bottom and 3 cm side-walls. This allows for 5–6 cm long electrodes. The electrode geometry shown in Figure 5.1 has been chosen for several reasons. Efficient cooling of the ungrounded electrode is provided by clamping it to the aluminium block with a Boron Nitride block as a spacer. Boron Nitride has reasonably high thermal conductivity and low dielectric constant, see Table 5.1. A preshaped Berullium Oxide block, which would have had even better thermal conductivity, could also have been used. The electrode geometry allows direct visual observation of the discharge from the top. The separation of the electrodes can

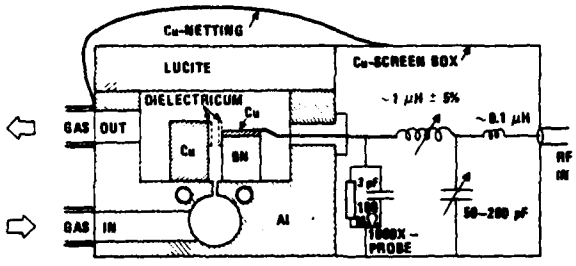

Figure 5.1 Cross-section of the high-pressure rf-discharge chamber and schematics of the impedance matching network

The 1000X high-voltage probe is a Tektronix P6015.

be varied continuously over a wide range. In the experiments, electrodes with various sizes, and both pure metal electrodes and electrodes covered with various dielectric materials have been tried.

The electrical feedthrough goes through a teflon bolt which is screwed into the aluminium side-wall.

The gas flows into the chamber through a 2 mm wide slit extending the full length of the electrodes. Two ZnSe windows are located on opposite side-walls perpendicular to the longitudinal axis of the discharge. In this way a CO_2-laser beam can be directed through the discharge region for measurement of the optical gain in the discharge. The ZnSe windows are 0.5 cm thick and anti-reflection (AR) coated for 10 μm radiation.

MATERIAL	HEAT CONDUCTIVITY $Wm^{-1}°C^{-1}$	DIELECTRIC CONSTANT @ 1 MHz – 10 GHz	DIELECTRIC CONSTANT @ 30 THz	DIELECTRIC STRENGTH kV/cm @ 60 Hz	DISSIPATION FACTOR	ELECTRIC RESISTIVITY 10^{16} Ω cm	REF
SAPPHIRE	0.38 @ 0°C 0.3 @ 100°C	9 – 11		480	0.00008 @ 10 GHz		130
ALUMINA	0.32 @ 0°C 0.3 @ 100°C	9 – 10	$(1.15 - i\,1.42 \cdot 10^{-2})^2$ n	100 – 240	0.0002		130 103 n 104 n
BeO	3.36 @ 0°C 2.1 @ 100°C	6.4 @ 1 MHz	$(4.2 \cdot 10^{-2} - i\,1.1)^2$ n	240	0.0001 – 0.0002		133 103 n 134 n
BORON NITRIDE							135
GRADE HP	0.67 @ 0°C ⊥ 0.61 @ 100°C ⊥ 0.4 @ 100°C ∥	4.1		375	0.001 @ 1 MHz		
GRADE A	0.23 @ 100°C ⊥ 0.44 @ 100°C ∥			310	0.0008		
PYREX	0.01 @ 0°C	4 – 6			0.01 – 0.001	0	136
COPPER	4.0 @ 27°C 3.9 @ 127°C					1.72	123
ALUMINIUM	2.2 @ 27°C 2.1 @ 127°C					2.82	123
STAINLESS STEEL	0.12					90	123

Table 5.1 Electrical and thermal properties of some materials

5.3 The high-pressure laser

The design of the high-pressure laser is similar to the design of the high-pressure discharge chamber. The laser is made of an aluminium base-plate and Lucite side-walls and top-cover. A picture of the laser with the side-walls and top-cover removed was shown in Figure 2.2. In Figure 5.2 the laser is shown with only the top-cover removed. (Also shown is the box containing the impedance matching network, which will be discussed in the next section.) The inner dimensions of the laser chamber are 27 cm × 8 cm bottom and 5 cm side-walls. The Lucite side-walls and top-cover are 2.5 cm thick.

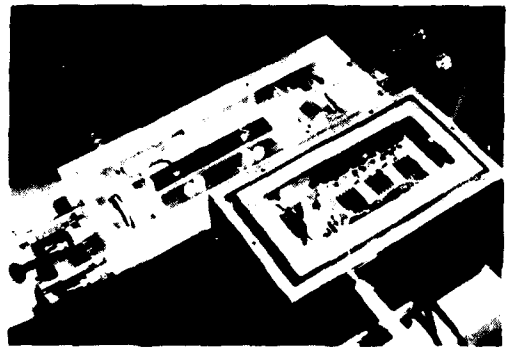

Figure 5.2 The high-pressure rf-excited CO_2-laser with screen-box and top-cover removed

Also shown is the box containing the impedance matching network.

The electrodes used in the experiments described in this report are 13.5 cm long. The ungrounded electrode is 2 mm wide. The waveguide is formed by polished sapphire ribbons (130) which are 15 cm long, 0.75 mm thick and 12.5 mm wide. The optical components in the resonator are mounted either onto Lucite brackets which are fastened to the electrodes, or to the baseplate. The alignment of the optical components can be adjusted from outside the chamber by means of six screwdriver pins which go through the chamber side-walls, with o-ring tightening. The screwdriver pins can be seen in Figure 5.2.

The optical components in the laser resonator shown in Figure 5.2 are an output-mirror on a piezoelectric translator (to the left) and an extra mirror, an etalon and a grating (to the right). The output from the laser resonator comes out of the laser chamber through a 0.75 cm thick ZnSe window. The window is AR-coated for 10 μm radiation. The window is tilted 5° from perpendicular to the resonator optical axis to avoid any feedback of the laser-output into the resonator.

5.4 The impedance matching network

In these experiments the problem of matching the complex impedance of the discharge and the laser head to the 50 Ω source was first studied for the high-pressure discharge chamber. An impedance matching network design which was found to be suitable for the high-pressure discharge experiments has also been used for the laser. Here this impedance matching network will be described. Numerical values are taken from the laser and the impedance matching network used for the laser.

The electrical characteristics of the discharge were considered in section 3.6.3. The electric equivalent circuit diagram of the laser head and the gas discharge is shown in Figure 5.3a. R is the discharge resistance and C_r is the capacity in parallel with R. Before gas breakdown, R is infinitely large. After gas breakdown R is typically 0.1 – 10 kΩ, depending on the input power, gas pressure and gas mixture. At 10 atm gas pressure, with a $CO_2 : N_2 : He$ gas mixing ratio of 2:2:96 and with ~7 kW input rf-power R~ 1 kΩ. The capacitive impedance $X_r = (\omega C_r)^{-1}$ in parallel with R is typically 1.5 kΩ. C_d is the capacity of the dielectric material on the electrodes and the dark space regions. $X_d = (\omega C_d)^{-1}$ is typically 300 Ω (0.75 mm sapphire ribbons and

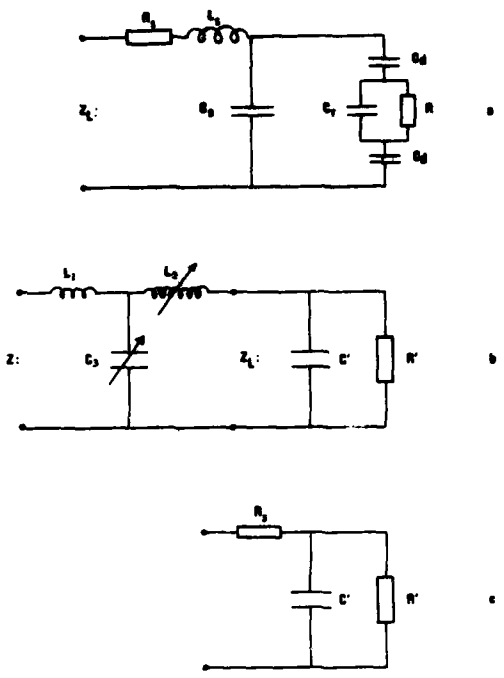

Figure 5.3 Electric equivalent circuits of the laser and the impedance matching network

The various impedances are described in the text.

a) *Electric equivalent circuit of the laser head*
b) The laser head (Z_L) and the impedance matching network
c) Electric equivalent circuit of the laser and the effective resistance R_s describing the power losses in the laser and in the impedance matching *network without the discharge*

0.1 mm dark space region with ϵ=1). C_s is a stray capacity between electrode and the rest of the laser structure. The stray capacity is much larger than the discharge gap capacity. $X_s = (\omega C_s)^{-1} = 250\,\Omega$ has been measured, which gives $C_s \sim 15$ pF. L_s is the inductance of the current loop from the electrical input contact to the ground, and R_s is an effective resistance in series with the discharge due to various losses in the network, see below. The skin-depth in copper is $\sim 10\,\mu$m (see section 3.6.6) and consequently $R_s \approx 0.8\,\Omega/m$ in a 1 mm diameter copper wire (123). This is a negligibly small value. Both L_s, and R_s due to the lead resistivity, can in practice be neglected.

The complex impedance Z_L of the network in Figure 5.3a can be described by a resistance R′ in parallel with a capacity C′, where R′ and C′ depend on all the impedances shown in Figure 5.3a. This is illustrated in Figure 5.3b.

The impedance Z_L can be transformed to the internal impedance $Z_0 = 50\,\Omega$ of the power source by a number of reactive networks (131). The network that has been used in the experiments described in this report is shown in Figure 5.3b. A tunable capacitor allows tuning of C_3 from $200\text{ pF} > C_3 > 50\text{ pF}$. ($20\,\Omega < X_3 < 80\,\Omega$, where $X_3 = (\omega C_3)^{-1}$). The inductance $L_2 \sim 1\,\mu$H is provided by a ~5 turn single-layer solenoid with diameter ~3 cm. L_2 is tunable typically ±5% by variation of the length of the solenoid. $L_1 \sim 0.15\,\mu$H.

By analysis of the network in Figure 5.3b it can be shown that under the condition

$$X_2 + X_3 + X_{C'} = 0 \qquad (5.1)$$

the impedance matching condition $Z = Z_0$ is satisfied for

$$X_3 \approx \sqrt{\frac{Z_0}{R'}}\, X_{C'} \qquad (5.2)$$

$$X_1 \approx \sqrt{\frac{Z_0}{R'}}\, X_2 \qquad (5.3)$$

It was noted above that the resistance in a 1-mm diameter copper wire could be neglected in these experiments. However there are other rf-power loss sources which should be taken into consideration. There will inevitably be radiation losses from the solenoids and the current loops in the impedance matching network. The electric and magnetic fields induce currents in the environments. Therefore metals with very low resistivity (copper, aluminium) and dielectric materials with low dielectric losses should be used in the laser and in the box containing the impedance matching network. Specifically iron, glass and Turbax should be avoided. In these experiments the impedance matching network is housed in a copper box, and the screening box for the laser is made of aluminium. An effective resistance $R_s \approx 1\ \Omega$ due to the losses in the network without the discharge has been measured in these experiments, see section 5.7.1. This resistance R_s can dissipate a significant portion of the rf-power incident on the discharge, see Figure 5.3c. This is because most of the current that goes through R_s passes through the capacity in parallel with the discharge when the capacitive impedances in parallel with the discharge are smaller than the resistivity of the discharge. Therefore it is important that the stray capacity C_s is as small as possible. An analysis of the circuit shown in Figure 5.3c (6) shows that for $R_s = 1\ \Omega$ usually less than 5% of the input power is dissipated in R_s in the experiments described in this report.

5.5 The rf-power source

The rf-power source is shown schematically in Figure 5.4. The output from a cw 40.68 MHz oscillator is attenuated by a variable attenuator for control of the final output power. The output from the attenuator is pulse-modulated by a modulator (a mini-circuit SRA-1 double-balanced mixer) driven by a variable-pulse generator. The output from the modulator is amplified by a 50 W, 47 dB gain amplifier (Ailtech model 5020, 1–200 MHz). Approximately 30 W peak-power maximum from the Ailtech amplifier is fed into eight "RF Power Labs" model V360 dc 500 W solid state amplifiers. These are originally designed for the 50–54 MHz radio-amateur band, and have been tuned down to 41 MHz by the manufacturer. They have been further modified here at the NDRE, and are driven with 40 V dc in class C operation. (They were originally designed for 28 V input and class AB operation.) Peak output power is approximately 7–8 kW. In Figure 5.5 is shown a picture of the rack containing the 50 W amplifier (at the bottom) the 40 V power-supply (in the middle) and the eight final-stage amplifiers. (At the top of the pile of amplifiers is an oscillator/modulator unit which has not been used in these experiments.)

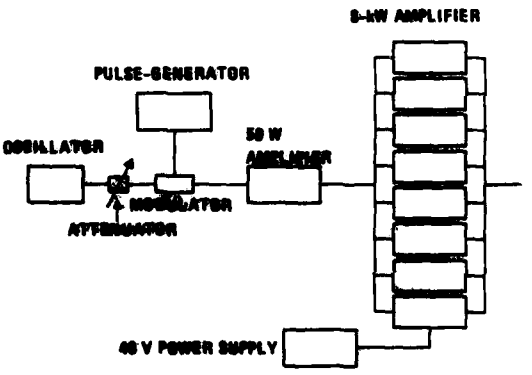

Figure 5.4 The rf-power source

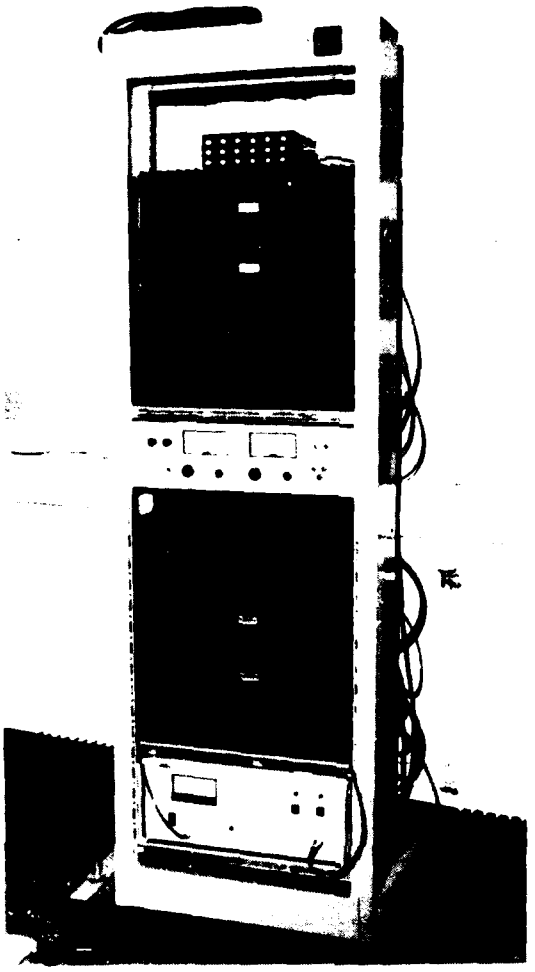

Figure 5.5 The rf-amplifier system

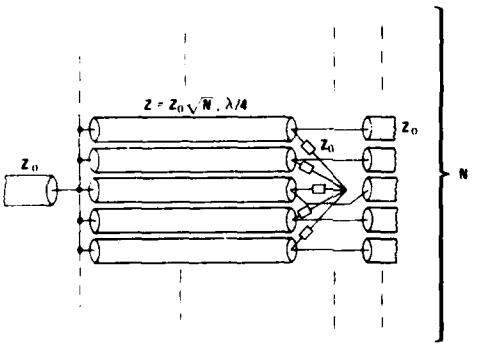

Figure 5.6 Wilkinson divider/combiner (after (132))

For feeding the rf-power from the 50 W amplifier into the eight final-stage units and for combining the output from the eight units, "Wilkinson dividers/combiners" (132) have been used. The diagram for an N-way Wilkinson divider/combiner is shown in Figure 5.6. Z_0 is the impedance at the input and output terminals. The N-way divider/combiner consists of N quarter-wavelength transmission lines (coaxial cables) with characteristic impedance $Z = Z_0\sqrt{N}$. At the N-way terminal side (to the right) the centre-conductors are connected to a common junction (not ground) with resistive loads equal to Z_0. When the one-terminal side (to the left) is terminated with an impedance Z_0, the impedance seen from each of the N terminals to the right will be equal to Z_0, regardless of what is the impedance of the (N−1) other terminals to the right.

In these experiments the 8-way power-splitter/combiner has been realized with two 4-way and one 2-way splitters/combiners at the input and output sides of the final stage amplifier.

From the output of the amplifier system the power is fed to the laser with an RG214U double braided 50 Ω coaxial cable.

5.6 The gas-handling equipment

The gas-handling equipment is shown schematically in Figure 5.7. It is designed for use both with gas recirculation and for blowing the gas through the discharge and out into the air.

When the gas is blown through the discharge and out, valve 1 (Figure 5.7) is closed and valves 2, 3 and 5 are open. The gas pressure is adjusted with the reduction valve on the gas bottle and the gas flow is adjusted with valve 4. Premixed gas mixtures on 10 l and 40 l bottles at up to 150 atm have been used. Before entering the discharge region the gas flows through a water-cooling system and through a gas filter (Matheson 6164, P4). The gas pressure is monitored with a pressure gauge (Vika, class 0.6) and the gas flow is monitored with a flowmeter (Fisher & Porter 10A1190 variable area flowmeter), downstream from the laser. The gas exit is through valve 5 and the vacuum pump.

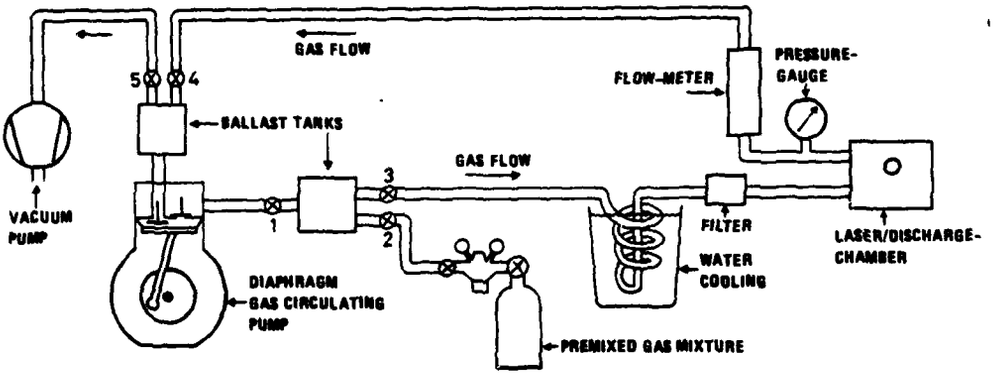

Figure 5.7 The gas handling equipment

When the gas is recirculated, the whole gas system is first evacuated with the vacuum pump to about 0.1 torr. The premixed gas mixture is circulated by the diaphragm pump (Dawson MacDonald & Dawson, UK, type D1416/657 Series 4). Maximum flow-rate is 20 l/min (by volume) and maximum pressure in the pump is 7 bar (gauge). The ballast tanks at the input and output of the pump are used to ensure a smooth gas flow through the laser. The gas flow-rate can bee adjusted by valves 3 and 4.

Textile armed rubber pipes (from Norgas A/S) are used between the various elements in the gas system. The pipes are flexible and do not collapse when the gas system is evacuated. Inner and outer diameter are 8 mm and 12 mm respectively.

The volume of the gas recirculation system is approximately 2.5 l.

5.7 Measurement techniques

5.7.1 Gas discharge characteristics

The gas discharge could be observed visually from the top through the Lucite top-cover both in the gas cell and in the laser. A copper netting was usually put on top of the gas cell for screening of the rf-radiation which is inevitably generated by the discharge and the electrical network. The aluminium screen-box on the laser had a copper netting on the top.

The input and reflected rf-power were measured with 40 dB directional couplers (Bird Thruline, series 4274 rf directional coupler plug-in elements). This was shown schematically in Figure 2.1 and can also be seen in Figures 5.8 and 5.9. The voltage across the electrodes in the gas cell was measured with a Tektronix P6015 1000X high-voltage probe. The probe was built into the impedance matching network and connected to the input wire as close to the discharge chamber as possible. This was shown schematically in Figure 5.1. The inductance in the current loop from the input to ground was negligibly small.

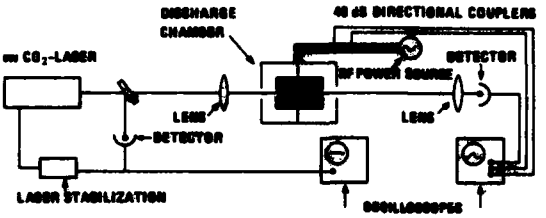

Figure 5.8 The experimental set-up for measurement of gain in the discharge

The reactive impedances of the laser head and the impedance matching circuit were measured with an rf vector impedance meter (HP 4815A). The effective R_s in series with the discharge (Figure 5.3c) was derived from measurement of the Q-value of the circuit in Figure 5.3b without the discharge. The circuit could be tuned into resonance, and the impedance was measured with the vector impedance meter.

5.7.2 Gain measurements

The experimental set-up for measurement of small-signal gain in the discharge is shown schematically in Figure 5.8. The linearly-polarized beam from a stabilized cw CO_2-probe-laser was directed through the discharge region in the high-pressure discharge chamber. The lens at the input side collimated the probe beam so the beam-waist through the discharge region was approximately 0.75 mm. The beam collimation length 2b was ≈9 cm (section 4.1.1). A 5 cm focal-length lens focused the transmitted beam on the detector (a Labimex R005 room-temperature CMT-detector).

There are several error sources in the gain-measurement experiments. Care must be taken so that the probe beam goes through the centre of the discharge region parallel to the electrodes, and that the whole beam-waist is well within the discharge cross-section. The heat, the electron density and the shock waves generated in the discharge cause fluctuations in the index of refraction of the discharge. This can deviate and spread the probe beam. When the probe beam is focused on the detector, some portion of the incident power is reflected back into the laser. This feedback to the probe laser causes fluctuations in the laser output. (This feedback disturbance of the probe laser could have been avoided by insertion of a quarter-wave-plate in the beam, but this has not been done).

It was observed that when the detector and the lens in front of it were not well aligned, the probe-beam signal was heavily disturbed by the discharge from the start of the discharge pulse till several hundred microseconds after the pulse had been turned off. No interpretation of gain was possible under these circumstances. When

the lens and the detector and the probe beam were well aligned, the probe-beam signal was constant between the discharge pulses. A photograph of the probe-beam signal during the discharge under these conditions is shown in Figure 6.10.

The detector that was used in the gain measurements had a frequency response varying typically from 45 mV/W at dc to 30 mV/W at 100 MHz. The large variation in the response versus frequency was not discovered until after the gain measurements had been performed. The detector has not been calibrated at the frequency adequate for the gain measurements. It is assumed that the response adequate for the gain measurements is close to the high-frequency response.

Because of all the measurement uncertainties described above, little weight has been put on the gain measurements in the work described in this report. The gain measurements were performed in an early stage of this work.

5.7.3 Laser-output and frequency tuning measurements

The experimental set-up for measurement of the laser-output power and the laser frequency is shown in Figure 5.9. The output from the laser is split by a ZnSe-wedge. The beam transmitted directly through the wedge is incident on a 1-meter grating spectrometer (Jobin Yvon HR1000). The frequency resolution (FWHM) of the monocromator is ~4 GHz, which is approximately 1/10 of the frequency separation between CO_2 line-centre frequencies. The beam reflected twice in the ZnSe wedge is focused onto a pyroelectric detector (Molectron P3-01). The fraction of the power incident on the wedge that reaches the pyroelectric detector is measured and calculated theoretically with good consistency. This provides a measurement of both the pulse-shape and absolute output power from the laser with the pyroelectric detector.

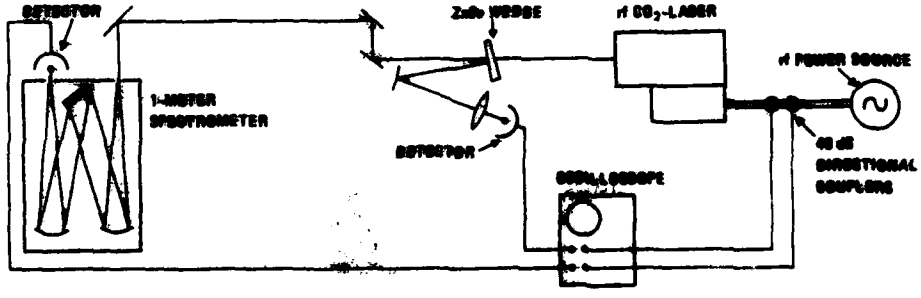

Figure 5.9 The experimental set-up for measurement of laser output power and laser frequency

The signals from the detectors and the 40 dB directional couplers are displayed either on a Tektronix 7603 or a Tektronix 7104 oscilloscope.

In Figure 5.10 is shown the experimental apparatus, including the 1-meter spectrometer (to the left), the table with the laser, the beam-handling optics and the pyroelectric detector (in the foreground), the rf-amplifiers (in the background to the right) and the rack containing the rf-pulse controls, 3 oscilloscopes, the regulation system for the cw CO_2-laser, the vector impedance meter etc (to the right).

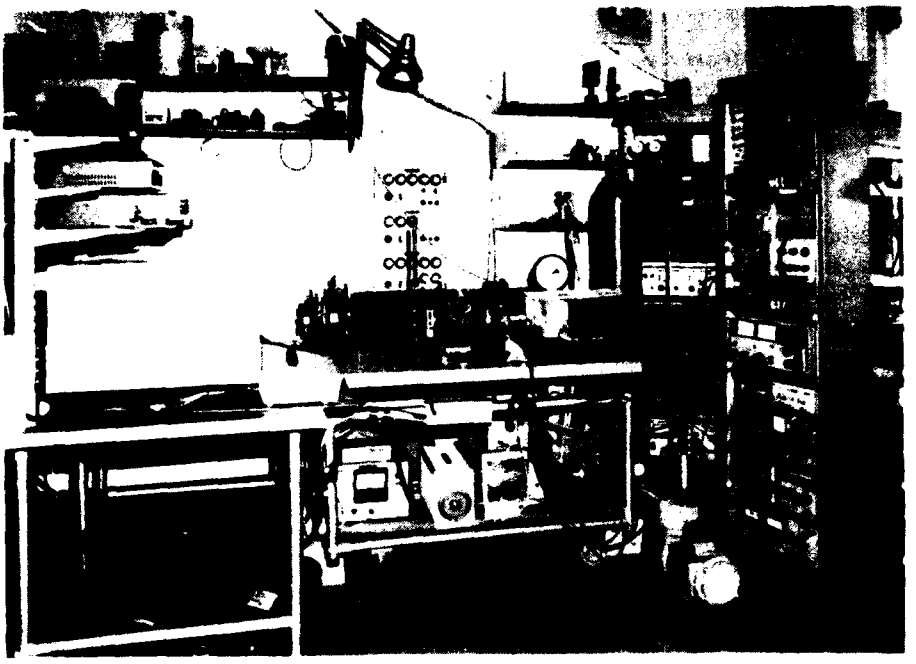

Figure 5.10 Photograph of the experimental set-up shown in Figure 5.9, see text

In the measurements of the high-frequency modulation of the laser output, the output beam was incident on the R005 CMT detector, which has a bandwidth of approximately 1 GHz. This is approximately equal to the frequency separation between two neighbouring resonance frequencies of the laser cavity. This experiment was performed in order to investigate whether the laser oscillated on two neighbouring resonator frequencies simultaneously. The same detector was used in heterodyne measurements where the output from the laser was mixed with the output from a cw CO_2-laser. This experiment was performed in order to measure the variation in the laser output frequency during the pulse and from pulse to pulse with better resolution than is obtainable with a grating spectrometer. The signals were displayed on a Tektronix 7104 oscilloscope.

6 EXPERIMENTAL RESULTS AND DISCUSSION

The goal of the experiments described in this report has been to investigate whether it is possible to develop a continuously tunable rf-excited CO_2-laser. As has been pointed out previously, the gas pressure required for continuous frequency tuning of a CO_2-laser between line-centre frequencies is approximately 10 atm when a single isotope is used (8) and 5 atm when a mixture of CO_2 isotopes is used (7).

The experimental results will be presented in four main sections. First will be presented and discussed typical characteristics of the rf-discharges between parallel plate electrodes. In Chapter 6.2 will be presented and discussed results from discharge experiments performed in order to attain a stable glow-discharge at 5–10 atm with long enough duration and with high enough rf-energy input-coupling to give sufficient gain for the pumping of a laser. In these experiments the stability and duration of the glow-discharge before a large number of arcs began to develop was measured for various gas mixing ratios and discharge geometries. Experiments were also made in order to determine the E/N ratio in the gas discharge and to measure the discharge impedance. These are central parameters in the description of the discharge, and they will be discussed in connection with the theory in Chapter 3. In section 6.3 will be presented laser performance characteristics for pressures up to 10 atm when a low-loss, non-tunable laser resonator is used. The results show laser output power, pulse shape and pulse stability which are typically obtainable with input rf-power levels up to 7–8 kW. They also show typical minimum input rf-power required to reach threshold for laser oscillation. The estimate of the small signal gain per rf pump energy made in section 3.7 will be compared to measurements of small signal gain and the measured rf pump power required to reach threshold for laser oscillation. In section 6.4 will be described experiments made in order to demonstrate continuous frequency tuning between line-centre frequencies. Several of the tunable resonators discussed in Chapter 4 have been investigated experimentally. No experiments have been performed to measure the total frequency range for which continuous frequency tuning can be obtained.

Several conditions have been common to the experiments. 40.68 MHz rf excitation frequency has been used throughout. In almost all the experiments a premixed gas mixture has been blown from a gas bottle through the discharge and out into the air without any precooling or preheating. The discharge pulse-repetition rate has been typically some hundred Hz. The gas flow transverse to the optical axis has been adjusted so that the gas in the discharge volume has been renewed approximately from between each pulse to between each second pulse. The discharge characteristics and laser output characteristics for various gas pulse-repetition rates and gas exchange rates will be discussed in section 6.3.4.

Preliminary experiments have been made with gas circulation in a closed gas system and with variation of the temperature of the gas and the electrodes between 8° and 30°C. The closed gas system was intended for continuous frequency tuning experiments at 5 atm pressure with a gas mixture containing $C^{12}O_2^{18}$ and $C^{12}O_2^{18}$. These experiments have not yet been performed. Results from the preliminary gas recirculation experiments will be presented and discussed in section 6.3.5.

Since all experiments have been aimed towards development of a continuously tunable rf-excited CO_2-laser, the results describing the gas discharge characteristics and laser performance are not at all complete.

6.1 Characteristics of rf-discharge between parallel plate electrodes

Visually the discharge appears typically as shown in Figure 6.1. Here the copper electrodes are covered by 1 mm thick polished alumina ribbons. The discharge volume is 55 mm x 2 mm x 1.5 mm (the discharge gap). The gas pressure is 5 atm and the gas mixing ratio of $CO_2 : N_2 : He$ is 5:5:90. Input rf-power is a few hundred watts. The picture shows several superimposed pulses.

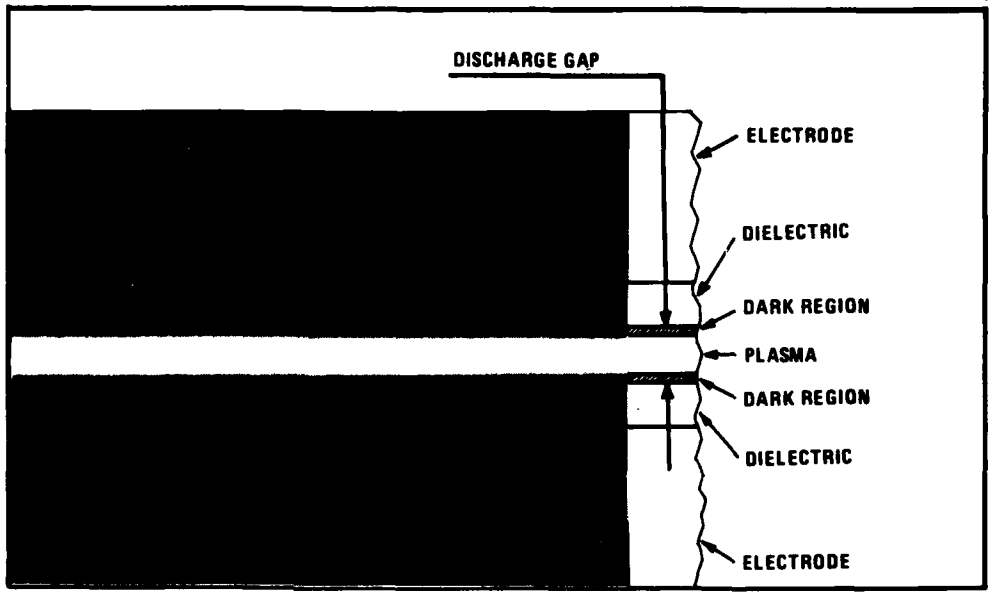

Figure 6.1 Photograph of typical rf-discharge between parallel plate electrodes
Gas pressure is 5 atm. The electrodes are covered with 1 mm thick polished alumina-ribbons. The discharge gap is 1.5 mm.

The dark space regions between the dielectric "electrodes" and the plasma region are clearly seen in Figure 6.1. The widths of the dark space regions are approximately 0.13 mm and thus they occupy approximately 15–20% of the volume between the electrodes.

Typical electrical characteristics of the discharge are shown in Figure 6.2. Cuves A and B show the input rf-power and the rf-power reflected from the discharge, respectively. Curve C shows the voltage across the electrodes. The electrodes, the discharge gap, the gas pressure and gas mixing ratio are the same as in Figure 6.1. The input rf-power is 1 kW and pulse repetition rate is 1 kHz.

Approximately 1.5 μs after the beginning of the rf-pulse the gas has been "broken down" to a homogenous glow discharge. It is seen from curve B that after this point perfect input power coupling is achieved. Less than 1% of the input rf-power is reflected back towards the power source. It is seen from curve C that the voltage amplitude across the electrodes at gas breakdown is approximately 7.5 kV. Assuming that the conduction current in the discharge is very small at that point, this voltage amplitude corresponds to an electric field strength amplitude E_0 = 44 kV/cm or $E_0/N = 3.5 \cdot 10^{-16}$ Vcm^2 in the gas.

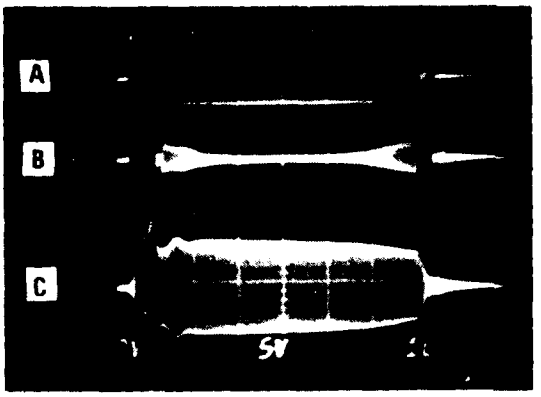

Figure 6.2 Electrical characteristics of the rf-discharge

A is the input rf-power (5 V/div) and B is the rf-power reflected from the discharge (2 V/div), measured with 40 dB directional coupler elements, see Figures 2.1, 5.8 and 5.9. C is the voltage across the electrodes, measured with a Tektronics P6015 1000X high-voltage probe (5 V/div). Input power is approximately 1 kW. Gas pressure is 5 atm, the discharge gap is 1.5 mm, and the electrodes are covered with 1 mm thick polished alumina-ribbons. Gas mixture is 5:5:90 of CO_2:N_2:He.

Figure 6.3 Picture of the rf-discharge with a few arcs

Discharge gap is 1 mm and gas pressure is 5 atm

It is also seen from Figure 6.2 that after about 5 μs from the start of the input power pulse there is an increase in the power reflected from the discharge (curve B). Also, the voltage across the discharge drops (curve C) and the input power is slightly reduced (curve A). This is caused by an increasing number of arcs building up in the discharge. The arcs lower the impedance of the discharge. This change in discharge impedance causes impedance mismatch and consequently more power is reflected from the discharge back to the power source.

Visually the arcs appear like narrow strings flickering around the whole electrode length and extending the full gap between the electrodes. A few arcs are shown in Figure 6.3. When the power reflected from the electrodes increases as it does in Figure 6.2 at the end of the pulse, the number of arcs is much larger than shown in Figure 6.3. It looks like small arc discharges and a glow discharge can exist simultaneously in the rf discharge. This cannot be determined from Figure 6.3 since the arcs develop primarily at the end of the pulse and the picture in Figure 6.3 is exposed over a much longer period than one pulse duration. It is observed visually that when the gas pressure and input power are increased, a few arcs seem to be present even for very short duration pulses. From the measurements of small signal gain and laser performance, these few small arcs do not seem to seriously affect the small signal gain and laser performance. However, when a considerable number of arcs begin to develop so that the discharge impedance is altered like at the end of the pulse shown in Figure 6.2, this is observed to be detrimental to the pumping of the upper laser level and the laser performance. It has thus been necessary to optimize the gas mixing ratio and discharge geometry so that the time from gas breakdown until a considerable number of arcs begin to develop is as long as possible, in order to be able to integrate enough power to reach threshold for laser oscillation. These experiments will be described in the next section.

6.2 Results from gas discharge experiments

The experiments described in this section have been made with the high-pressure discharge chamber described in section 5.2. The electrode length is 50–60 mm and the electrode width 2 mm.

Stable glow discharges could be obtained up to at least 5 atm gas pressure with only polished copper electrodes without any dielectric ribbons on them. In this case striking the glow discharge was more difficult and the rf-power that could be deposited in the discharge before arcing was much less compared to when the electrodes were covered with dielectric ribbons. When pure metal electrodes were used, the onset of arcing usually terminated the glow discharge completely and all the subsequent pulses were arc discharges. Thus in the following only gas discharge experiments where dielectric "electrodes" have been used will be described.

6.2.1 Time before arcing for various gas mixing ratios

In these experiments only equal portions of CO_2 and N_2 in the gas mixtures have been used. This is because according to (49) equal portions of CO_2 and N_2 are best for maximum small signal gain. Equal portions of CO_2 and N_2 are used in most high-pressure CO_2 lasers (8, 22, 27, 49–52). The most common $CO_2 : N_2 : He$ mixing ratios at multiatmospheric pressures are 10:10:80 and 5:5:90. The time from gas breakdown to formation of considerable amounts of arcs depends strongly on the content of CO_2 and N_2. This is shown in Figure 6.4a and 6.4b.

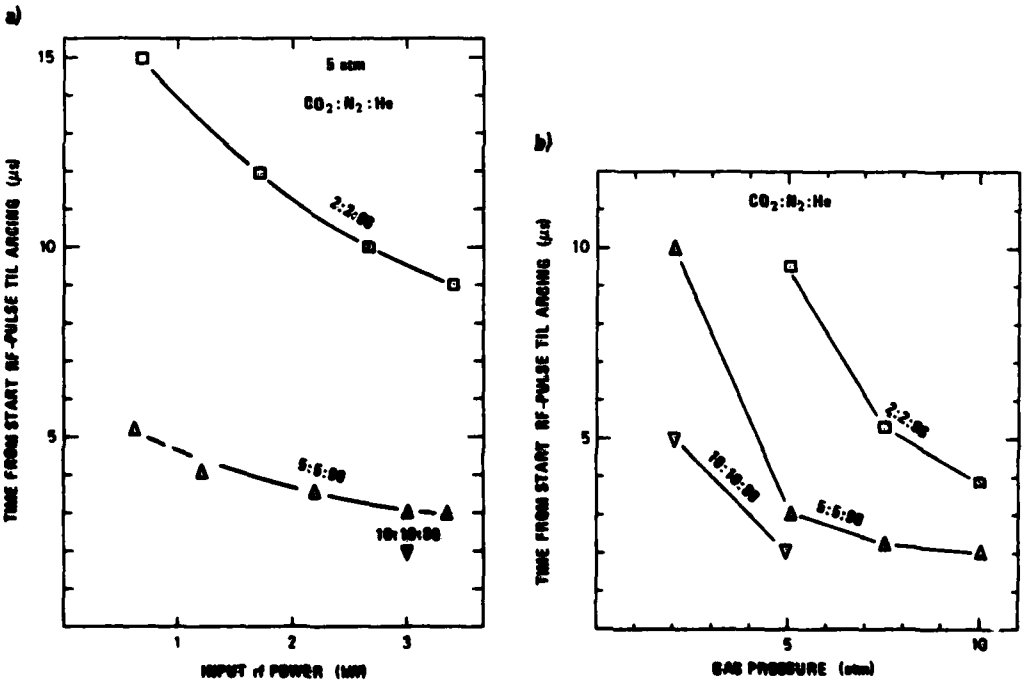

Figure 6.4 *Time from start of input rf pulse till developement of large number of arcs*
Development of arcs is taken to occur when there is an increase in the power reflected from the discharge, see Figure 6.2.

a) Time before arcing for various $CO_2 : N_2 : He$ gas mixing ratios, versus input rf-power. Gas pressure is 5 atm. The gas volume is 50 mm x 2 mm x 1.5 mm (the discharge gap). The electrodes are covered with 0.5 mm thick polished sapphire-ribbons

b) Time before arcing for various gas mixing ratios versus gas pressure. Input rf-power is 3 kW. The discharge geometry is the same as in Figure 6.4a.

Figure 6.4a shows measurements of the time from the start of the discharge pulse till there is a significant increase in the power reflected from the discharge because of considerable formation of arcs, see Figure 6.2. The gas pressure is 5 atm. The discharge gap is 1.5 mm and the electrodes are covered with 0.5 mm thick polished sapphire ribbons. The gas exchange rate is approximately 250 Hz and the pulse repetition rate approximately 400 Hz. It is clearly seen that the time before arcing increases with decreasing CO_2 and N_2 content. In a discharge with pure He no arcs were observed for pulse durations longer than several tens of microseconds.

Figure 6.4b shows the time before arcing versus gas pressure for various gas mixing ratios. The discharge geometry is the same as in Figure 6.4a. The input rf-power is 3 kW. The input power density is comparable to what has been used in the laser. It is clearly seen how the time before arcing decreases with increasing gas pressure. The gain decay time constant is approximately 30 $\mu s \cdot$atm, see sections 3.2.2 and 6.2.5. Thus in Figure 6.4b only the glow discharge with the 2:2:96 gas mixing ratio lasts longer than the gain decay time constant.

6.2.2 Time before arcing for various discharge geometries

It was shown in Figure 3.16 that the glow discharge should last at least 2–3 times the gain decay time constant in order to minimize the rf-power required to reach the threshold for laser oscillation. This is not the case for any of the gas mixtures in the measurements illustrated in Figure 6.4a and 6.4b for the relevant input power densities. Longer duration glow discharge could be obtained by using even less CO_2 and N_2 than in the 2:2:96 mixture. However, laser experiments indicated that the small signal gain in a 1:1:98 mixture was significantly lower than in the 2:2:96 mixture for relevant pump power densities. Experiments were therefore made with various discharge geometries in order to maximize the glow discharge duration for the 2:2:96 gas mixture.

It was expected that a dielectric material on the electrodes with high thermal conductivity and low electric capacity for large ballasting would be the best for long duration glow discharge, see section 3.6. Large electric ballasting would be provided by a thick dielectric ribbon with low dielectric constant. Experiments have been made with 0.5 mm thick polished sapphire, 1 mm thick polished alumina and 1 mm thick cover glass on the electrodes. The thermal and dielectric properties of sapphire and alumina were shown in Table 5.1. Measurements of glow discharge durations at 10 atm gas pressures with these various dielectrics on the electrodes are shown in Figure 6.5. The gas mixing ratio is 2:2:96 of $CO_2 : N_2 :$ He. The gas exchange rate is approximately equal to or faster than the 250–400 Hz pulse repetition rate for all but one of the measurement series, which is indicated in Figure 6.5. The discharge gap is 1.2 mm or 1.5 mm. The results are shown versus input power density. The glow discharge duration before arcing was approximately constant for fixed input power density and dielectric material when the discharge gap d was varied from 1 mm to 1.5 mm.

It is clearly seen that the longest glow-discharge duration before arcing is obtained with the 1 mm thick alumina ribbons on the electrodes. A comparison between the experiments with 1 mm alumina and 0.5 mm sapphire shows the main effect of increasing the thickness of the dielectric, since the dielectric and thermal properties of these materials are close, see Table 5.1. The largest discharge ballasting is obtained with the 1 mm thick cover-glass ribbon, since this has the smallest dielectric constant. However, the thermal conductivity of glass is much poorer than for Al_2O_3. (It should also be noted that glass has larger dielectric losses than Al_2O_3). From Figure 6.5 can also be seen the effect of various gas exchange rates relative to the pulse repetition rate. The "bottom" curve with 0.5 mm thick sapphire plates is taken with

gas exchange rate approximately half of the pulse repetition rate. In the other curve with 0.5 mm thick sapphire the gas flow rate is significantly higher than the pulse repetition rate. In this latter case the glow-discharge duration is significantly longer. This will be commented on further in section 6.3.4.

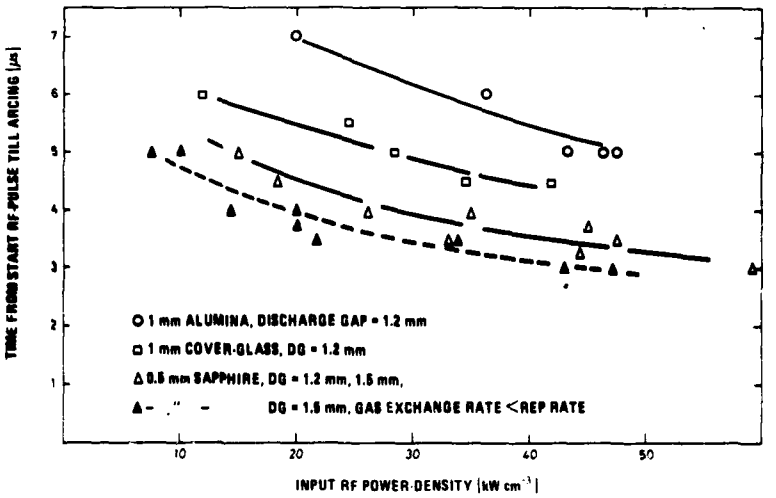

Figure 6.5 Time from start of input rf-pulse till developement of large number of arcs, for various dielectric ribbons on the electrodes

Gas pressure is 10 atm. $CO_2 : N_2 : He$ gas mixing ratio is 2: 2: 96. The gas exchange rate is faster than the pulse repetition rate for all measurement series except for the one indicated.

It would have been of interest to try other dielectric materials at several thicknesses to maximize the glow discharge duration. Especially is it expected that BeO would be superior to all the materials described above because it has much higher thermal conductivity and a lower dielectric constant than Al_2O_3, see Table 5.1. Boron nitride should also be a good material (Table 5.1).

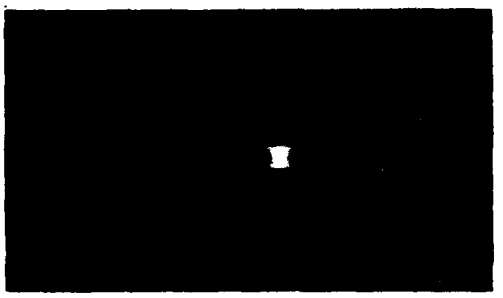

Figure 6.6 Constricted glow-discharge

Gas pressure is 5 atm and discharge gap is 1.5 mm

Glow-discharge experiments have been performed with discharge gaps between 0.5 mm and 2 mm. Measurements of the glow discharge duration have been made with discharge gaps between 0.9 mm and 1.5 mm. In these experiments no significant difference in the glow discharge duration for fixed input power density (kW/cm^3) has been observed. When the discharge gap was larger than 1.5 mm, when the gas exchange rate was considerably slower than the pulse repetition rate and for high input power levels, the discharge tended to be confined to a narrow glow discharge extending the full gap between the electrode, that is, with no dark space region. Such a discharge is shown in Figure 6.6. This discharge is no arc discharge, the voltage- current characteristic is that of a glow discharge. No optical gain measurements or laser experiments have been performed with such a discharge.

6.2.3 Electrical characteristics of the discharge

It was shown in Figure 6.2 that at the start of the discharge pulse the voltage across the electrodes rises to a certain level and then drops to a constant lower value. Before the voltage has reached its maximum value a large fraction of the rf-power incident on the electrodes is reflected. When the voltage has stabilized, a steady state situation is obtained where perfect input coupling efficiency is obtained. Gas breakdown, that is, when the charge density in the gas drastically increases from approximately zero, is assumed to occur at the point where the voltage across the electrodes is at its maximum value in Figure 6.2.

The electric field strength in the gas at gas breakdown can be calculated from the measurement of the breakdown voltage under the assumption that the plasma conductivity still is very low at this point. In Figure 6.7 are shown E_0/N ratios at gas breakdown from measurements of the breakdown voltage for various gas mixing ratios. E_0 is the electric field strength amplitude, and N is the neutral particle density. In all these measurements the gas exchange rate has been lower than the 400 Hz pulse repetition rate. In a few cases the gas exchange rate was increased to above the pulse repetition rate without any significant increase in the breakdown voltage taking place. The bars indicate variations in the measured voltage at 5 atm and 10 atm gas pressure for various input power levels, pulse repetition rates and discharge gaps between 1.0 mm and 1.5 mm. For the 10: 10: 80 gas mixing ratio only one measurement has been made at 5 atm.

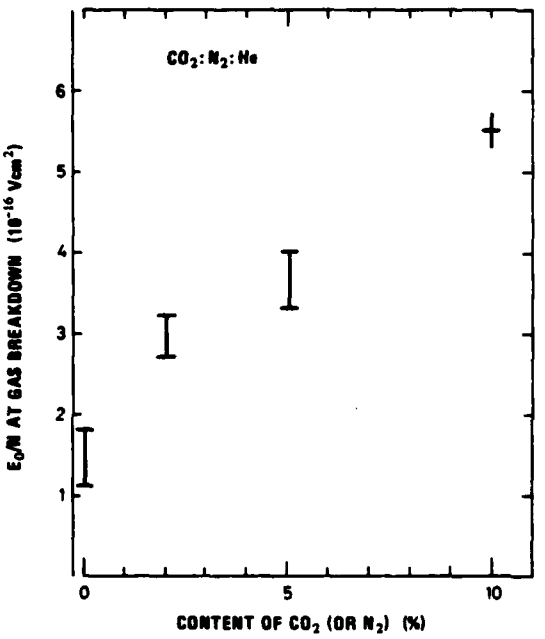

Figure 6.7 *E_0/N ratio (electric field strength amplitude/neutral particle density) at gas breakdown versus content of CO_2 in the gas mixture*

The gas mixtures of $CO_2 : N_2 : He$ contain equal portions of CO_2 and N_2, and the rest is He. The bars indicate variations in the measured E_0/N at 5 atm and 10 atm gas pressure for various input power levels, pulse repetition rates, and discharge gaps between 1.0 mm and 1.5 mm.

It is clearly seen from Figure 6.7 that the E_0/N at gas breakdown depends strongly on the gas mixing ratio. No attempts have been made in this work to calculate ionization and electron loss coefficients from the measured E_0/N ratios at gas breakdown.

In Figure 6.8 is shown the E_0/N for various discharge gaps. The gas mixing ratio of $CO_2 : N_2 : He$ is 2: 2: 96. The electrodes are covered with 0.5 mm sapphire or 1 mm alumina. The gas exchange rate is faster than the pulse repetition rate.

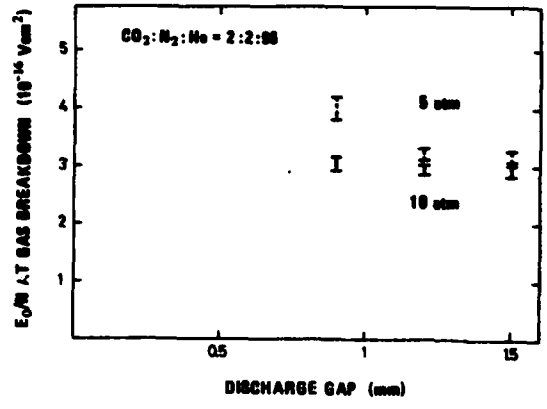

Figure 6.8 *E_0/N ratio (electric field strength amplitude/neutral particle density) at gas breakdown for various discharge gaps*

The gas pressure is 5 atm (upper points) and 10 atm (lower points), and the gas mixing ratio is 2:2:96 of $CO_2:N_2:He$.

It is seen from Figure 6.8 that for discharge gaps d = 1.5 mm and d = 1.2 mm the E_0/N at breakdown are approximately equal. At d = 0.9 mm the E_0/N is larger, especially at 5 atm gas pressure. According to equation (3.5) the electron displacement peak-to-peak is 0.8 mm for $E_0/N = 4 \cdot 10^{-16}$ Vcm^2 assuming $\nu_m = 1.75 \cdot 10^{12}$ s^{-1} atm^{-1}. Thus the increase in E_0/N for gas breakdown at d = 0.9 mm can possibly be explained by the discharge gap becoming close to the electron displacement.

In Figure 6.9 is shown the voltage amplitude across the electrodes after gas breakdown, when the voltage amplitude has stabilized. The voltage is shown versus input rf-power at 5 atm and 10 atm gas pressures for various gas mixing ratios. The discharge gap is 1.5 mm and the electrodes are covered with 0.5 mm sapphire ribbons. The gas exchange rate is slower than the 400 Hz pulse repetition rate.

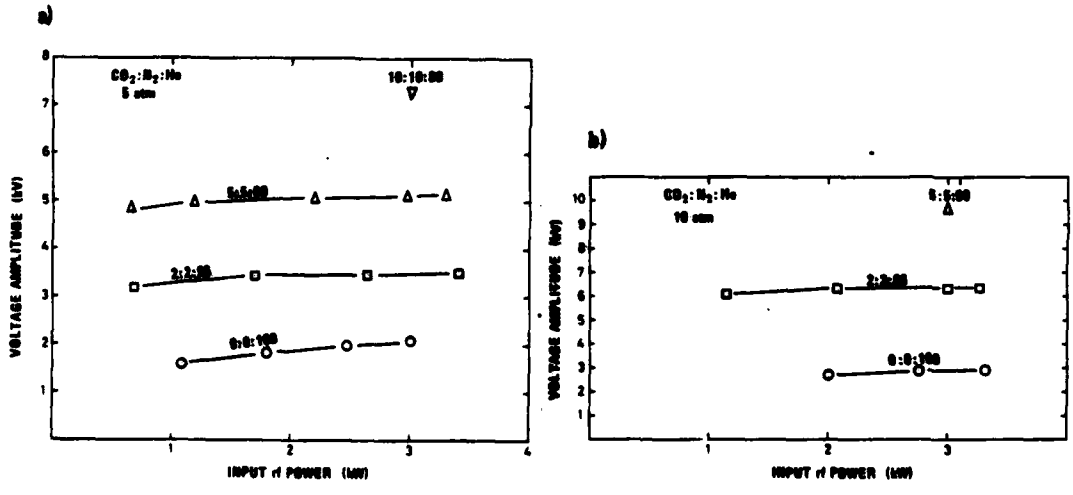

Figure 6.9 *Voltage amplitude across the electrodes when the discharge has stabilized*

Values are shown for various $CO_2:N_2:He$ gas mixing ratios. Discharge volume is 50 mm x 2 mm x 1.5 mm (discharge gap), and the electrodes are covered with 0.5 mm polished sapphire-ribbons.

a) gas pressure is 5 atm

b) gas pressure is 10 atm

It is seen that the steady state voltage depends on the gas mixing ratio in approximately the same manner as the breakdown voltage does, see Figure 6.7. It is also seen that the voltage does not vary much with the input power level. This indicates that the resistance of the plasma is larger than the capacitive impedance in series with the discharge, see Figure 3.13.

The E/N ratio in the glow discharge cannot be determined as straightforwardly as at gas breakdown. The voltage across the electrodes depends on the input rf-power, the resistance of the plasma and the capacities of the plasma region, the dark space region and the dielectric, see Figure 3.13 or 5.3. In the experiments performed with the high-pressure discharge chamber the reactive impedance X_R in parallel with the plasma resistance R is approximately 4 kΩ for a 1 mm thick plasma region. The reactive impedances of the dielectric and the dark space regions are approximately 200–400 Ω, assuming 0.5 – 1 mm thick dielectrics of Al_2O_3 and 0.1 mm thick dark space regions. From measurements of the voltage across the electrodes, the plasma resistance R and the voltage across the plasma region can be calculated by using the electric equivalent circuit diagram shown in Figure 3.13 or 5.3 when the reactive impedances are known. The equation is of second power in R. Since R in general decreases with increasing input rf-power, one of the two solutions can be excluded.

R and E/N in the glow discharge have been derived from measurements of the voltage across the electrodes and the power dissipated in the discharge at 10 atm gas pressure for a discharge volume 5 cm×2 mm×1.2 mm (discharge gap). The electrodes were covered with 0.5 mm thick sapphire ribbons and the gas mixing ratio of $CO_2 : N_2 : He$ was 2:2:96. At 2 kW input power R was found to be 3.5 – 4 kΩ. According to equation (3.13) this corresponds to an electron density $n \approx 1.7 \cdot 10^{12}$ cm^{-2}. R was found to be approximately inversely proportional to the input rf-power, which was varied from about 2 kW to 7 kW. The E_{rms}/N ratio, where E_{rms} is the root-mean-square electric field strength in the plasma region, was found to be $1.0 - 1.2 \cdot 10^{-16}$ Vcm^2 for 2–7 kW input rf power. In a measurement with the 10:10:80 gas mixing ratio at 5 atm and with a discharge gap of 1.5 mm, the resistance R was found to be approximately 5 kΩ for 3 kW input power. The E_{rms}/N ratio was found to be approximately $2.5 \cdot 10^{-16}$ Vcm^2.

In (67) is measured the E/N in a pulsed dc-excited self-sustained glow discharge for a 10:10:80 gas mixture of $CO_2 : N_2 : He$ at 7–13 atm to be $2.5 \cdot 10^{-16}$ Vcm^2. Below 1200 torr E/N = $2.7 \cdot 10^{-16}$ Vcm^2 has been measured (68, 137). These values are close to the E_{rms}/N that has been measured in this work for the same gas mixture at 5 atm. It is thus reasonable to assume that the dominating electron loss mechanism in the rf-discharge described above is attachment loss, as in (67, 68, 137) for this gas mixing ratio. This was also expected, see section 3.4. According to (54) the E/N ratio for most efficient pumping of the upper laser level in CO_2 is $1.2 \cdot 10^{-16}$ Vcm^2 for a $CO_2 : N_2 : He$ gas mixing ratio of 10:10:80. It seems reasonable to assume that the E/N for efficient pumping of the upper laser level is lower but close to this value for the 2:2:96 gas mixing ratio, see (54) and section 3.3. Thus, from the measurement and derivations described above one should be able to draw the conclusion that the rms-value of the E/N ratio in the rf glow discharge is close to what is good for efficient pumping of a CO_2 laser. This is also indicated by the gain measurements and laser performance measurements described in the following sections.

In this report the electric field strength in the glow discharge has not been derived for the various discharge geometries, gas mixing ratios, gas pressures and input power levels, for one thing because the width of the dark space regions has not been measured under the various conditions. It is expected that several parameters concerning the electron production and loss rates could be determined from such measurements of the E/N ratio in the discharge, see section 3.4.

6.2.4 Gain measurements

The gain was measured with a 200 mW cw CO_2 probe laser oscillating on the R(18) line at 10.28 μm. Figure 6.10 shows the amplified probe laser beam after propagation through the discharge at 5 atm gas pressure. The discharge gap is 1.5 mm and the $CO_2:N_2:He$ gas mixing ratio is 5:5:90. Input rf power is 1 kW in 4 μs.

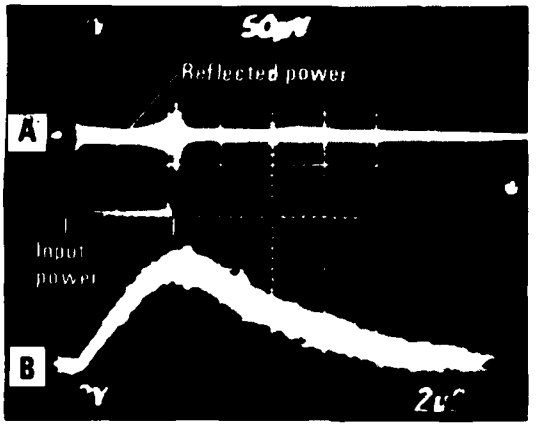

Figure 6.10 Measurement of small-signal gain
A) Input and reflected rf-pulses from ~ 40 dB directional couplers (2 V/div)
B) Amplified probe-laser beam (R(18) 10.4 μm band). (50 μV/div). Input rf-power is approximately 1 kW, and peak small signal gain is 1.0–1.5 %/cm (see text). Discharge volume is 55 mm x 2 mm x 1.5 mm. Gas mixture is 5:5:90 of $CO_2:N_2:He$.

As was pointed out in section 5.7.2 the detector response has not been determined precisely at the frequency relevant for the gain measurements. Assuming the response of the detector in the gain measurements is equal to the response at several MHz, the peak small signal gain in the measurement shown in Figure 6.10 is 2.8%/cm. Figure 6.10 is representative for all the gain measurements performed at 5 atm with the 5:5:90 gas mixture. According to predictions of the small signal gain pr input rf-power density made in section 3.7, the peak small signal gain in the experiment described above should be 2.15%. All the input rf-power is then considered to be deposited in the plasma region occupying 85% of the volume between the electrodes, see Figure 6.1. The gain decay time-constant was taken to be 30 μs atm, see below. Thus the measured peak gain is 30% larger than expected.

As was pointed out in section 5.7.2, the gain measurements have several possible error sources. In the experiments described above control measurements were made with a gas containing only He. When the probe-beam and the detector were well aligned, no variation in the probe-beam signal during the discharge was observed.

The peak small signal gain pr input rf-power density will be discussed further in section 6.3.3 in connection with measurements of input power threshold for laser oscillation.

Figure 6.10 also shows the gain decay after the rf-power has been turned off. The time for the gain to have decayed to e^{-1} times the maximum value has been measured between 1 and 5 atm for the 5:5:90 gas mixing ratio to be 30 μs atm, inversely proportional to the gas pressure. According to equation (3.1) and the discussion in section 3.2.2 the gain decay time-constant was expected to be 31.4 μs atm. This corresponds very well with the measured values.

6.3 Laser output characteristics

6.3.1 Typical pulse shape characteristics and pulse-to-pulse stability

Figure 6.11 show typical laser output pulses at 5 atm and 10 atm gas pressure. The gas mixing ratio of $CO_2 : N_2$:He is 2 : 2 : 96. Each pulse has the form of a gain-switched spike approximately 300 ns long, followed by a tail at lower power. At 5 atm gas pressure relaxation oscillations following the gain-switched spike can be clearly seen. At 5 atm the tail has an approximately constant power level till the input power pulse is turned off. For input-power pulse lengths longer than shown in Figure 6.11 the output pulse would eventually self-terminate. At 1 atm gas pressure, pulse tails longer than 80 μs have been measured. At 10 atm the relaxation oscillations are not observed and the pulse tail is much shorter than at 5 atm.

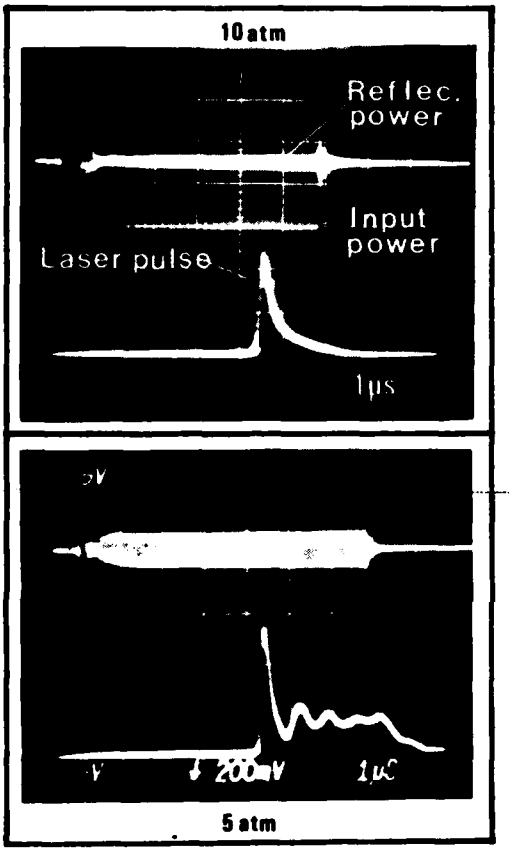

Figure 6.11 Typical laser output pulses at 10 atm (above) and 5 atm gas pressure (below)
The pictures show superpositions of 5–10 pulses.

In Figure 2.3 was shown laser output pulses at 10 atm for a gas mixing ratio of 1:1:98, and 2 kW input rf power. Here the pulse tail is longer than at 10 atm in Figure 6.11. In general it was observed that the higher the gas flow the longer duration would the pulse tail have. No systematic experiments have been performed in order to measure pulse shapes for various gas mixing ratios and gas flow rates.

Figures 2.3 and 6.11 show superpositions of approximately 10–20 consecutive laser output pulses. The oscilloscope sweep trace is triggered by the input rf pulse. The pictures illustrate typical pulse-to-pulse stabilities.

Figure 6.12 shows 17 superposed laser output pulses at 10 atm gas pressure. The gas mixing ratio is 2:2:96, the pulse repetition rate 250 Hz, the input rf-power ~7 kW and the discharge gap 1.2 mm. The laser resonator consists of a grating, an etalon, an extra mirror and a 0.5% transmission output coupler. The wavenumber of the laser radiation is 971.3 cm^{-1}, which is between the R(12) and R(14) line at 10.2 μm. The oscilloscope trace is triggered by the laser pulse. The full width at half maximum of the peak pulse shape is seen to be 300 ns. In Figure 6.12 the laser resonator has been carefully adjusted and the pulse repetition rate relative to the gas exchange rate has been optimized for maximum pulse-to-pulse stability. This will be commented later. Figure 6.12 represents the best pulse-to-pulse stabilities which have been obtained at 10 atm with a tunable resonator in these experiments. It should be noted that some of the output pulse-to-pulse variations seen in Figures 6.11 and 6.12 are caused by variations in the input rf-power level.

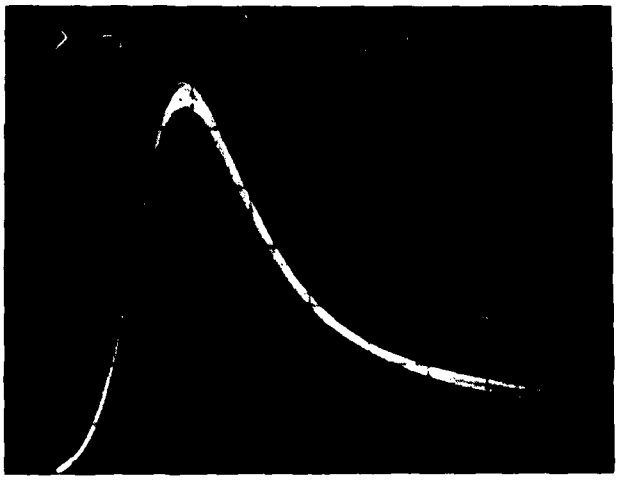

Figure 6.12 Superposition of ~ 17 laser-output pulses at 10 atm gas pressure

6.3.2 Peak output power

In Figure 6.13 is shown the peak laser output power versus input rf-power for 5 atm and 10 atm gas pressures. Also shown is the time delay from the start of the input rf-pulse till the laser output pulse. The laser output mirror is a plane dielectric coated Ge mirror with 2% transmission. It is mounted as close to the waveguide as possible. The other laser mirror is a dielectric coated ZnSe mirror with 0.75 m radius of curvature and it is mounted approximately 2 mm from the other end of the waveguide. The pulse repetition rate is 200 Hz. The gas exchange rate is approximately equal to the pulse repetition rate. The discharge gap is 1.5 mm and 1.2 mm at 5 atm and 10 atm respectively. The frequency of the laser output has not been determined.

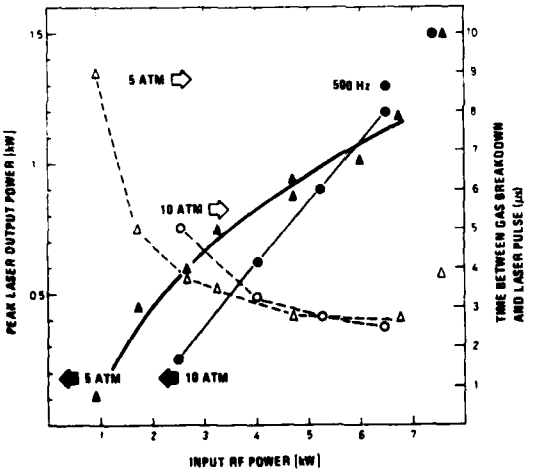

Figure 6.13 Peak laser-output power, and time between gas-breakdown and start laser-pulse, versus input rf-power at 5 atm and 10 atm gas pressures

Discharge gap is 1.2 mm at 10 atm and 1.5 mm at 5 atm. Output-coupler transmission is ~ 2 %. The gas mixing ratio of CO_2: N_2: He is 2: 2: 96.

At 10 atm for 6.2 kW input power is also shown the peak output power when the pulse repetition rate and the gas exchange rate have been increased to 500 Hz. It is clearly seen that the peak output power is higher in this case. When the measurement series shown in Figure 6.13 were performed, the rf-power source did not give out more than about 6.5 kW peak rf-power. Both at 5 atm and 10 atm the laser has given about 1.5 kW peak output for approximately 7.5 kW peak input rf-power. These values are incorporated in Figure 6.13. At 10 atm gas pressure a laser efficiency (laser output energy/input rf-energy) of approximately 2% has been measured for a 300 ns duration pulse. No experiments have been performed in order to maximize the laser efficiency.

6.3.3 Estimate of small signal gain

In section 3.7 an estimate was made of the rf-power required for pumping a continuously tunable rf-excited CO_2 laser. The estimate was based on the assumption that input energy densities of 12.5 J/l atm, 10 J/l atm and 7 J/l atm would give a peak small-signal gain of 0.5%/cm at 1 atm, 5 atm and 10 atm gas, respectively. Corrections were made for the duration of the pump pulse relative to the gain decay time-constant, which was taken to be 30 μs atm.

It will be seen from Figure 6.13 that the input rf-power threshold for laser oscillation is approximately 2 kW at 10 atm gas pressure. According to the estimates of the gain per input rf-power made in section 3.7, and assuming the gain is a linear function of the input energy density, the round trip gain in the resonator for the 2.5 kW input power measurement shown in Figure 6.13 would be ~4–4.5% when the laser starts to oscillate. The decay time constant is taken to be 3–3.5 μs. (The gas mixing ratio is not the same as in the gain measurements described in the previous section. According to equation (3.1) and the discussion in section 3.2.2, the gain decay time-constant would be 36 μs atm for the 2:2:96 gas mixture ratio.) All the input rf-power is considered to be deposited in the plasma region occupying ~85% of the volume between the electrodes, see Figure 6.1. The resonator round-trip loss due to the transmission in the laser mirrors is 2.5%.

In another experiment at 10 atm gas pressure a gold-coated grating was used as an end reflector in the laser resonator. The losses at the grating were estimated to be 6–7% due to estimated ~1% coupling loss and according to the value for grating efficiency given by the grating manufacturer (107). The output coupling of the dielectric output mirror was ~0.5%. According to the estimated gain per pump energy density described above, the gain would be 11–12% when the laser started to oscillate and was well above threshold. (The laser oscillated on the R(16) line at 10.4 μm.)

The build-up time from one photon in the resonator mode till the laser output pulse is of the order of microseconds when the net resonator round-trip gain is only a few per cent. Because of the arcs which inevitably build up at the end of the discharge pulses, more accurate measurements of the threshold for laser oscillation than described above have not been made.

In section 6.2 was described measurement of small-signal gain which was 30% higher than was expected according to the estimated gain per pump energy density. In those experiments the gas mixing ratio of $CO_2 : N_2 : He$ was 5:5:90. It has been observed in this work that the small signal gain is less for a gas mixing ratio of 1:1:98 compared to that for the 2:2:96 mixing ratio. As was discussed in section 6.2, the E/N ratio in the discharge varies with the gas mixture. It is therefore reasonable to believe that the pumping efficiency also varies with the gas mixing ratio, see section 3.4.

We summarize this discussion about the small signal gain per rf pump-energy density with the conclusion that the estimate made in section 3.7 is reasonably accurate for gas mixing ratios between 2:2:96 and 5:5:90. More experiments are needed in order to determine the peak small signal gain for the various gas mixing ratios and gas pressures more precisely. It should also be noted that the gain between line-centre frequencies has not been considered in this report, and this gain is of particular importance for a continuously tunable laser.

6.3.4 Laser output and discharge characteristics versus gas flow and pulse repetition rate

It has been observed that the laser performance and some gas discharge characteristics to some extent depended on whether the gas was removed from the discharge volume faster or slower than the discharge pulse repetition rate. The main observations are shown in Figure 6.14, which also indicates within which domain the pulse repetition rate has been varied.

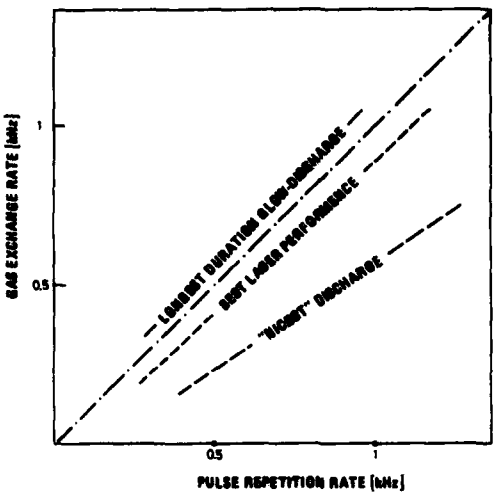

Figure 6.14 Gas-discharge characteristics and laser performance characteristics versus ratio of gas exchange rate to gas flow rate

Visually the glow discharge appeared to be most stable and "nice" when the pulse repetition rate was faster than the gas exchange rate. The higher the pulse repetition rate the more stable and "nice" the discharge seemed to be. This observation can be attributed to electrons and ions and possibly atoms and molecules in excited metastable states being present in the gas from the preceding pulse. This was discussed in section 3.6.2. A similar observation has been made by Smith *et al* (129). On the other hand, the duration of the glow discharge before arcing was slightly shorter than when the pulse repetition rate was lower than the gas exchange rate. This was shown in Figure 6.5.

When the pulse repetition rate was lower than the gas exchange rate, the time from the start of the input power pulse to gas breakdown could vary slightly from pulse to pulse. This was especially pronounced when the input power was close to threshold for sustaining a glow discharge. This observation seems reasonable from the fact that the gas breakdown is of a statistical nature and starts from some electrons and ions which are always present in the gas, for one thing because of cosmic radiation (71–75).

Initial laser performance experiments were made at 1 – 1.5 atm gas pressure with copper electrodes without any dielectricum on them. Input rf-power levels up to 1 kW were used. In these experiments the optimum flow rate for maximum laser output power was approximately half the pulse repetition rate, that is, the gas was renewed approximately between each second pulse. Thus it looked as though the preionization from the preceding pulse was important for the laser performance under these conditions. As has been pointed out previously, striking of the discharge in general was more difficult when pure copper electrodes were used, compared to when these were covered by a dielectricum.

In the multiatmospheric pressure laser only electrodes covered with sapphire ribbons have been used. In these experiments the optimum gas exchange rate for maximum output power was close to the pulse repetition rate. At 10 atm gas pressure it was observed that under certain circumstances the output power depended critically on the ratio between the pulse repetition rate and gas exchange rate. The output power could be zero both for pulse repetition rates higher than approximately 10–20%

above the gas exchange rate and for pulse repetition rates lower than 10–20% below the gas exchange rate. When these rates were approximately equal, the output power could be relatively high. This behaviour was not expected because visually and electrically the discharge did not look very different under these conditions. This observation has not been given a satisfactory explanation. It probably has something to do with the homogenity of the laser active medium, preionization from the preceding discharge pulse or discharge lensing effects. It was observed that the behaviour described above was pronounced when the curvature of the laser resonator mirrors did not properly match the resonator "mode" defined by the waveguide and the discharge region, and when the resonator losses were relatively high. High resonator losses could be caused both by the above-described mirror curvature mismatch, one or more dispersive elements in the resonator, and high output power coupling. When the laser resonator was well designed, was carefully aligned and had low losses, the laser would oscillate for pulse repetition rates much lower than the gas exchange rate with approximately constant output power, independent of the pulse repetition rate. The laser would also oscillate for pulse repetition rates higher than the gas exchange rate with output power decreasing with increasing pulse repetition rate. Under all circumstances the laser output power was highest when, according to our calibrations, the pulse repetition rate was approximately equal to, but slightly below, the gas exchange rate.

As has been mentioned previously, it was observed that the higher the gas flow rate and pulse repetition rate the higher was the output power, the more stable were the output pulses and the longer duration had the pulse tails. Below 5 atm gas pressure the laser could be operated at a few Hz pulse repetition rate without any gas flow at all. No systematic measurements of the maximum and minimum pulse repetition rates for various gas exchange rates, gas pressures and gas mixing ratios have been performed.

6.3.5 Gas recirculation experiments

Initial gas recirculation experiments were performed in order to be able to recirculate gas containing a mixture of CO_2 isotopes. The experiments were performed at 5 atm gas pressure, which should be adequate for continuous frequency tuning with such a mixture (7) and which is close to the pressure limit of the pump. Only a few gas recirculation experiments have been performed because successful frequency tuning experiments were performed at 10 atm gas pressure, see section 6.4.

In preliminary gas recirculation experiments the temperature of the gas and the electrodes was varied from 8°C to 30°C. It was observed that at 8°C the problem with arcs in the discharge was considerably larger than at 20°C. This also seemed to be the case in a subsequent experiment where prechilled gas was just blown through the discharge and out into the air. These are the only experiments that have been performed with cooling of the electrodes and the gas.

When the gas was recirculated and the water-cooling was at room temperature, the laser performance in approximately the 10^4 first shots was approximately equal to when the gas was just blown through the laser and out into the air. When the laser was operated at 350 Hz pulse repetition rate the laser could be operated continuously for approximately 4–5 minutes before arc discharges seriously limited the laser performance. This corresponds to approximately 10^3 shots. Then the laser could be turned off while the gas continued to be recirculated for 10 minutes. When the laser was turned on again it would oscillate approximately as at the start of the experiment, but the time till arcs limited the laser performance was only approximately 1 minute.

We believe that the above-described behaviour is caused by gas dissociation in the discharge. We have not measured the gas composition after the experiments and we have not measured the gas temperature nor the temperature of the electrodes during the experiments. The above described experiments indicate for how long the laser can be operated with a simple gas recirculation system with no catalyst to regenerate CO_2 from CO and O_2 and with a simple water-cooling system.

6.4 Frequency tuning experiments and spectral characteristics of the laser output

Initial measurements of the laser output frequency when no dispersive elements were used in the resonator showed that the laser always oscillated on the strongest lines in the R-branch at 10.4 μm. This was also expected according to the calculated gain-curves shown in Figure 3.4. All the frequency tuning experiments have been performed within the R-branch at 10.4 μm. The $CO_2 : N_2 :$ He gas mixing ratio has been 2: 2: 96 unless otherwise stated.

6.4.1 Frequency tuning with grating

Initial frequency tuning experiments were performed with the simplest tunable resonator shown in Figure 4.8a, that is, with a diffraction grating as the only resonator tuning element. The grating was a PTR-Optics gold-coated master-ruled grating with 135 lines per millimeter, blazed for 10.6 μm. It was mounted as close as possible to the waveguide. The laser output mirror was either a 0.75 m or a 1.3 m radius of curvature dielectric mirror with approximately 0.5% transmission, mounted close to the other end of the waveguide. The relative output power on the various line-centre frequencies in the R-branch at 10.4 μm at 5 atm gas pressure is shown in Figure 6.15. Input rf-power is 6–7 kW.

It can be seen from Figure 6.15 that the laser oscillates on the transitions from R(6) to R(30) and that the strongest lines are from R(10) to R(20). The relative strength of the various lines is determined by the rotational temperature of the CO_2 molecule, see section 3.2. The laser was observed to oscillate close to only one line-centre frequency at a time when the grating was fine-tuned for maximum output on a line-centre frequency.

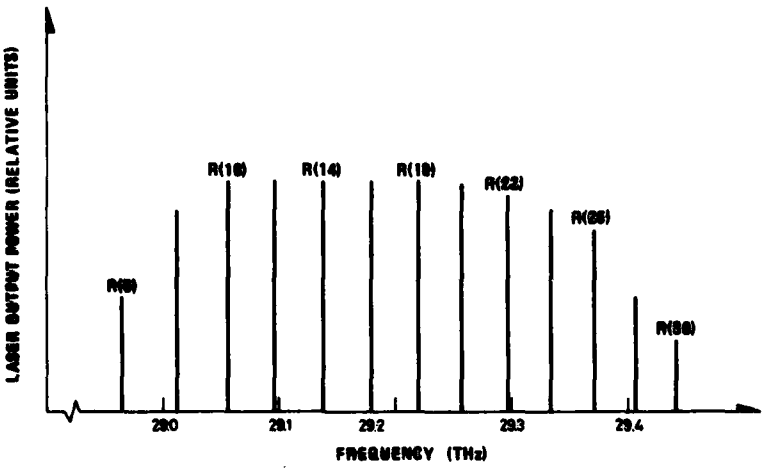

Figure 6.15 Relative peak laser-output at various line-centre frequencies in the R-branch, 10.4 μm band, at 5 atm gas pressure

At 10 atm gas pressure the laser oscillated only close to the line-centre frequencies from R(12) to R(20). No frequency tuning between line-centre frequencies was possible with this laser resonator.

At 5 atm, frequency tuning was also attempted with this resonator and with a gas mixture of 1.5% $C^{12}O_2^{16}$, 1.5% $C^{12}O_2^{18}$, 3% N_2 and 94% He. The gas was recirculated. The laser was observed to oscillate close to the line-centre frequencies between R(18) and R(26) of $C^{12}O_2^{16}$ and between R(12) and R(18) of $C^{12}O_2^{18}$, see Figure 3.5. The output power was comparable to the output power with a single CO_2 isotope. The tuning range was much smaller. No further or more detailed measurements with the isotope mixture have been performed.

6.4.2 Frequency tuning with beam-expander/grating combination

Frequency tuning experiments were performed with a beam-expander with magnification M = 2.5 in front of the grating. This was shown schematically in Figure 4.8b. The beam-expander consisted of a 1 cm diameter 1 cm negative focal-length lens and a 2.5 cm diameter 2.5 cm positive focal-length lens separated by 1.5 cm. The lenses were made of ZnSe and were AR-coated for 10 μm. The transmission through the beam-expander was measured to be 97.5% ± 1%. A beam-expander with larger magnification could not be used because of the limited space available inside the laser chamber. With a 2 mm beam diameter in the waveguide the frequency resolution of the grating with the M = 2.5 beam-expander would be 30 GHz, according to the Rayleigh criterion. This resolution should allow frequency tuning between line-centre frequencies.

With the beam-expander/grating combination the laser would not oscillate at gas pressures above 6.5 atm, due to the frequency-independent losses and the limited available rf-power.

To increase the maximum reflection from the beam-expander/grating combination, an extra partial reflecting mirror with 50% reflectivity was inserted between the waveguide end and the beam-expander, as close to the waveguide as possible. With this configuration no laser oscillation was obtained at all. This is probably due to transverse mode coupling losses between the coupled resonators, see Chapter 4. It was also observed that the beam-expander was not perfectly aligned with the lenses parallel and colinear to each other. As was pointed out in Chapter 4, the alignment of the beam-expander/grating combination is very critical and this was also observed in the experiments without the extra partial reflector. No further experiments were performed with the beam-expander/grating combination, even though a more careful alignment of the beam-expander, the grating and the extra mirror would probably have given better results.

6.4.3 *Frequency tuning with grating/etalon/extra-mirror combination*

The resonator with the grating/etalon/extra-mirror combination (the GEM-reflector) was shown schematically in Figure 4.8d. The reflection from the GEM-reflector versus frequency was analyzed in section 4.2.4. In the experiments the extra mirror was mounted as close to the waveguide as possible, and the etalon and the grating were mounted close to the extra mirror. The distance between the waveguide and the grating was 2–2.5 cm. A discharge gap d of 1.2 mm was used. The corresponding confocal parameter b of the free space Gaussian mode which most closely would resemble the (one-dimensional) waveguide mode with d = 1.2 mm would be 5.5 cm, see section 4.1.1. According to equation (4.6) and the discussion in section 4.1.2, the coupling losses from the grating placed 2 cm from the waveguide end would be approximately 6%.

In the experiments described here the output mirror was a dielectric coated Ge-mirror with approximately 0.5% transmission and 1.3 m radius of curvature. It was mounted on a piezoelectric translator for fine-adjustment of the resonator frequencies. The grating was not mounted on a piezoelectric translator as it should have been for control of the resonance frequencies of the extra-mirror/grating reflector relative to the etalon resonance frequency, see section 4.2.4. This was primarily because of the limited available space inside the laser chamber. All the experiments described in this section were performed at 10 atm gas pressure.

The first experiments were performed with a 50%-reflectivity extra mirror and an uncoated 2 mm thick ZnSe etalon. The angle between the surfaces of the etalon was 2 arc minutes, measured in a He-Ne laser interferometer. Laser oscillation between line-centre frequencies was observed with this configuration.

Subsequent experiments were performed with a 70%-reflectivity extra mirror and an etalon with surface parallelism better than 5 arc seconds, according to the specifications. Two different etalons were tried separately; one was a 2 mm thick uncoated ZnSe etalon and the other was a 0.75 mm thick ZnSe etalon with 51% reflectivity coating on each surface. The peak transmission through the etalons was measured to be 99% (±0.5%) and 96% (±1%) (single pass) respectively.

Frequency tuning between line-centre frequencies was obtained both with the 2 mm uncoated etalon and with the 0.75 mm 51% coated etalon. The laser oscillated most easily with the 2 mm uncoated etalon, but the laser frequency sometimes jumped from one etalon resonance frequency to the neighbouring one.

Frequency tuning measurement between R(10) and R(16) line-centre frequencies with the 0.75 mm thick 51% coated etalon is shown in Figure 6.16. In that experiment the grating angle has not been varied, only the tilt angle of the etalon has been varied from about 0° to 10°. The measured laser output frequency is shown versus the etalon resonance frequency, which has been calculated from the measured etalon tilt angle. The resonance frequency at 0° was determined from measurement of the laser output frequency for etalon tilt angles close to 0°. In the experiment described above it was necessary to carefully adjust the gas flow rate versus pulse repetition rate for maximum laser output power. Pulse repetition rate was 200 Hz. Peak output power was approximately 200–300 W. For some etalon tilt angles it was necessary to fine-adjust the distance between the grating and the extra mirror. This was probably for situations when the resonance frequencies of the etalon coincided with the resonance frequencies of the combined grating/extra-mirror reflector. This fine-adjustment was accomplished by pressing the grating-adjustment screwdriver into the grating mount.

6.4.4 Laser frequency characteristics

In the measurements presented in Figure 6.16 the bandwidth of the laser output was measured to be less than the ~4 GHz resolution of the 1 m grating spectrometer. In order to investigate whether the laser oscillated on two or more resonator frequencies simultaneously the output pulse was detected with an uncooled CMT detector with bandwidth larger than 1 GHz, and the pulse signal was displayed on a Tektronix 7104 oscilloscope. In Figure 6.17 are shown typical results at 10 atm gas pressure. The lower trace shows a single output pulse and the upper trace shows an expanded part of the output pulse, approximately at the top of the pulse shape. In the picture to the left, a pulse amplitude modulation of approximately 1 GHz can be clearly seen. This is assumed to be the beat-frequency between neighbouring resonator frequencies, which are separated by approximately 1 GHz. (The resonator length is approximately 15 cm.) Thus, in that measurement the laser oscillates on two neighbouring resonator frequencies simultaneously. In the picture to the right the resonator length has been adjusted, by adjusting the voltage to the piezoelectric translator which supports the laser output-mirror, to minimize the 1 GHz amplitude modulation.

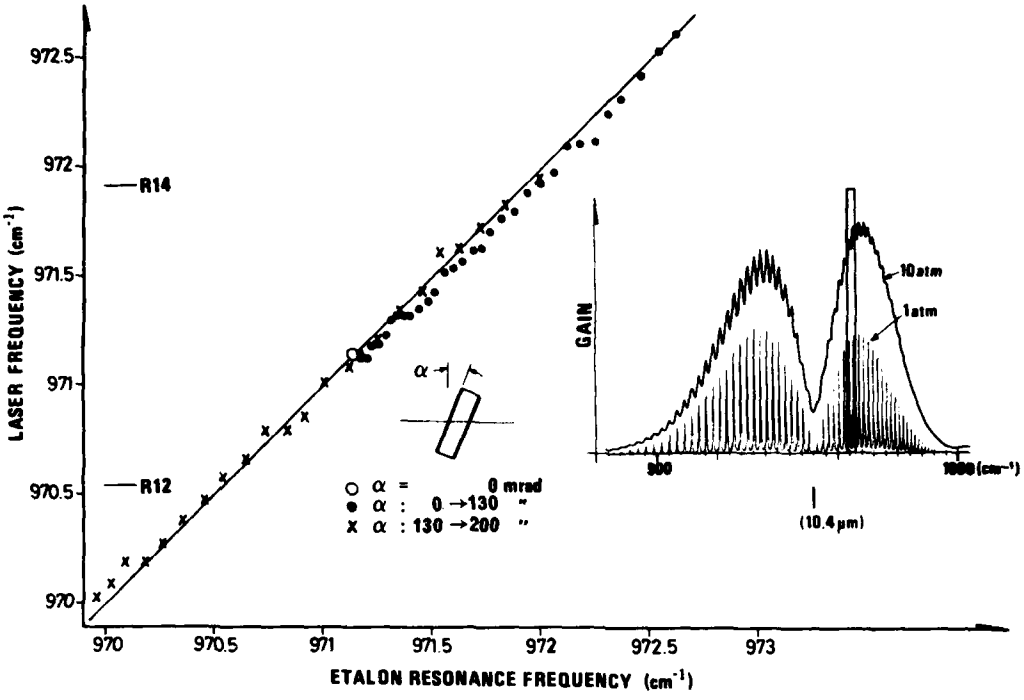

Figure 6.16 Frequency tuning between R(10) and R(16) line-centres in the 10.4 μm band, with a resonator with a grating/etalon/extra-mirror combination
The 0.75 mm thick ZnSe etalon has 51% reflectivity on each surface. The extra-mirror has 70% reflectivity. The etalon tilt angle α is varied from 0 to 200 mrad.

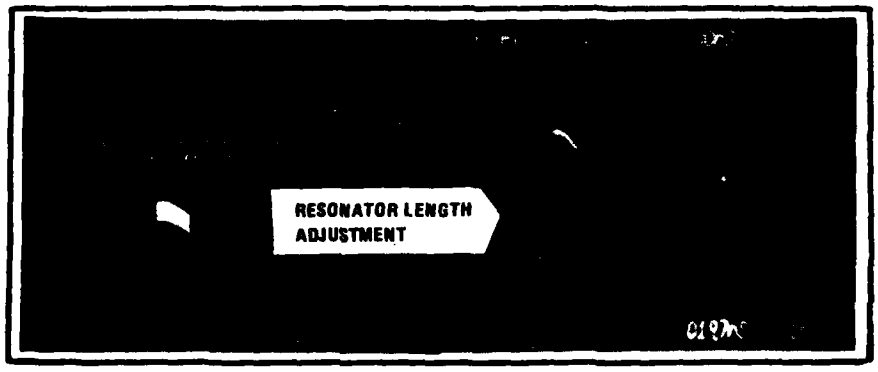

Figure 6.17 Measurement of amplitude-modulation of the laser-output at 10 atm gas-pressure
Lower trace shows laser-output pulse (100 ns/div). Upper trace shows expanded part of the top of the laser-pulse (5 ns/div to the left, 1 ns/div to the right).

It should be noted that the depth of the 1 GHz modulation frequency and consequently the ratio of the intensities of the two frequencies cannot be determined from the pictures in Figure 6.17. This is because the frequency response of the detector and the detector circuitry is not at all constant up to 1 GHz.

At 2 GHz the response of the detector and detector circuitry is very low. It cannot be seen from the right-handside picture whether the laser oscillates on two resonator frequencies separated by 2 GHz or more. This can be the case because of the resonances of the grating/extra-mirror combination, which have not been controlled in these experiments. We believe, however, that when these resonance frequencies can be controlled, for example by mounting the grating or the extra mirror on a piezoelectric translator, the laser can be a single-line laser.

The variation in laser frequency during the laser pulse was investigated in a heterodyne experiment, where the output from the rf-laser was mixed with the output from a cw CO_2-laser on the 1 GHz-bandwidth CMT-detector. The cw CO_2-laser was stabilized on the R(12) line-centre. Figure 6.18 shows typical measurements at 4 atm and 9 atm gas pressure. In each picture are shown three traces. In the middle is the laser output pulse. The sinusoidal upper and lower traces are expanded views of the first and second intensified portion respectively of the laser output pulse. Each trace is a single-sweep trace and the traces are taken at approximately 1-second intervals.

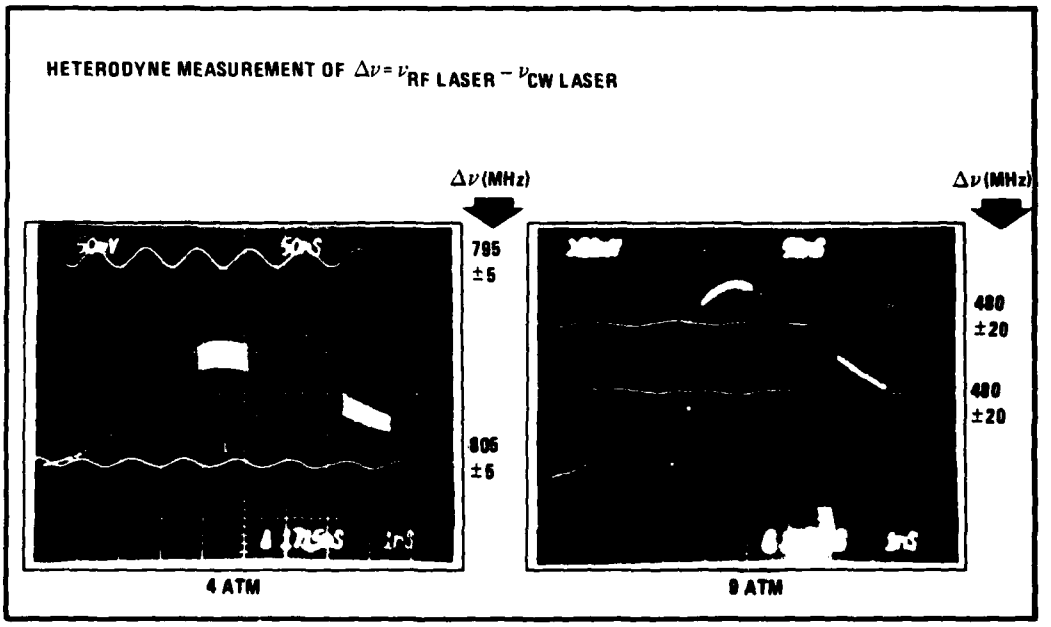

Figure 6.18 Heterodyne-measurement of variations in the output-frequency from the rf-excited CO_2-laser at 4 atm and 9 atm

The cw CO_2-laser oscillate on the R(12) line in the 10.4 μm band. Output from the cw CO_2-laser is 200 mW and peak output from the rf-excited CO_2-laser is ~ 200 W.

The output power of the cw CO_2 laser is 200 mW while the peak output power of the rf-laser is 200 W. Not all the power from the rf-laser is incident on the detector. The modulation depth of the beat-signal between the two laser frequencies depends on the relative strengths on the two beams, on the frequency response of the detector and detector circuitry and on the overlap of the wavefronts and the polarization vector of the two laser beams at the detector surface. Little effort has been made to maximize

the beat-signal modulation depth. It is seen from Figure 6.18 that the modulation depth is much smaller at 9 atm than at 4 atm. A good explanation for this has not been found. It may be that the mode quality of the output from the rf-laser is poorer at 9 atm than at 4 atm, or that the rf-laser also oscillates on other resonator frequencies, see the discussion above.

In any case, it is seen from Figure 6.18 that the variation in laser output frequency from pulse to pulse and during the laser pulse is reasonably low. The frequency chirp during the pulse and the pulse-to-pulse frequency variation seem to be less than 10 MHz. It was observed that when the resonator was well adjusted, the traces shown in Figure 6.18 remained stable for a much longer time than the 3 seconds used to take each picture.

The experiments described in this section have only been performed once. More experiments, with the grating or the extra-mirror mounted on a piezoelectric translator, should be done in order to investigate the frequency in the laser pulse more thoroughly. The long term stability of the laser has not been measured.

6.4.5 The transverse mode profile

The transverse mode structure of the laser output has not been investigated in detail. When the resonator mirrors were slightly misaligned, beat frequency between transverse modes oscillating simultaneously could easily be observed. The beat frequencies were approximately 80 MHz. It was also observed that the laser could jump from one transverse mode to another in the tail of a long-duration pulse at lower pressures than 10 atm. When the laser mirrors were well aligned, and when the output pulses were not too long, like in Figures 6.11 for example, the laser was believed to oscillate on a single transverse mode.

The beam profile has only been measured with liquid-crystal paper. Oscillation on a higher-order mode in the open direction of the parallel-plate waveguide has been observed. Usually the laser seemed to oscillate on the fundamental mode in both transverse directions. The divergence of the beam was smallest in the open direction of the parallel-plate waveguide, as expected.

7 CONCLUSIONS

In the work described in this report the concept of pumping a CO_2-laser with a radio-frequency discharge at multiatmospheric pressures in order to obtain continuous frequency tuning has been investigated both theoretically and experimentally. Emphasis has been laid on investigation of parameters of importance to attain a stable and homogenous rf glow-discharge in a CO_2 laser gas mixture at 5–10 atm, and how to couple enough energy into such a discharge to reach threshold for laser oscillation. Experimentally, discharges between parallel plate electrodes have been investigated and 40.68 MHz rf-excitation at up to 7–8 kW peak-power has been used. A multiatmospheric-pressure rf-excited CO_2 waveguide laser has been built based on results from the rf-discharge experiments. Continuous frequency tuning of this laser between vibrational/rotational line-centre frequencies of CO_2 has been demonstrated. The frequency tuning range of the laser has not yet been measured.

7.1 Results from measurements of rf-discharge characteristics at multiatmospheric pressures

In an rf glow-discharge between parallel plate electrodes the peak-to-peak displacement of the oscillating electrons should be less than the electrode separation. At 40 MHz the electron displacement will be 0.4 – 0.8 mm. Experimentally it is observed that an electrode separation of 1 – 1.5 mm is best for a stable glow discharge. It is necessary that the electrodes be covered with a dielectric material in order to be able to strike the discharge easily and to attain a stable glow discharge without arcing with long enough duration to reach threshold for laser oscillation. At 10 atm the gain decay time constant is 3 – 3.5 μs. At multiatmospheric pressures it has been observed that considerable amounts of small arcs which are detrimental to the laser performance inevitably build up when the discharge duration is longer than typically a few times the gain decay time-constant.

It looks as though a few small arcs can be present simultaneously with the glow discharge without significantly reducing the pumping efficiency of the upper laser level and reducing the laser performance. To obtain a long-duration glow-discharge without large amounts of arcs it has been necessary to use a dielectric material on the electrodes with sufficiently large capacitive ballasting of the discharge. Experiments have been performed with 0.5 mm and 0.75 mm thick sapphire ribbons, 1 mm thick alumina ribbons and 1 mm thick cover glass ribbons on the electrodes. It has been observed that longer-duration arc-free discharges are obtained with the 1 mm alumina than with the 0.5 mm sapphire ribbon. Relatively long-duration arc-free glow discharges were also obtained with the 1 mm cover glass. Discharges with BeO ribbons on the electrodes have not been investigated.

To obtain a 6–10 μs duration glow discharge at 10 atm without large amounts of arcs it has also been necessary to use a gas mixture with relatively low content of CO_2 and N_2 compared to what is used in conventional TE–CO_2-lasers. A $CO_2 : N_2 : He$ gas mixing ratio of 2: 2: 96 has been used in most of the laser experiments. This seemed to be an optimum gas mixing ratio for large small-signal gain and sufficiently long duration arc-free discharges for the input power level and the electrode geometry used in this work. Discharges with other gases than CO_2, N_2 and He have not been investigated.

7.2 Laser performance

The laser has been operated with a gas flow transverse to the optical axis. The electrodes were covered with 0.75 mm thick polished sapphire ribbons. The laser pulse repetition rate has been varied from ~10 Hz to 2 kHz.

With no dispersive elements in the laser resonator and with a 2% laser output coupler, input rf-power threshold for laser oscillation was ~2 kW at 10 atm gas pressure. With the same output coupling 1.5 kW peak laser output power has been obtained at 10 atm with 7–8 kW input rf-power. The output pulse has the form of a ~300 ns duration gain-switched pulse followed by a tail at lower power. An amplitude stability from pulse-to-pulse better than ± 5% has been obtained. A laser efficiency (input rf-energy/laser-output energy) of ~2% has been measured at 10 atm for the gain-switched pulse. Experiments in order to maximize the laser output power and efficiency have not been performed.

Continuous laser-frequency tuning between CO_2 line-centre frequencies has been demonstrated between the R(12) and R(14) lines in the 10.4 μm band. The optical elements in the tunable laser resonator were a 0.5% output coupler, a grating, an etalon and an extra mirror. The grating was used as a coarse frequency-tuning element. The laser frequency was fine-tuned between the R(12) and R(14) line-centres by tuning the tilt-angle of the etalon. The extra mirror was used to enhance the peak reflectivity of the grating/etalon combination. Peak laser-output power was 200–300 W. The laser-output frequency was measured to follow the resonance frequency of the tunable laser resonator approximately within the measurement uncertainties. No pulling of the laser frequency towards line-centre frequencies was observed. The spectral bandwidth of the laser pulse was determined to be less than the 3–5 GHz resolution bandwidth of the grating spectrometer which was used to measure the laser frequency. Frequency tuning experiments has not been performed in other parts of the CO_2 laser gain spectrum.

Measurements of amplitude-modulation of the laser-output pulse indicated that the laser could oscillate on a single resonator-frequency when the resonator length was controlled with a piezoelectric translator. Heterodyne measurements of the laser-output frequency indicated that the variation in the laser frequency during the laser pulse could be less than 10 MHz, and that the pulse-to-pulse frequency stability within a few seconds could be equally good. These features have not been investigated in full detail.

The laser has been operated frequently during more than half a year without changing the electrode material. Damage to the optical components in the laser resonator has not been observed.

It has been observed that best laser performance was obtained when the gas in the volume between the electrodes was renewed between each laser pulse. In some experiments at 10 atm (see section 6.3.4) the laser-output was considerably lower and more unstable both when the gas exchange rate was faster and slower than the pulse repetition rate. A satisfactory explanation for this has not been found.

7.3 Conclusions and recommendations regarding future work

The rf-excited continuously tunable CO_2 waveguide laser described above has been operated with higher pulse-repetition rates than pulsed dc avalanche-discharge excited continuously tunable lasers. The peak-output power and output-pulse energies have been considerably lower. The experiments indicate that very good pulse-to-pulse stability (±5%) good frequency stability ($\nu/\Delta\nu > 10^6$) and good frequency tuning control are obtainable with the rf-excited CO_2 waveguide laser. The laser can be operated with pulse repetition rates in excess of 1 kHz. A continuously tunable laser as described above should provide useful applications for spectroscopy, remote sensing optical pumping of other laser media, isotope separation and short-pulse generation. Several applications of a continuously tunable source in the 10 μm region require considerably higher peak powers and higher pulse energies than those from the rf-excited CO_2-laser. A good solution can then be to use the rf-excited CO_2-laser as a master oscillator for injection-locking of a 10 atm dc avalanche discharge-excited CO_2-laser. Alternatively, the output from the rf-excited laser could be amplified by dc-excited CO_2-amplifiers. Scaling up the laser cross-section for more output energy is probably limited by the small discharge gap $\sim 1 - 1.5$ mm which must be used to attain a stable and sufficiently long duration glow-discharge.

For the rf-excited CO_2-laser to become a practical tunable radiation source, first of all a more suitable, more compact, more reliable and probably more powerful rf-power source than has been used in these experiments must be found. Experiments should be performed to investigate alternating-current glow-discharge characteristics at other frequencies. It is expected that the lower the frequency the more difficult will it be to obtain a long-duration stable glow discharge without arcs. The laser structure and impedance-matching network design used in these experiments can be used at least up to 100 MHz.

In the GHz frequency domain magnetrons are available which can provide several hundred kilowatt peak output power. Magnetrons are compact power sources with very high efficiency. In this frequency domain another discharge geometry than has been used in these experiments must be applied.

The tunable resonator used in the final laser-frequency tuning experiments is relatively complicated. A laser-frequency scan requires tuning of both the grating tilt angle, the etalon tilt angle and the distance between the grating and the extra mirror. If more powerful rf-excitation can be provided, the extra mirror can probably be omitted. The frequency resolution of a grating alone is not sufficient for continuous tuning between line-centres, so either an etalon or a beam-expander must be used in addition to the grating. Which of these solutions is the better has not been determined. At the present time we believe that a resonator with a low-finesse etalon and a grating will give the most stable and compact solution and will provide the most accurate laser frequency control.

Work should also be done in order to gain a better theoretical understanding of rf glow-discharge characteristics at multiatmospheric pressures. This is important for a better understanding of the laser performance and for the best utilization of the rf-discharge excitation technique. Special attention should be paid to the arcing problem, and the relation between gas exchange rate and the pulse repetition rate. The charge distribution in the discharge has not been considered in detail in this work.

The excitation efficiency of the upper laser level of CO_2 in the rf-discharge has not been investigated in detail in this report. The optimum E/N ratio for most efficient excitation of the upper laser level of CO_2 has not been determined for the gas mixing ratios used in these experiments. The E/N(rms) for which the self-sustained rf glow-discharges operate has not been considered in detail theoretically for the various gas

mixing ratios, and it has not been determined very accurately experimentally. The discharge stabilizing effect of the dielectric materials on the electrodes should be more thoroughly investigated. More dielectric materials and various thicknesses should be tried out experimentally. An optimum gas mixing ratio and electrode dimension for sufficiently long-duration glow discharge without arcs and for as high pumping efficiency of the upper laser level as possible should be found. The effect of the gas temperature on the gain and on the arcing problem should be investigated more thoroughly.

Finally it should be noted that a continuous-wave continuously tunable CO_2-laser has not yet been demonstrated. The rf-discharge excitation technique would perhaps be the most suitable excitation technique for such a laser. This is because it has been shown that a stable rf glow-discharge can be generated between narrow-gap electrodes with a fast transverse gas-flow at 10 atm. The electrode structure both confines and cools the gas discharge and serves as a waveguide for the optical field. The main problems that must be solved are the gas cooling and gas dissociation. The necessary transverse gas flow rate will probably be determined by the time duration for which the discharge can be kept free for arcs.

Acknowledgements

This work has been done under the supervision of Gunnar Wang, to whom the author is deeply grateful for numerous valuable discussions and advice. The author is also indebted to Tycho Jæger for inspiring discussions and encouragement during this work. Christian Holm is sincerely thanked for coating several laser mirrors. The technical assistance from Øyvind Christensen, especially with the rf-power amplifiers, and the help and advice from Arne Stav in the self-service workshop is greatly appreciated. The author is also very grateful to Knut Stenersen and Stig Landrø for helpful assistance and cooperation.

References

(1) Laakmann K: Proc International Conference on Lasers '78, 11–15 Dec 1978, p 741. Paper TUKK3 CLEOS, San Diego, 1980.

(2) Chenausky P P, Laughman L M, Wayne R J (1980): Paper TUKK4 CLEOS San Diego.

(3) Lachambre J L, MacFarlane J, Otis G, Lavigne P (1978): A transversely rf-excited CO_2 waveguide laser, *Appl Phys Lett* 32, 10, 652.

(4) Christensen C P, Powell F X, Djeu N (1980): Transverse electrodeless rf discharge excitation of high-pressure laser gas mixtures, *IEEE J Quantum Electron* QE-16, 949.

(5) Sutter L V (1981): Gain-switched pulsed rf CO_2 waveguide lasers, *Opt Eng* 20, 5, 769.

(6) Allcock G, Hall D R (1981): An efficient rf excited waveguide CO_2 laser, *Opt Commun* 37, 49.

(7) Gibson R B, Boyer K, Javan A (1979): Mixed isotope multiatmosphere CO_2 laser. *IEEE J Quantum Electron* QE-15, 1224.

(8) Carman T W, Dyer P E (1979): Continuous tuning characteristics of a small high pressure uv preionized CO_2 laser, *Opt Commun* 29, 218.

(9) Walther H, Rothe K W (Eds) (1979): Laser Spectrocoopy IV, Proceedings of the Fourth International Conference, 1979, Springer Series in Optical Sciences 21, Springer-Verlag, Berlin, Heidelberg, New York.

(10) McKellar A R W, Oka T, Stoicheff B P (Eds) (1981): Laser spectroscopy. V, Proc Fifth International Conference, 1981, Springer Series in Optical Sciences 30, Springer-Verlag, Berlin, Heidelberg, New York.

(11) Demtroder W (1981): Laser spectroscopy, Springer Series in Chemical Physics 5, Springer-Verlag, Berlin, Heidelberg, New York.

(12) Hochstrasser R, Kaiser W, Shank C V (Eds): Picosecond phenomena II, Springer Series in Chemical Physics 14, Springer-Verlag, Berlin, Heidelberg, New York.

(13) Zewail A H (Ed): Advances in laser chemistry, Springer Series in Chemical Physics 4, Springer-Verlag, Berlin, Heidelberg, New York.

(14) Proceedings from Workshop on Optical and Laser Remote Sensing, Monterey, 9–11 February 1982. To be published.

(15) Rockwood S (1976): Uranium isotope separation and its demand on laser development. In: Tunable lasers a- applications, Eds A Mooradian, T Jæger. P Stokseth, Springer Series in Optical Sciences 3, Springer-Verlag, Berlin, Heidelberg, New York.

(16) Tobin M S, Sattler J P, Daley T W (1982): New SMMW laser transitions optically pumped by a tunable CO_2 waveguide laser, *IEEE J Quantum Electron* QE-18, 79.

(17) Moulton P F, Mooradian A (1979): Tunable transition-metal-doped solid state lasers. In ref (9).

(18) Walling J C (1982): Alexandrite lasers: physics and performance, *Laser Focus* 18, 2, 45.

(19) Freed C (1968): Stability measurement of CO_2-N_2-He lasers at 10.6 μm wavelength, *IEEE J Quantum Electron*, QE-4, 404.

(20) DeMaria A J (1973): Review of cw high-power CO_2 lasers, *Proc IEEE* 61, 731.

(21) Abrams R L (1974): Gigahertz tunable waveguide CO_2 laser, *Appl Phys Lett* 25, 304.

(22) Alcock A J, Fedosejevs R, Walker A C (1975): Gain characteristics of a multiatmosphere uv-preionized CO_2 laser, *IEEE J Quantum Electron*, QE-11, 767.

(23) Chang T Y, Wood O R (1977): Optically pumped continuously tunable high-pressure molecular lasers, *IEEE J Quantum Electron* QE-13, 907.

(24) Stenersen K (1982): Continuously tunable optically pumped high-pressure DF→CO_2 transfer laser, NDRE/PUBL–82/1003, Norwegian Defence Research Establishment.

(25) Yu I, Bychkov *et al* (1978): High-power pulsed CO_2 laser continuously tunable over a wide frequency range, *Sov J Quantum Electron* 8, 870.

(26) Harris N W, O'Neill F, Whitney W T (1976): Wideband interferometric tuning of a multiatmospheric CO_2 laser, *Opt Commun* 16, 57.

(27) Alcock A J, Leopold K, Rickardson M C (1973): Continuously tunable high-pressure CO_2 laser with uv photopreionization, *Appl Phys Lett* 23, 562.

(28) Blanchard M *et al* (1974): Superatmospheric double-discharge CO_2 laser, *J Appl Phys* 45, 134.

(29) Jain R K, Wood O R, Maloney P J, Smith P W (1977): Characteristics of high-field preionized discharges for transversely excited waveguide lasers, *Appl Phys Lett* 31, 260.

(30) Cobine J D (1958): Gaseous conductors, Dover, New York.

(31) Patel C K N (1964): Continuous-wave laser action on vibrational-rotational transitions of CO_2, *Phys Rev Lett* 336A, 1187.

(32) Bellisio J A, Freed C, Haus H A (1964): Noise measurements on He-Ne laser oscillators, *Appl Phys Lett* 4, 5.

(33) Eckbreth A C, Davis J W (1972): RF augmentation in CO_2 closed-cycle dc electric-discharge convection laser, *Appl Phys Lett* 21, 25.

(34) Handy K G, Brandelik J E (1978): Laser generation by pulsed 2.45 GHz microwave excitation of CO_2, *J Appl Phys* 49, 3753.

(35) Nichols D B, Brandenberg W M (1972): Radiofrequency preionization in a supersonic transverse electrical discharge laser, *IEEE J Quantum Electron* QE-8, 718.

(36) Brown C O, Davies J W (1972): Closed-cycle performance of a high-power electric-discharge laser, *Appl Phys Lett* 21, 480.

(37) Schock W, Hügel H, Hoffmann P (1981): A new concept for a 1.5 kW CO_2-laser, *Laser + Electro-Optik* 13, 2, 76.

(38) Paananen R A, Bobroff D L (1963): Very high gain gaseous (Xe-He) optical maser at 3.5 μm, *Appl Phys Lett* 2, 99.

(39) Collinson J A (1965): A stable single-frequency rf excited gas laser at 6328 Å, *Bell Syst Techn J* 44, 1511.

(40) Yndin V I (1973): Investigation of a helium-neon laser with high-frequency excitation, *Sov J Quantum Electron* 3, 274.

(41) Schock W, Schall W, Hügel H, Hoffmann P (1980): CW carbonmonoxide laser with rf excitation in the supersonic flow, *Appl Phys Lett* 36, 793.

(42) Brandelik J E, Smith G A (1980): Br, C, Cl, S and Si laser action using a pulsed microwave discharge, *IEEE J Quantum Electron* QE-16, 7.

(43) Laakmann Electro Optics Inc, 33052 Calle Aviador, San Juan Capistrano, CA 92675, USA.

(44) Laser Applications Ltd, Goethenburg Way, Sutton Fields Industrial Estate, Hull HU8 0YE, England.

(45) Mendelsohn A J, Normandin R, Harris S E, Young J F (1981): A microwave-pumped XeCl laser, *Appl Phys Lett* 38, 603.

(46) Bakarev A E *et al* (1980): Waveguide CO_2 laser with a pulsed high-frequency discharge, *Sov J Quantum Electron* 10, 243.

(47) Landrø S E (1979): Vekselstrømeksitasjon av CO_2-bølgelederlaser, Intern rapport E-302, Norwegian Defence Research Establishment.

(48) Løvold S, Wang G (1982): Ten atmospheres high repetition rate rf-excited CO_2 waveguide laser, *Appl Phys Lett* 40, 13.

(49) Hasson V (1980): Compact high-pressure CO_2 lasers, *SPIE* 227, 35.

Brink D J, Hasson V (1978): High-power photopreionization carbondioxide waveguide lasers operating at gas pressures of up to 13 atm, *J Appl Phys* 49, 2250.

(50) Taylor R S, Alcock A J, Sarjeant W J, Leopold K E (1979): Electrical and gain characteristics of a multiatmosphere uv preionized CO_2 laser. *IEEE J Quantum Electron* QE-15, 1131.

(51) Carman T, Dyer P E (1978): Studies of a small gap multiatmospheric-pressure CO_2 laser, *J Appl Phys* 49, 3742.

(52) Dyer P E, Tait B L (1980): A compact repetitively pulsed superatmospheric-pressure CO_2 laser with high output power density, *Appl Phys Lett* 37, 356.

(53) O'Neill F, Whitney W T (1977): A high-power tunable laser for the 9–12.5 μm spectral range. *Appl Phys Lett* 31, 270.

(54) Lowke J J, Phelps A V, Irwin B W (1973): Predicted electron transport coefficients and operating characteristics of CC_2-N_2-He laser mixtures, *J Appl Phys* 44, 4664.

(55) Cherrington B E (1979): Gaseous electronics and gas lasers, International series in natural philosophy 94, Pergamon Press, Oxford.

(56) Herzberg G (1947): Molecular spectra and molecular structure, II, Infrared and Raman spectra of polyatomic molecules, D van Nostrand, New York.

(57) Freed C, Bradley L C, O'Donnell R G (1980): Absolute frequencies of lasing transitions in seven CO_2 isotopic species, *IEEE J Quantum Electron* QE-16, 1195.

(58) Siemsen K J, Whitford B G (1977): Heterodyne frequency measurements of CO_2 laser sequence-band transitions, *Opt Commun* 22, 11.

(59) Whitford B G, Siemsen K J, Reid J (1977): Heterodyne frequency measurements of CO_2 laser sequence-band transitions, *Opt Commun* 22, 261.

(60) Dang C, Reid J, Garside B K (1980): Gain limitations in TE CO_2 laser amplifiers. *IEEE J Quantum Electron* QE-16, 1097.

(61) Yatsiv S *et al* (1971): Pulsed CO_2 gas-dynamic laser, *Appl Phys Lett* 19, 65.

(62) Cool T A, Stephens R R (1970): Efficient purely chemical cw laser operation, *Appl Phys Lett* 16, 55.

(63) Pockler T D, Shander M, Walker R E (1972): High-pressure pulsed CO_2 chemical transfer laser, *Appl Phys Lett* 20, 497.

(64) Stenersen K, Wang G (1981): Optically pumped high-pressure DF–CO_2 transfer laser, *Opt Commun* 39, 251.

(65) Smith K, Thomson R M (1978): Computer modeling of [illegible] lasers, Plenum Press, New York, London.

(66) Schulz, G J (1964): Vibrational excitation of N_2, CO and H_2 by electron impact, *Phys Rev* 135A, 988.

(67) Carman T W, Dyer P E (1978): Voltage-current characteristics of superatmospheric pressure CO_2 laser discharges, *Appl Phys* 17, 27.

(68) Denes L J, Lowke J J (1973): V-I characteristics of pulsed CO_2 laser discharges, *Appl Phys Lett* 23, 130.

(69) Nighan W L, Wiegand W J (1974): Causes of arcing in cw CO_2 convection laser discharges, *Appl Phys Lett* 25, 633.

(70) Turner R (1981): The glow-to-arc transition in a pulsed high-pressure gas discharge, *J Appl Phys* 52, 681.

(71) Howatson A M (1965): An introduction to gas discharges, Pergamon Press, Oxford.

(72) Brown S C (1966): Introduction to electrical discharges in gases, John Wiley & Sons, New York.

(73) Nasser F (1971): Fundamentals of gaseous ionization and plasma electronics, Wiley-Interscience.

(74) Meek J M, Craggs J D (Eds) (1978): Electrical breakdown of gases, Wiley series in plasma physics, Chichester.

(75) Hirsh M N, Oskam H J (Eds) (1978): Gaseous electronics. I, Electrical discharges, Academic Press, New York.

(76) Gänger B (1943): Der hochfrequenzdurchschlag verdichteter gase, *Archiv für Elektrotechnik* 37, 267.

(77) Babat G I (1947): Electrodeless discharges and some allied problems, *J Inst Elec Eng* 94, 27.

(78) Hatch A J, Heuckroth L E (1970): Retuning effects and dynamic instability of a radio-frequency capacitive discharge, *J Appl Phys* 41, 1701.

(79) Asmussen J jr *et al* (1974): The design of a microwave plasma cavity, *Proc IEEE* 62, 109.

(80) Fehsenfeldt F C, Evenson K M, Broida H P (1965): Microwave discharge cavities operating at 2450 MHz, *Rev Sci Instrum* 36, 294.

(81) Maksimov A I (1967): Electron density and energy in a microwave helium discharge, *Sov Phys Techn Phys* 11, 1316.

(82) Schmieder R W (1979) Pressure dependence of gas breakdown by combined laser and microwave fields, *J Appl Phys* 50, 712.

(83) Schneider F (1954): Zum mechanismus der hochfrequenzentladung zwischen ebenen platten, *Z Angew Physik* 6, 456.

(84) Butler H S, Kino G S (1963): Plasma sheath formation by radio-frequency fields, *The Physics of Fluids* 6, 1346.

(85) Sager O (1972): High frequency discharge and its application in sputtering plants, Balzers aktiengesellschaft, High Vacuum Report VBE 1.

(86) Brown S C (1959): Basic data of plasma physics, Techn Press MIT and Wiley, New York.

(87) Marcatili E A J, Schmeltzer R A (1964): Hollow metallic and dielectric waveguides for long distance optical transmission and lasers, *Bell Syst Techn J* 43, 1783.

(88) Krammer H (1976): Field configuration and propagation constants of modes in hollow rectangular dielectric waveguides, *IEEE J Quantum Electron* QE-12, 505.

(89) Laakmann K D, Steier W E (1976): Waveguides: Characteristic modes of hollow rectangular dielectric waveguides, *Appl Opt* 15, 1334.

(90) Laakmann K D (1976): Hollow rectangular dielectric waveguide: Errata, *Appl Opt* 15 2029.

(91) Hanna D C, Sawyers C G, Yuratich M A (1981): Large volume TEM_{00} mode operation of Nd:YAG lasers, *Opt Commun* 37, 359.

AD-A118 877 NORWEGIAN DEFENCE RESEARCH ESTABLISHMENT KJELLER F/G 20/5
CONTINUOUSLY-TUNABLE HIGH-REPETITION RATE RF-EXCITED CO2 WAVEGU--ETC(U)
JUL 82 S LOEVOLD
UNCLASSIFIED NDRE/PUBL-82/1002 NL

(92) Pechersky M (1981): Shock waves in pulsed gas lasers, *Laser Focus* 17, 12, 65.

(93) Miles R O, Grow R W (1978): Characteristics of a hollow-core distributed feedback CO_2 laser, *IEEE J Quantum Electron* QE-14, 275.

(94) Javan A (1979): Development of tunable high pressure CO_2 laser for lidar measurements of pollutants and wind velocities – January 1976 to December 1977, NASA Contractor Report 3175 Contract NASI.14289, Massachusetts Institute of Technology.

(95) Fox A G, Li T (1961): Resonant modes in a maser interferometer, *Bell Syst Tech J* 40, 453.

(96) Degnan J J (1976): The waveguide laser: A review, *Appl Phys* 11, 1.

(97) Smith P W, Wood O R, Maloney P J, Adams C R (1981): Transversely excited waveguide gas lasers, *IEEE J Quantum Electron* QE-17, 1166.

(98) Abrams R L, Chester A N (1974): Resonator theory for hollow waveguide lasers, *Appl Opt* 13, 2117.

(99) Abrams R L (1972): Coupling losses in hollow waveguide laser resonators, *IEEE J Quantum Electron* QE-8, 838.

(100) Degnan J J, Hall D R (1973): Finite-aperture waveguide-laser resonators, *IEEE J Quantum Electron* QE-9, 901.

(101) Avrillier S, Verdonck J (1977): Coupling losses in laser resonators containing a hollow rectangular dielectric waveguide, *J Appl Phys* 48, 4937.

(102) Henderson D M (1976): *Appl Opt* 15, 1066.

(103) Gorton E K, Redding J R (1980): Two methods of operation of a CO_2 transversely excited waveguide laser, *J Phys E* 13 335.

(104) Häfele H G (1963): Das infrarot spektrum des Rubins, *Z Naturforsch* 18A, 331.

(105) Garmire E, McMahon T, Bass M (1980): Flexible infrared waveguides for high-power transmission, *IEEE J Quantum Electron* QE-16, 23.

(106) Diffraction gratings ruled and holographic, Handbook, Jobin Yvon optical systems.

(107) PTR-Optics Corp, 145 Newton Street, Waltham, Massachusetts 02154, USA.

(108) II–VI Inc, Saxonburg Blvd, Saxonburg, PA16056, USA.

(109) Hercher M (1969): Tunable single mode operation of gas lasers using intracavity tilted etalons, *Appl Opt* 8, 1103.

(110) Burleigh Instruments Inc, Burleigh Park, Fishers, NY 14453, USA.

(111) Bjorkholm J E, Damen T C, Jagdeep Shah (1971): Improved use of gratings in tunable lasers, *Opt Commun* 4, 283.

(112) Peters P J M, Witteman W J (1982): Stable sealed-off transition selective CO-laser at room temperature, Paper ThN5, CLEO '82, Tucson, Arizona, USA.

(113) Deka B K, Dyer P E, Winfield R J (1981): Single mode operation of a continuously tunable TE CO_2 laser using a three mirror resonator, *Opt Commun* 39, 255.

(114) Radio-Research Instrument Co Inc, 2 Lake Avenue Extension, Danbury, Connecticut 06810, USA.

(115) "Heath Kit", Heath Company, Benton Harbor, Michigan 49022, USA.

(116) RF Power Labs Inc, 21820-87th SE, Maltby Industrial Village, Woodinville, WA 98072, USA.

(117) Hall D R, Hull University, Physics Department, Hull, UK, private communication.

(118) Wood O R, Smith P W, Adams C R, Maloney P J (1975): Excitation of transversely excited CO_2 waveguide lasers, *Appl Phys Lett* 27, 539.

(119) Homann Ch, Hübner H, Bötticher (1978): Determination of the recombination coefficient in CO_2 laser discharges, *Appl Phys Lett* 33, 417.

(120) Gerber R A, Sauter G F, Oskam H J (1966): Studies of decaying Helium plasmas. *Physica* 32, 2173.

(121) Ishchenko V N, Lisitsyn V N, Sorokin A R (1978): Excitation of high-pressure laser media by a discharge through an insulator, *Sov J Quantum Electron* 8, 453.

(122) Christensen C P (1979): Pulsed transverse electrodeless discharge excitation of a CO_2 laser. *Appl Phys Lett* 34, 211.

(123) Howard W Sams & Co Inc (subsidiary of ITT), Indianapolis (1975): Reference data for radio engineers, 6 Ed.

(124) Young J F, Harris S E, Wisoff P J K, Mendelsohn A J (1982): Microwave excitation of excimer lasers, *Laser Focus* 18, 4, 63

(125) Bagratashvili V N *et al* (1976): Investigation of a high-pressure continuously tunable CO_2-laser, *Sov J Quantum Electron* 6, 541.

(126) Reid J, Garside B K, Ballik E A (1979): Vibrational relaxation measurements in CO_2 employing an incremental TEA laser gain technique, *IEEE J Quantum Electron* QE-9, 602.

(127) Cheo P K (1971): CO_2 lasers. In: Lasers vol 3, Eds A K Levine, A J DeMaria, Marcel Dekker Inc, New York.

(128) Cheo P K *Appl Phys Lett* 11, 38 (1967): *IEEE J Quantum Electron* 4, 587 (1968).

(129) Smith P W, Maloney P J, Wood O R II (1979): Waveguide TEA laser, *Appl Phys Lett* 23, 524.

(130) Saphikon, Tyco Industries, 51 Powers Street, Milford, NH03055, USA.

(131) The Radio Amateur's Handbook 1980, 57 Ed, The American Radio Relay League, Newington, CT06111, USA.

(132) Wilkinson E J (Jan 1960): An N-way hybrid power divider, IRE Transact Microw Theory and Techn, 116.

(133) Brush Wellman Inc, 17876 St Clair Ave, Cleveland, O 44110.

(134) Loh E (1968): Optical phonons in BeO crystals, *Phys Rev* 166, 673.

(135) Carborundum Company, Graphite Products Division, PO Box 577, Niagara Falls, New York, USA: Technical information on Boron Nitride.

(136) Coors Porcelain Company, Bulletin 955, 600 Ninth Street, Golden, Colorado 80401, USA.

(137) Dyer P E, James D J (1975): *J Appl Phys* 46, 1679.

(138) Handbook of Chemistry and Physics, 55 Ed, CRC Press Inc, Cleveland, Ohio, USA.

(139) Abrams R L (1974): Broadening coefficients for the P(20) CO_2 laser transition, *Appl Phys Lett* 25, 609.

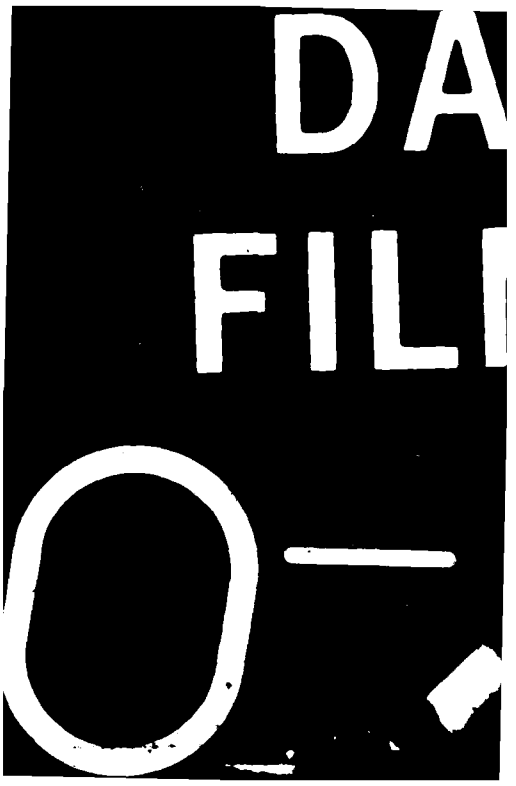
DA
FIL